Detachment Faulting and Mantle Exhumation Beneath an Allochthonous Carbonate Cover: Insights From the Gouffre Georges (Lherz Massif, Pyrenees, France)

Riccardo Asti, Nicolas Saspiturry, Michel de Saint Blanquat, Patrick Sorriaux, Eric C. Ferre

Tectonics®

RESEARCH ARTICLE
10.1029/2024TC008757

Detachment Faulting and Mantle Exhumation Beneath an Allochthonous Carbonate Cover: Insights From the Gouffre Georges (Lherz Massif, Pyrenees, France)

Riccardo Asti[1,2,3], Nicolas Saspiturry[4], Michel de Saint-Blanquat[5], Patrick Sorriaux[7], and Eric C. Ferré[6]

[1]Department of Biological, Geological and Environmental Sciences – BiGeA, Alma Mater Studiorum, University of Bologna, Bologna, Italy, [2]Université Côte d'Azur, OCA, CNRS, IRD, Géoazur, Valbonne, France, [3]Univ Rennes, CNRS, Géosciences Rennes, UMR 6118, Rennes, France, [4]Géosciences Montpellier, Université de Montpellier, CNRS, Montpellier, France, [5]Géosciences Environnement Toulouse, Université de Toulouse, CNES, CNRS, IRD, UPS, Toulouse, France, [6]Department of Geological Sciences, New Mexico State University, Las Cruces, NM, USA, [7]Retired TOTAL petroleum geoscientist and Spéléo Club du Haut Sabarthez, Tarascon sur Ariège, France

Abstract The Cretaceous North Pyrenean hyperextended rift system recorded HT-LP metamorphism in the pre- and syn-rift sedimentary cover during lithospheric mantle exhumation. We describe and analyze for the first time the rocks exposed in the Gouffre Georges, a deep cave in the Lherz peridotite massif (Ariège, France). The cave walls expose the lithospheric detachment between the Mesozoic pre-rift sedimentary cover hanging wall and the mantle rock footwall. Extensional structures have been preserved despite the positive inversion of the North Pyrenean rift system during the Pyrenean Orogeny. The extension direction is downdip WNW, consistent with rifting models of transtensional left-lateral regime during the final stage of rifting. Field, microstructural, and petrographic data document a continuum of extensional deformation from high- to low-temperature conditions. This detachment fault underwent high-temperature hydrothermalism, with a possible contribution from evaporite-born fluids. New observations also strongly suggest the formation of a hot, low-viscosity material along the detachment interface. This material was then injected in the uppermost part of the peridotite body during the final stage of mantle exhumation. We consider three possible scenarios: (a) partial melting at the base of the pre-hyperextension carbonates; (b) precipitation from carbonate-rich hydrothermal fluids; and (c) flow of hyper-ductile marble due to extreme plasticity of calcite under high temperature. Likewise, the base of the pre-hyperextension cover recorded intense hydraulic and tectonic brecciation during extension. As indicated by their lack of syn-rift sedimentary reworking, the Lherz peridotite recorded partial exhumation at the base of the Jurassic sedimentary cover, without exposure to the seafloor.

Key Points:

- A large exceptional cave at the contact between marbles and peridotite (mantle rocks) exposes a major detachment
- Carbonate microstructures in the carbonate hanging wall document high-temperature regime and progressive cooling in a continuum of extension
- The top-to-the-WNW kinematics of this detachment and related extensional structures are preserved after Pyrenean positive inversion

Supporting Information:

Supporting Information may be found in the online version of this article.

Correspondence to:

R. Asti,
riccardo.asti2@unibo.it

Citation:

Asti, R., Saspiturry, N., de Saint-Blanquat, M., Sorriaux, P., & Ferré, E. C. (2025). Detachment faulting and mantle exhumation beneath an allochthonous carbonate cover: Insights from the Gouffre Georges (Lherz Massif, Pyrenees, France). *Tectonics*, *44*, e2024TC008757. https://doi.org/10.1029/2024TC008757

Received 1 DEC 2024
Accepted 11 DEC 2024

Author Contributions:

Conceptualization: Riccardo Asti, Nicolas Saspiturry, Michel de Saint-Blanquat
Data curation: Riccardo Asti
Formal analysis: Riccardo Asti, Nicolas Saspiturry, Michel de Saint-Blanquat
Funding acquisition: Riccardo Asti, Michel de Saint-Blanquat
Investigation: Riccardo Asti, Nicolas Saspiturry, Michel de Saint-Blanquat, Patrick Sorriaux, Eric C. Ferré
Validation: Patrick Sorriaux, Eric C. Ferré

1. Introduction

Hyperextension on continental margins is among the most exciting geodynamic discoveries of the past decades and is currently at the core of the scientific debate about how continents form, breakup and evolve through time. Defined as stretching of the continental crust such that the lower and upper parts remain coupled and embrittled, allowing major faults to penetrate to the mantle, hyperextension happens during the last phases of crustal thinning that splits tectonic plates to form new oceanic crust (e.g., Alves et al., 2006, 2009; Boillot et al., 1987; Larsen et al., 2018; Manatschal, 2004; Sauter et al., 2023; Pérez-Gussinyé and Reston, 2001; Whitmarsh et al., 2001). Conceptual rifting models spanning from the pioneer pure-shear model (McKenzie, 1978) to the later simple-shear models (Wernicke, 1981, 1985) have been subsequently replaced by "polyphase" models based on new data from Atlantic-type passive margins (Lavier and Manatschal, 2006). DSDP, ODP, and IODP drilling expeditions along the Atlantic Ocean margins demonstrated that hyperextension is a common phenomenon in distal continental margins. These expeditions also allowed the development of novel numerical models explaining lithosphere-scale extension and sub-continental mantle denudation (Brune et al., 2014, 2017; Huismans & Beaumont, 2003, 2008, 2011). Moreover, syn-rift, breakup, and drift sedimentary sequences on continental margins were correlated with major phases of crustal thinning, lithospheric breakup, and oceanic spreading (Alves & Cunha, 2018; Alves et al., 2020; Soares et al., 2012). Passive margins recording important mantle exhumation were found to develop under conditions dominated by high thermal gradients and mantle heat flow due to asthenospheric rise (Clerc et al., 2015, 2018; Morgan, 1982; Pérez-Gussinyé et al., 2024; Reston and Morgan, 2004; Sapin et al., 2021).

Visualization: Riccardo Asti, Nicolas Saspiturry, Michel de Saint-Blanquat
Writing – original draft: Riccardo Asti, Nicolas Saspiturry
Writing – review & editing: Riccardo Asti, Nicolas Saspiturry, Michel de Saint-Blanquat, Patrick Sorriaux, Eric C. Ferré

The Pyrenees are one of the most famous analogs of hyper-extended rifted margin and have been extensively studied in the last decades. Indeed, they are the locus of debates and emergence of new concepts about mantle exhumation by low-angle detachments, pertinent to rifting and breakup mechanisms in general (e.g., Asti, Lagabrielle, et al., 2019; Clerc & Lagabrielle, 2014; Jammes et al., 2009; Lagabrielle and Bodinier, 2008; Lagabrielle et al., 2010; Lescoutre and Manatschal, 2020; Manatschal et al., 2021; Masini et al., 2014; Tugend et al., 2014). Several outcrops of exhumed sub-lithospheric mantle are scattered along the mountain range (e.g., Clerc & Lagabrielle, 2014; Lagabrielle et al., 2010; Monchoux, 1970; Tugend et al., 2014), or imbricated into the orogen (Espurt et al., 2019; Saspiturry et al., 2020a, 2024), but the related syn-breakup detachment faults are rarely and discontinuously exposed in outcrop (Asti, Lagabrielle, et al., 2019; Lagabrielle et al., 2019a, 2019b). They are somehow mapped, but they remain highly hidden, which fuels active debates that have flourished during the last decades. In particular, numerous recent studies have investigated the structural and tectono-thermal evolution of the Cretaceous paleo-passive margin preserved in the NPZ (e.g., Asti, Lagabrielle, et al., 2019; Asti et al., 2021; Clerc & Lagabrielle, 2014; Clerc et al., 2015, 2016; Ducoux et al., 2019, 2021; Duretz et al., 2020; Saspiturry et al., 2019a, 2020b, 2021a; Lescoutre et al., 2019; Motus et al., 2022). These studies highlight the fundamental differences in structural architecture, sedimentary systems and thermal regime between pre-rift evaporite-rich passive margins, as in the case of the Pyrenean margins, and other types of so-called magma-poor passive margins, often considered as archetypal for extended margins (e.g., Alves et al., 2006, 2009; Manatschal et al., 2010; Mohn et al., 2012; Whitmarsh et al., 2001; Péron-Pinvidic et al., 2013).

The main characteristics of the Cretaceous North Pyrenean paleo-passive margin include: (a) the predominance of ductile deformation during continental crust thinning in the distal part of the margin, resulting in crustal boudinage and the lack of major tilted blocks (e.g., Asti, Lagabrielle, et al., 2019; Asti et al., 2021; Clerc & Lagabrielle, 2014); (b) the deposition of up to 5 km of syn-rift sedimentary series in overall synform-shaped basins (e.g., Lagabrielle et al., 2020; Saspiturry et al., 2021a, and references therein); (c) the high thermal regime resulting in HT-LP syn-rift metamorphism of Mesozoic sedimentary cover (Albarede & Michard-Vitrac, 1978; Boulvais, 2016; Clerc et al., 2015; Ducoux et al., 2021; Golberg & Leyreloup, 1990; Saspiturry et al., 2020b); (d) the presence of a decoupling layer between the thick Mesozoic sedimentary cover and its substratum, made of the 1 to 2 km-thick Upper Triassic (Keuper) low-strength evaporites (Canérot, 1988, 1989; Clerc & Lagabrielle, 2014; Clerc et al., 2016; Curnelle, 1983; Labaume & Teixell, 2020; Lagabrielle et al., 2010, 2020; Motus et al., 2022; Teixell et al., 2016). This low-strength evaporite layer is critical for the tectono-thermal evolution of pre-rift evaporites-rich passive margins. Rift systems where the presence of the pre-rift evaporites has played a fundamental role in their tectonic evolution are referred to in the literature as "*prerift salt basins*" (Jackson et al., 2017; Rowan, 2014) or "*smooth slopes basins*" (Lagabrielle et al., 2020). This weak mechanical layer allows the pre-rift sedimentary cover to slip above the thinning basement and to rest above the exhumed mantle in the most distal part of the rift system. There, isotherm rise due to mantle uplift is more pronounced and allow the development of a ductile tectonic foliation parallel to the exhumation contact (Clerc & Lagabrielle, 2014; Duretz et al., 2020; Lagabrielle et al., 2010, 2020; Saspiturry et al., 2021a). This process promotes the deposition of thick syn-rift sedimentary series that increase heat accumulation at the base of the tectonic system due to important sedimentary burial (Clerc et al., 2015; Saspiturry et al., 2021a; Ducoux et al., 2021 and references therein). Thus, the combined effect of crustal thinning, mantle uplift, and sedimentary burial creates the conditions for HT-LP metamorphism of the sedimentary cover in the distal part of the system. This specific architecture leads to ductile thinning of both the crustal basement and its sedimentary cover in the distal part of the rift during mantle exhumation (Asti, Lagabrielle, et al., 2019; Asti et al., 2021; Clerc & Lagabrielle, 2014; Duretz et al., 2020).

One of the main implications of crustal thinning concurrent with high-temperature metamorphism under a thick pre- and syn-rift sedimentary cover is that the subcontinental mantle is mechanically decoupled from the brittle uppermost crust throughout the whole rifting history (Duretz et al., 2020; Saspiturry et al., 2021a). This mechanism prevents exposure of the subcontinental mantle to the seafloor, which is rather exhumed under a cover of allochthonous sedimentary series. This peculiar rheological layering at the scale of the lithosphere during rifting and hyperextension has of course major implications on the hydrothermal processes that take place along mantle-exhuming detachment faults.

The eponymous peridotitic Lherz Massif (Ariège, France) crops out in the central part of the NPZ. This area has received considerable attention in the past five decades not only from mantle petrologists and geochemists, but also more recently from the tectonic community. Indeed, this area has been pivotal for the emergence of new

concepts on hyperextension at magma-poor passive margins (Asti et al., 2021; Clerc et al., 2012; Lagabrielle et Bodinier, 2008; Lagabrielle et al., 2010, 2016; Uzel et al., 2020).

In this study, we present an extensive set of new structural observations based on exceptionally well-exposed underground outcrops in the Gouffre Georges, a >700 m deep cave located on the western edge of the Lherz Massif. This cave provides access to 3-D continuous exposures of the contact between mantle rocks exhumed during the Pyrenean Cretaceous extension and the overlying pre-rift sedimentary cover. These previously undescribed exposures allow to retrieve new critical information on processes taking place when decoupled pre-rift carbonates end up in contact with the exhumed lithospheric mantle during rifting, in a (hydro)thermal environment still very poorly constrained and understood. Also, by interpreting new macroscopic and microscopic observations, along with new structural data, we propose a new tectonic model for the formation of this exceptionally well-preserved detachment. Finally, we discuss the tectonic, kinematic and thermal implications of the model in the framework of the Cretaceous Pyrenean rift system and other similar rifted margins.

2. Geological Setting

The Pyrenean belt consists, from North to South, of three structural domains (Choukroune, 1976) (Figure 1): (a) the North Pyrenean Zone (NPZ), located between the North Pyrenean Frontal Thrust (NPFT) to the North and the North Pyrenean Fault (NPF), to the South; (b) the Axial Zone (AZ), which exposes mainly Paleozoic and locally Precambrian units that recorded the Variscan orogeny; (c) the South Pyrenean Zone (SPZ), located between the Axial Zone and the South Pyrenean Frontal Thrust (SPFT). The NPZ hosts a series of Cretaceous rift sedimentary basins, developed during the opening of the Bay of Biscay and eastward drift of the Iberian Plate (e.g., Asti et al., 2022; Choukroune & Mattauer, 1978; Debroas, 1990).

All along the southern part of the NPZ, the pre- and syn-Cretaceous rifting sedimentary cover has been affected by high-temperature/low-pressure (HT/LP) metamorphism during crustal thinning and lithospheric mantle exhumation during the Cretaceous rifting event (Albarede & Michard-Vitrac, 1978; Choukroune, 1976; Clerc et al., 2015; Golberg et al., 1986; Golberg & Maluski, 1988; Lescoutre et al., 2019; Montigny et al., 1986; Ravier, 1959; Saspiturry et al., 2020a, 2020b). This domain is generally referred to in the literature as Internal Metamorphic Zone (e.g., Choukroune, 1976; Ravier, 1959) and also includes the Aulus Basin (see below).

Substantial crustal thinning during the Cretaceous extension resulted in crustal breakup and lithospheric mantle exhumation (Fabriès et al., 1991, 1998; Jammes et al., 2009; Lagabrielle et al., 2010; Saint-Blanquat et al., 1986; Vielzeuf and Kornprobst, 1984). The syn-rift and breakup sedimentary sequences that correlate with major phases of crustal thinning and mantle denudation at rifted margin (Alves & Cunha, 2018; Alves et al., 2009, 2020; Soares, 2014; Soares et al., 2012), are respectively materialized in the NPZ by the Neocomian to Albian sediments witch exhibit several syn-rift megasequences (Arnaud-Vanneau et al., 1979; Asti et al., 2022; Canérot, 2008, 2017; Debroas, 1978, 1987, 1990, 1995; Peybernès, 1976, 1982; Puigdefàbregas and Souquet, 1986; Razin, 1989; Souquet et al., 1985) and by the Late Albian to Early Cenomanian succession (Canérot & Mediavilla, 2023; Debroas et al., 2010; Duée et al., 1984; Roux, 1983; Saspiturry et al., 2021a). The Early Cretaceous extensional episode is documented by the occurrence of numerous ultramafic bodies distributed all along the NPZ (Clerc & Lagabrielle, 2014; Lagabrielle et al., 2010; Monchoux, 1970; St Blanquat et al., 2016). Among these ultramafic bodies, the Lherz Massif is one of the largest (ca. 0.9 km^2) and the type locality where lherzolite was defined (Lacroix, 1894, 1900). The Lherz ultramafic body is imbedded in the metamorphosed and brecciated pre-rift sequence which constitutes the base of the Cretaceous Aulus Basin.

The Aulus Basin (Ariège, France) is an East-West elongated sedimentary basin developed during Cretaceous rifting in the NPZ (Figure 2). This basin is enclosed between the Paleozoic units of the Trois-Seigneurs Massif to the North and the Axial Zone to the South. Lenses of Variscan HT-LP granulites occur along the northern and southern edges of the basin (Azambre & Ravier, 1978; Vielzeuf and Kornprobst, 1984). These granulites, originally located at depths of ~20–24 km, subsequently recorded amphibolite facies ductile stretching during the Cretaceous rifting (Asti et al., 2021). In the internal part of the basin, several large ultramafic bodies, including the Lherz Massif, are exposed (Monchoux, 1970). These bodies constitute fragments of subcontinental mantle (e.g., Le Roux et al., 2007) that were disconnected from their original crustal hanging wall. Indeed, these ultramafic bodies are systematically surrounded by Mesozoic metamorphic carbonates and/or by various types of breccia (see later in this Section).

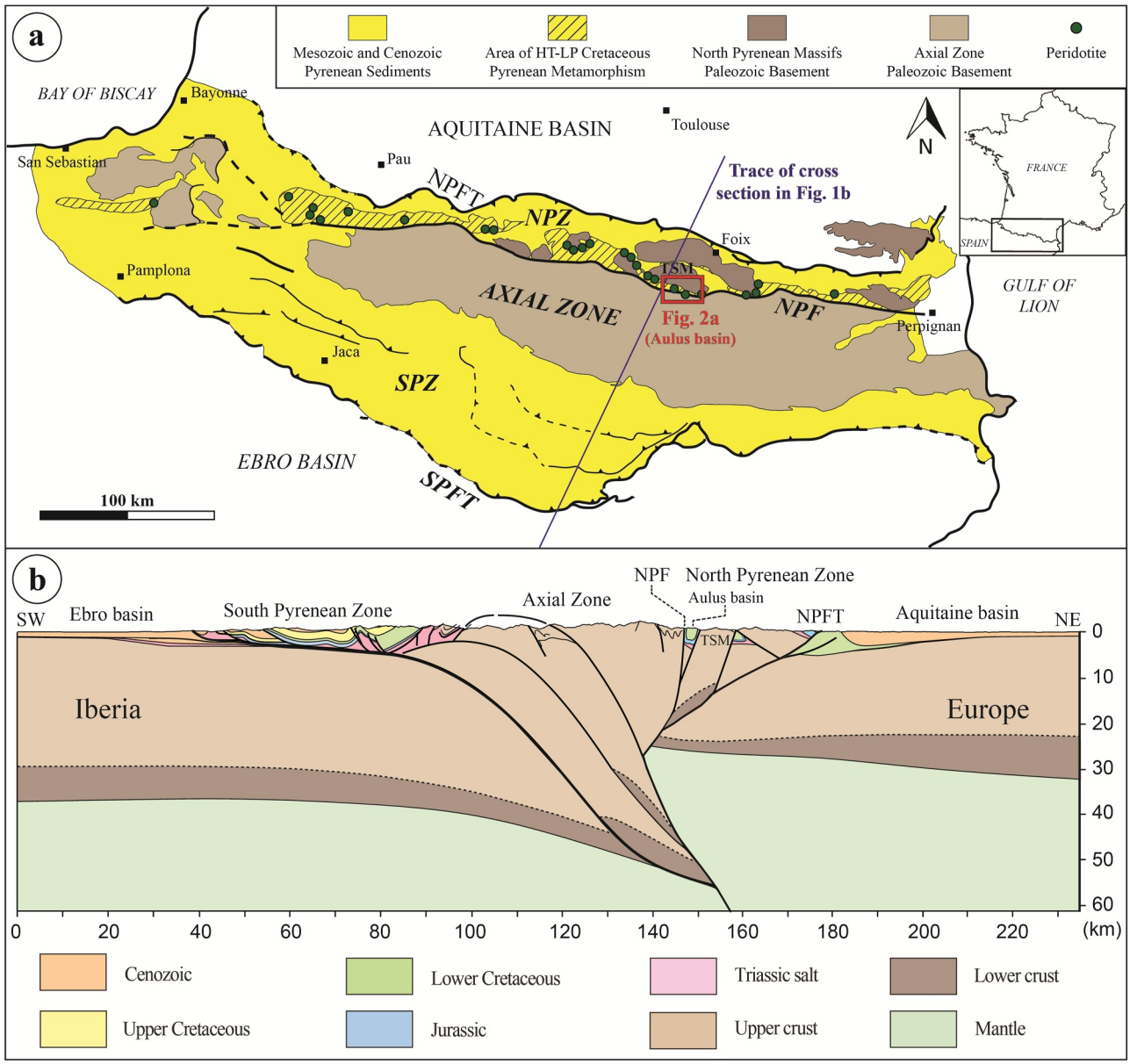

Figure 1. (a) Structural map of the Pyrenees reporting the distribution of the domains affected by the Cretaceous HT/LP metamorphism and of the main outcropping ultramafic bodies (redrawn and modified after Corre et al., 2018). (b) Cross section across the Central Pyrenees (see blue line in panel (a) for the location of the trace); redrawn and modified after Mouthereau et al. (2014). Acronyms: NPF, North Pyrenean Fault; NPFT, North Pyrenean Frontal Thrust; NPZ, North Pyrenean Zone; SPFT, South Pyrenean Frontal Thrust; SPZ, South Pyrenean Zone; TSM, Trois Seigneurs Massif.

Jurassic units of the Internal Metamorphic Zone and of the NPZ are commonly interpreted as pre-rift units, *sensu* (Alves & Cunha, 2018; Alves et al., 2006, 2009, 2020; Soares et al., 2012). The shallow marine Jurassic carbonates deposited during a period of relative tectonic quiescence (e.g., Delfaud & Henry, 1967; Peybernès, 1976; James, 1998; Lenoble, 1992; Ternet et al., 1997), even though the latest Jurassic deposits might have been affected by limited syn-depositional extensional faulting, but it remains highly speculative (see Calvet & Lucas, 2001; Debrand-Passard, 2001). Indeed, accommodation in the Jurassic is linked to thermal subsidence following the Permian-Triassic post-orogenic extension allowing the continental crust to return to its equilibrium state (e.g., Asti et al., 2022; Duretz et al., 2020; Saspiturry et al., 2019b; Vergés & García-Senz, 2001). This interpretation is coherent with what has been proposed for analog deposits in the Aquitaine Basin, the Parentis Basin, the Iberian Chain Basins, the North Iberian margin and the SPZ that are thought to have been deposited in an overall context

10.1029/2024TC008757

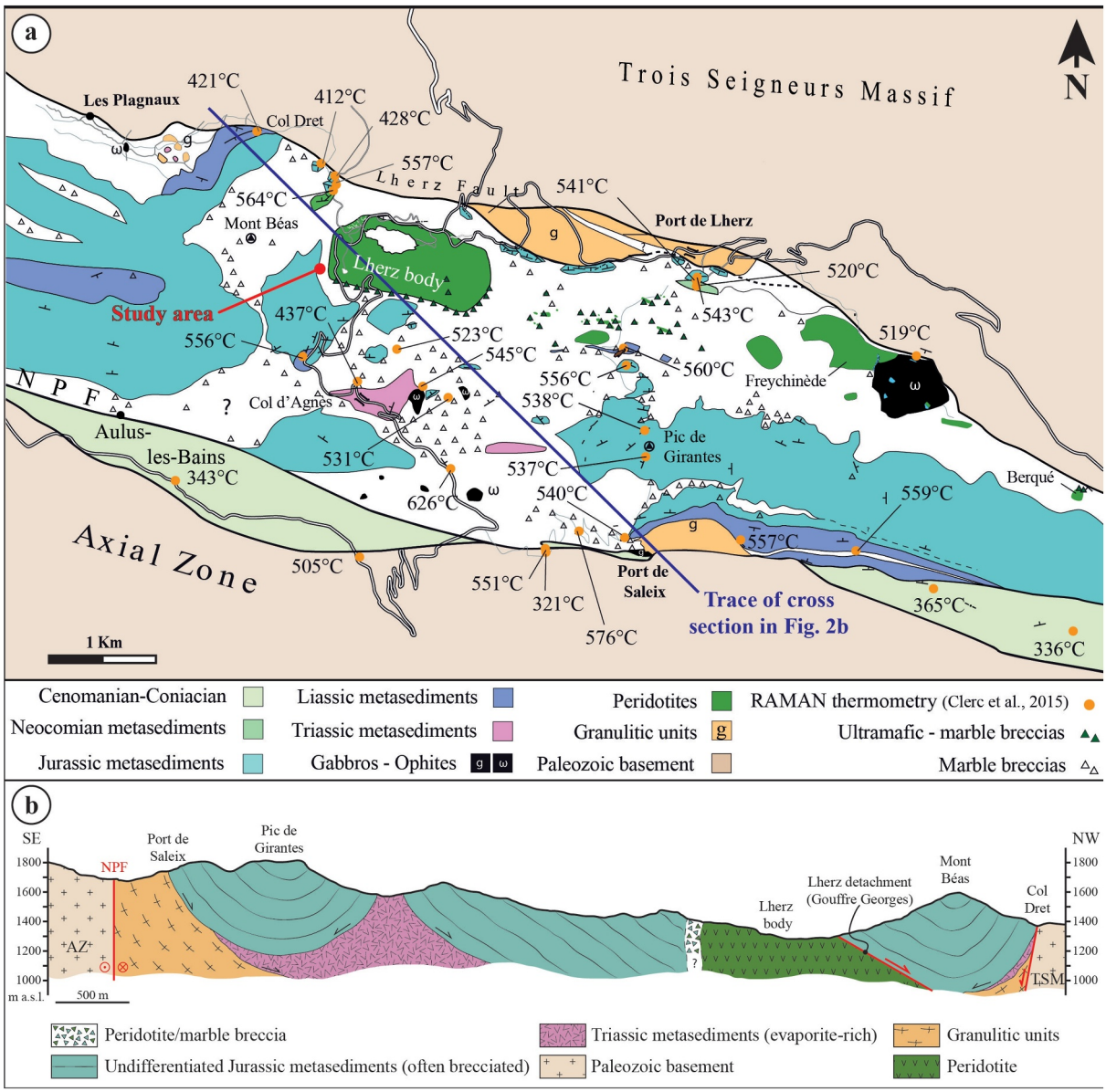

Figure 2. (a) Geological map of the central part of the Aulus Basin (modified after Lagabrielle et al., 2016) with location of the Gouffre Georges. (b) Geologic cross section across the Aulus Basin (see blue line in panel (a) for the location of the trace). Acronyms: AZ, Axial Zone; NPF, North Pyrenean Fault; TSM, Trois Seigneurs Massif.

of pre-rift flexural passive margins (e.g., Asti et al., 2022; Brunet, 1984, 1994; García-Senz et al., 2019; Gómez et al., 2019; Martín-Chivelet et al., 2019; Salas et al., 2001; Vergés & García-Senz, 2001 with references therein). However, recent studies reviewed this interpretation for the Iberian side of this system and proposed that Lower and Middle Jurassic deposits are related to an early (incipient) syn-rift episode (Aurell et al., 2019). Whatever the correct interpretation of Jurassic deposits is, the Cretaceous syn-rift and breakup episodes are clearly preceded by a phase of tectonic quiescence in the Pyrenees and the Jurassic units are pre-rift with respect to this latter extensional episode. For this reason, they will be considered as pre-rift units in the following, in agreement with many previous studies on the Cretaceous Pyrenean extension (e.g., Clerc & Lagabrielle, 2014; Ducoux et al., 2021; Duretz et al., 2020; Jammes et al., 2009; Masini et al., 2014; Saspiturry et al., 2021a).

Around the Lherz Massif, the Jurassic sedimentary units include in stratigraphic order (from bottom to top): (a) white and blue/gray banded marbles and dolomitic marbles (lower Lias); (b) black marbles, sometimes

banded, and fine-grained black schists (middle/upper Lias); (c) white dolomitic marbles and black dolostones (Dogger-Oxfordian); (d) white or gray marbles and dolomitic marbles (Kimmeridgian-Tithonian) (Ternet et al., 1997). Apart from the Liassic schists, all these lithological facies are similar and existing stratigraphic hierarchies are only tentative (Ternet et al., 1997). This is due to intense ductile deformation and metamorphism responsible for the banding commonly observed in the metamorphic Jurassic carbonates of the NPZ (Mahé, 2013). Indeed, as in the whole Internal Metamorphic Zone, the Mesozoic sedimentary series exposed in the Aulus Basin have been largely affected by the HT-LP metamorphism during crustal thinning and lithospheric mantle exhumation during the Cretaceous rifting event (Albarede & Michard-Vitrac, 1978; Choukroune, 1976; Clerc et al., 2015; Ducoux et al., 2021; Golberg & Maluski, 1988; Golberg et al., 1986; Montigny et al., 1986; Ravier, 1959). In this framework, the Aulus Basin recorded some of the highest paleotemperatures associated with this regional event (>500–550°C) (e.g., Clerc et al., 2015). Metamorphic minerals including scapolite, tremolite, muscovite and phlogopite are common in all the metamorphic Jurassic rocks in the Aulus Basin.

The Lherz peridotite body is in contact with several breccia formations that crop out all around and structurally above the body (Figure 2). These breccias are polymictic and range between two monomictic end-members where the clasts are exclusively peridotite or marble composition. The matrix also hosts variable proportions of disaggregated peridotite grains in a calcitic cement (Choukroune, 1973; Clerc et al., 2012; Lacroix, 1895; Lagabrielle and Bodinier, 2008; Lagabrielle et al., 2016). The interpretation of the origin of these breccias remains debated since their discovery (Lacroix, 1895, 1900), whether from the point of view of the geological process responsible for their formation, or their tectonic setting, or even of their thermal state. Indeed, these breccias were first interpreted as Cretaceous breccias related to: (a) explosion processes resulting from the emplacement of the hot peridotite within the Jurassic carbonate cover (Avé Lallemand, 1967; Minnigh et al., 1980; Ravier, 1959), or (b) hydraulic fracturing due to overpressured hot fluids formed during the Cretaceous (Dauteuil et al., 1987; Golberg, 1987; Ternet et al., 1997). Other hypotheses have been proposed, supporting a sedimentary origin: (a) Upper Jurassic sedimentary breccia (Lacroix, 1895); (b) post-inversion Eocene continental sedimentary breccia (Choukroune, 1973, 1976); (c) post-inversion (Cenozoic) karstic sedimentary breccia deposed within or close to tectonic and hydraulic breccia formed during the Cretaceous rifting (Debroas & Azambre, 2012; Debroas et al., 2013) and (d) tectono-sedimentary breccia formed during the Cretaceous extension which led to mantle exhumation (Clerc et al., 2012; Hall & Bennett, 1979; Lagabrielle and Bodinier, 2008; Lagabrielle et al., 2010, 2016). The latter group thus interprets these breccias as remnants of the breakup sequence (*sensu* Soares et al., 2012; Alves & Cunha, 2018; Alves et al., 2020) developed during the final stage of mantle denudation and its exposure on the seafloor. In addition, sapphirine-bearing rocks are also exposed around the Lherz peridotite (Monchoux, 1970). The formation of the sapphirine-bearing mineral suite occurred at temperatures ∼600–650°C during an event constrained by U-Pb ages on rutile at ∼100 Ma, synchronous with the Pyrenean HT metamorphic event, that is, during active peridotite exhumation (Uzel et al., 2020).

The Gouffre Georges is a remarkable cave located on the eastern flank of the Mont Béas peak (1903 m a.s.l.), right to the west of the Lherz peridotite and was discovered in 1967 by J.P. Claria and G. Prince (Cordée Spéléologique du Languedoc). With a current depth of −726 m from its uppermost entrance, this is one of the deepest cavities in the Pyrenees (Figure 3). While the upper part of the cave formed in carbonate breccia and Mesozoic marbles, its central part (between the Tube entrance located at 1390 m a.s.l. and the Famine room located at −445 m from the main entrance) runs along the contact between the Lherz peridotite body and its carbonate cover. This access to the cave (hereafter referred to as "Tube entrance") is protected by a locked door for safety reasons. Details on the accessibility and morphology of the cave are in Sorriaux et al. (2019) and Nováková et al. (2022). This geological contact is exceptionally exposed in three dimensions over a distance >200 m. Up to now, this underground contact had never been described from a geological viewpoint.

3. Results

3.1. Field Data

Successive underground observations performed between the Tube entrance and the Salle de la Famine chamber have allowed the identification of the main lithofacies exposed along the cave walls, enabling the unraveling of their relationships and the construction of a geological cross-section of the Gouffre Georges (Figure 4). This entire cave section develops along the main peridotite/carbonate cover contact. This boundary

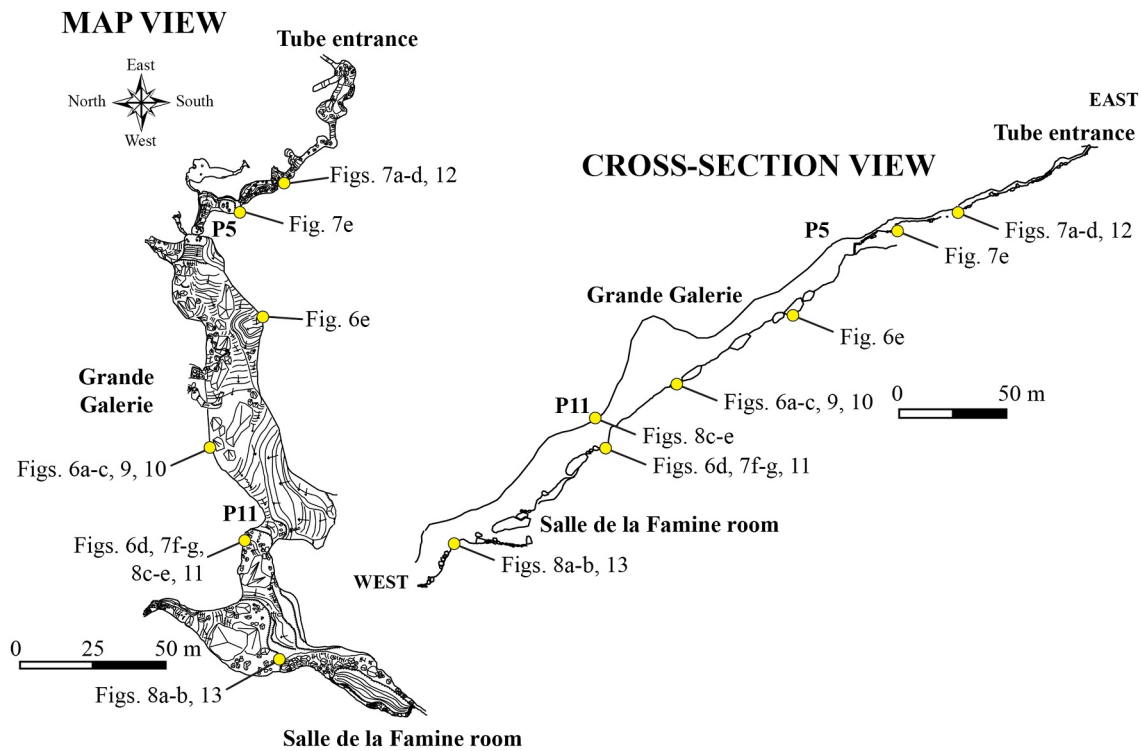

Figure 3. Topography of the Gouffre George between the Tube entrance and the Salle de la Famine room (modified after Sorriaux et al., 2019).

constantly dips toward the WNW with a low dip angle (~30°), with localized exceptions where the contact becomes steeper (~60–70°) at the level of the main pits (e.g., P5, P11). These steps correspond to normal fault scarps crosscutting the main low-angle contact. The walls on the sides of such pits commonly expose steeply-dipping slickensides with normal kinematics, and the main low-angle peridotite/carbonate contact is systematically downthrown toward the west (Figures 5d and 6d).

Five main lithofacies have been identified, listed from bottom to top: (a) peridotite, (b) carbonate vein/dikes intrusive within the uppermost part of the peridotite, (c) carbonate microbreccia on top of the peridotite, (d) coarse marble breccia and (e) marbles. The figures illustrating the rock exposures on the walls of the cave and referred to in this section (i.e., Figures 5–8) are also reported in the Supporting Information S1 without any line drawing or overrides.

The structurally deepest part of the section consists of relatively fresh brown to dark green peridotite, with a clearly visible websteritic layering marked by amphibole-bearing clinopyroxenite layers (Figure 5a). Toward the upper contact, the peridotite is progressively more penetratively serpentinized (mesh structure). Just below the contact, successive generations of centimeter-sized black veins of serpentinite crosscut the pervasively serpentinized peridotite (Figure 5b). In some places, the peridotite is black and almost completely serpentinized. Iddingsitization occur locally at the upper contact with the carbonate cover, where the peridotite displays a characteristic yellowish/ochre color (e.g., Figures 5f, 7b, and 7g) due to the formation of clays, Fe-oxides and hydroxides from olivine principally. Ophicalcites are commonly observed below the contact with the carbonate cover on a thickness of several decimeters (Figure 7a, upper right). They consist of a complex network of mm- to cm-sized calcite veins crosscutting the serpentinite veins (Figure 5c).

The uppermost part of the peridotite is deformed by anastomosed top-to-the-WNW extensional shear planes that define sigmoidal lenses of serpentinized peridotite (Figure 5d). Locally, these shear planes are intruded by NW-dipping to sub-horizontal decimetric carbonate veins (Figures 6a–6c). These veins are white to pinkish and mainly composed of mm-sized carbonate crystals. They also show a weak internal foliation sub-parallel to the contact with the host rock. The carbonate veins have remarkable lateral continuity (10–25 m) and are connected upward with the main contact between the peridotite and the overlying carbonate rocks (Figure 6a). The boundaries

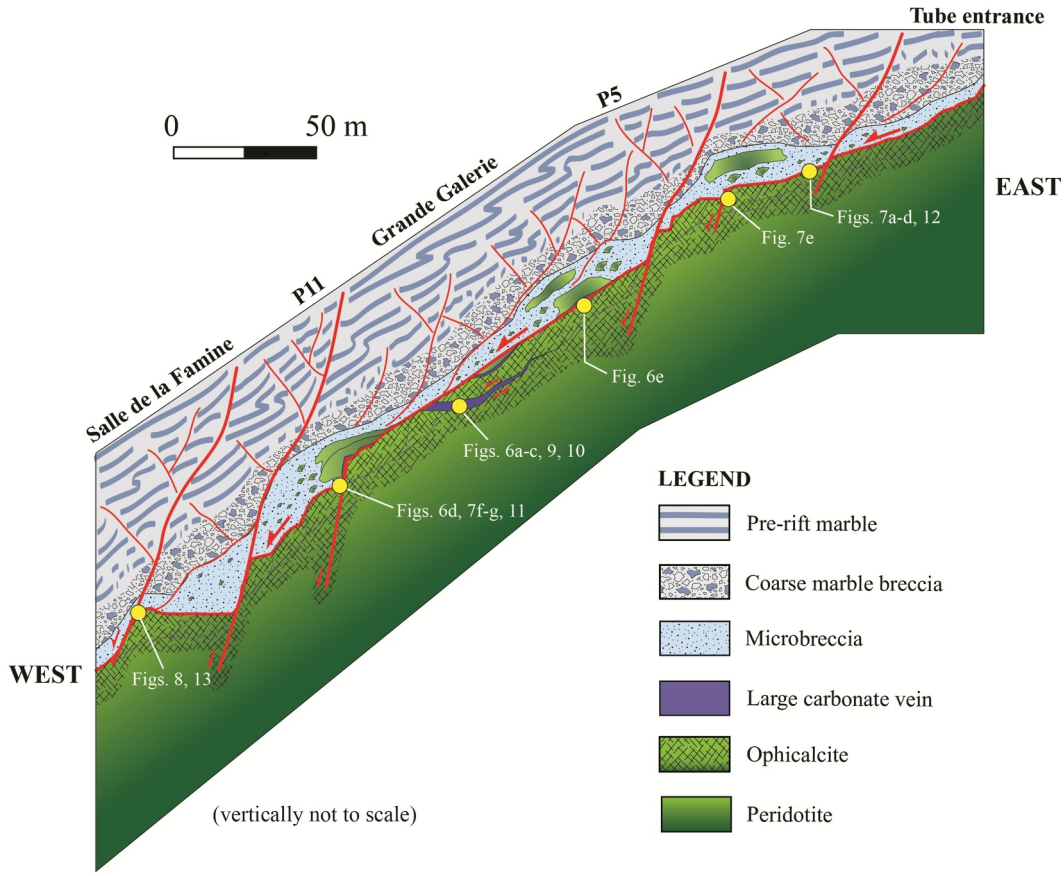

Figure 4. Schematic geologic cross section of the Gouffre Georges (vertically not to scale).

of the veins are often sheared, with shear planes (C-type) and R shear planes crosscutting the veins showing a normal top-to-the-NW sense of shear (Figures 6b and 6c). The veins locally branch into decimetric fine-grained green-to-gray foliated shear bands displaying an S-C fabric (*sensu* Berthé et al., 1979) compatible with a normal top-to-the-NW sense of shear (Figure 6c). Large remnants of boudinaged white carbonate veins can be found in the shear bands (Figure 6c).

The peridotite/microbreccia contact is slightly irregular at the centimeter scale, with a lobate cm-scale cauliflower shape in some places (Figure 7b), whereas elsewhere it consists of a sharp low-angle fault plane with dip-slip slickenside lineation (Figure 7c). The main contact is in turn cut by steeper NNE-SSW trending late normal faults (Figure 7), possibly representing R shear planes of a (locally) C-type main contact.

The overlying microbreccia is a pink-to-orange matrix-supported carbonate breccia, with mm to cm-sized ovoidal white marble grains (Figure 7d) and mm- to dm-sized irregular peridotite clasts (Figures 7b and 7c). This layer shows a foliation sub-parallel to the main contact (N025°, 49°W), marked by the alignment of the long axis of the larger ovoidal carbonate grains (Figures 4a and 4d). The microbreccia also embeds lens-shaped angular pluri-metric peridotite blocks (Figures 6e and 7e). This is clearly visible on the southern wall of the Grande Galerie and in a small room before the eastern access to the Grande Galerie. The base of these large peridotite blocks is sub-parallel to the main mantle/cover contact, and the foliation of the microbreccia wraps around them. All these blocks are variably serpentinized and display pervasive calcite veining (ophicalcites). The thickness of the microbreccia layer ranges from ∼1 m to less than 10 m.

Upwards, the microbreccia progressively transitions to a coarse breccia. This breccia is chaotic, poorly sorted, and mainly composed of white saccharoid marble and white/gray banded marble clasts. All these clasts derive from the base of the deformed pre-rift cover. The marble clasts are mm- to dm-sized, angular to sub-angular, and are embedded within a yellow, pink or orange carbonate matrix (Figures 8a and 8b). This type of breccia is

10.1029/2024TC008757

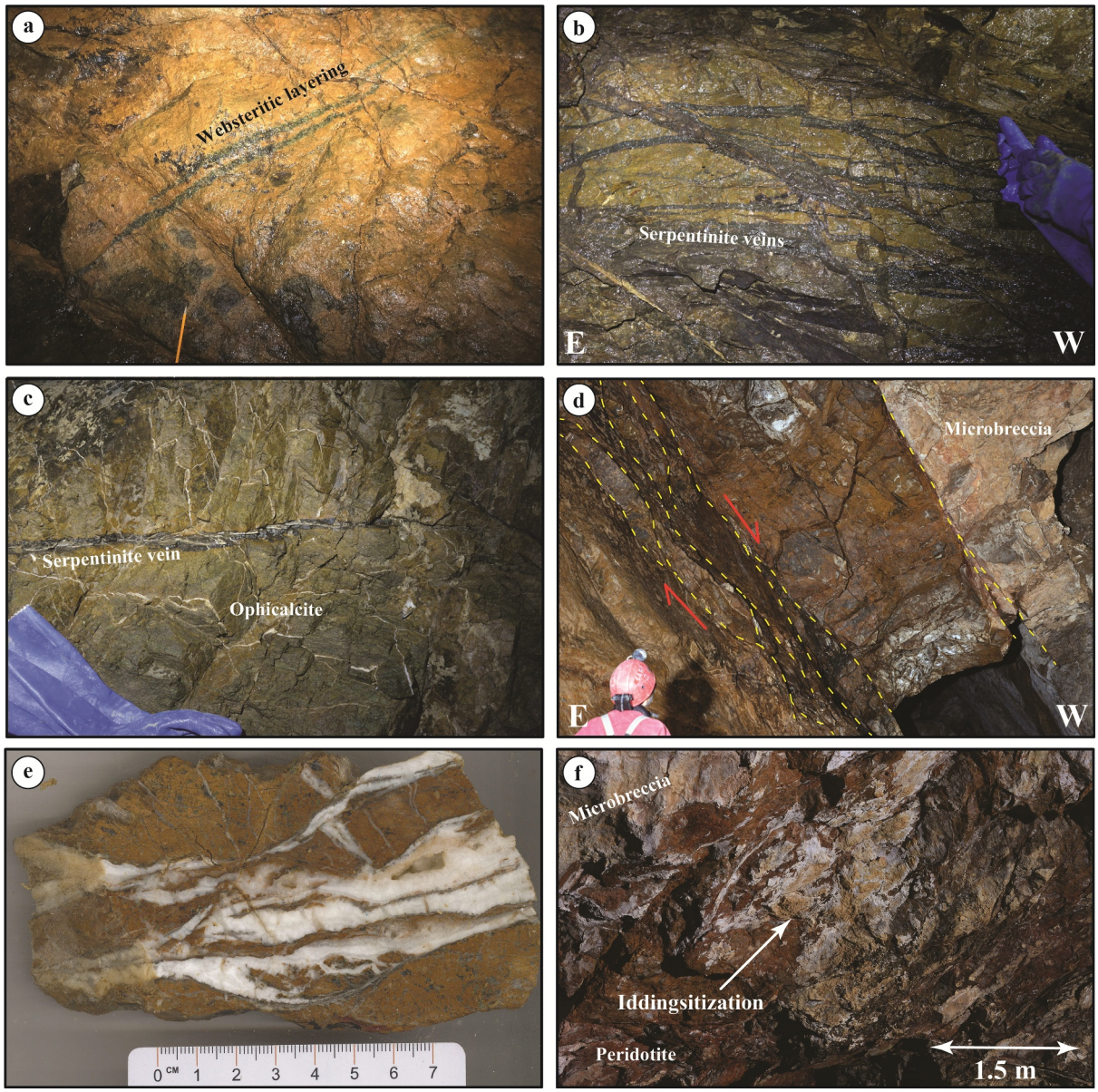

Figure 5. Some characteristic features of the peridotite outcropping in the Gouffre Georges. (a) Relatively fresh peridotite with its websteritic layering, lower part of the Grande Galerie. (b) Highly serpentinized peridotite with different generations of serpentinite veins, between the P11 pit and the Salle de la Famine room. (c) Serpentinized peridotite with serpentinite veins cross-cut by carbonate veins, middle part of the Grande Galerie. (d) Detail of the main contact showing sheared and cataclased peridotite; the top to the west sense of shear is deduced from the obliquity between different shear planes and is consistent with other kinematic indicators observed elsewhere on the same contact. (e) Hand specimen of peridotite crosscut by mm- to cm-thick veins of calcite of various orientations displaying evidence for crack-seal precipitation. (f) Uppermost part of the peridotite, below the contact with the carbonate microbreccia; note the characteristic yellowish/ochre color likely due to the presence of iddingsite.

extensively exposed at the surface, particularly around the Mont Béas peak, which is dominantly composed of this lithotype alternating with Jurassic marble lenses. Locally, the coarse breccia contains clasts of a former breccia, showing the reworking of an older breccia (Figure 8a), and some marble clasts show evidence of hydraulic fracturing (Figure 8b). This breccia does not display any sedimentary features, such as bedding, grading or sorting. The transition from the microbreccia to the marble breccia is irregular and diffuse. It is often challenging to trace a proper limit between these two facies. However, the coarse marble breccia does not host ultramafic clasts. Locally, the transition between the microbreccia and the overlying coarse breccia is marked by WNW dipping normal fault planes (Figure 7a).

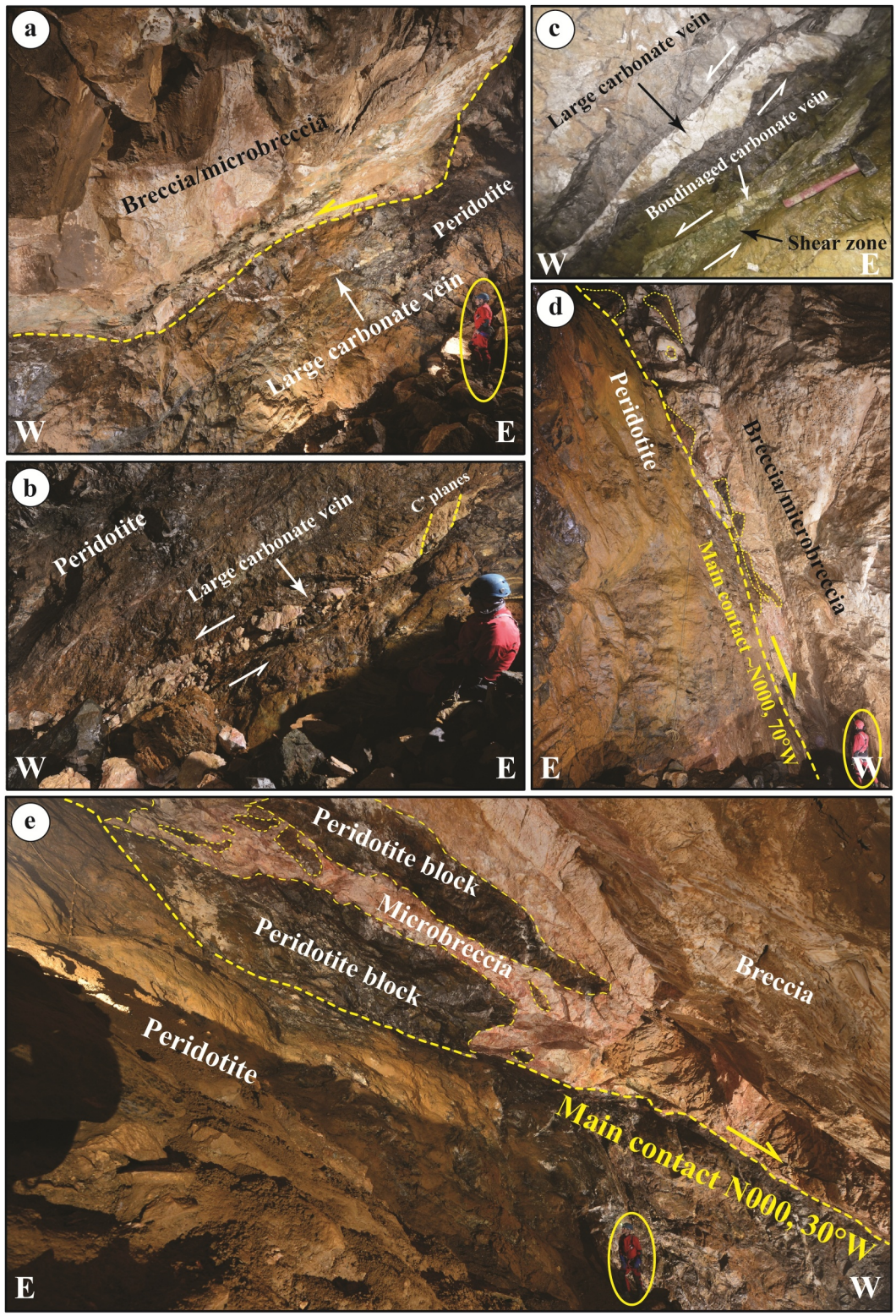

Figure 6.

The overlying marbles, representing the uppermost lithological unit exposed in the cave, mainly consist of banded white-and-gray/bluish marbles and massive white marbles. They have undergone syn-extensional ductile deformation expressed by an S_0/S_1 foliation that defines a characteristic banding, sub-parallel to the main peridotite/carbonate cover contact, and a WNW-ESE trending stretching lineation, more or less parallel to the long axis of the cave (Figure 8c). These marbles are mainly visible at the roof of the Grand Galerie and of the P11 pit and below the Famine room. Brittle shear planes and fractures cut the marbles, offset the banding, and isolate marble clasts (Figures 8d and 8e). The shear planes thicken and pass to pink microbreccia lenses, which locally develop between continuous layers of more or less cataclased marbles (Figure 8e). Locally, brecciated interlayers develop within the metamorphic foliation of the marbles. Conversely, more or less laterally continuous layers of foliated marbles can be observed within the mostly brecciated intervals. The volume of fractured/brecciated marbles increases downwards at the expense of the marble until and progressively transitions to the coarse marble breccia. In summary, the marbles display evidence of a progressive transition from a ductile (S_0/S_1 foliation) to a brittle (brecciation and cataclastic comminution) regime during stretching. In the cave, it is not clear if these marbles constitute a continuous layer overlying the coarse breccia unit, or if it represents large lenses preserved and enveloped by large volumes of breccia, as suggested by the relationship between marbles and coarse breccia observed in the Mont Béas peak right above the entrance of the cave.

3.2. Microscopic Description of the Main Lithofacies

Five main lithofacies have been distinguished in the Gouffre Georges and are, from bottom to top (Figure 4): (a) the peridotite (which may be more or less serpentinized), (b) the carbonate veins (emplaced within the uppermost part of the peridotite), (c) the microbreccia, (d) the coarse marble breccia, and (e) the Jurassic marbles. In the following, we describe their microscopic features.

3.2.1. Peridotite

In contrast to surface exposures, fresh peridotite occurs rarely in the cave. Relatively fresh outcrops where the magmatic microstructure of the peridotite are preserved between the P11 pit and the Salle de la Famine (Figure 5a). This fresh peridotite consists of olivine (Ol), clinopyroxene (Cpx), orthopyroxene (Opx), and spinel (Sp). Thin section observation shows various lithologies, lherzolite, harzburgite, websterite, spinel-pyroxenite, and amphibole-pyroxenite. The rock is marked by an HT foliation (shape preferred orientation of Ol, Opx and Cpx), with frequent boudinaged layers of pyroxenite. Lower temperature/higher shear stress cataclastic shears are common.

The peridotite is generally serpentinized, either in a pervasive way (mesh microtexture), or via black mm- to cm-thick serpentinite veins, or both (Figure 5b). The geometry and the microstructure of the serpentinite veins suggest a dynamic serpentinization with a sub-vertical extension evidenced by crack-seal vein texture, associated to a top to the west shearing, evidenced by the C-C'-like geometric organization of serpentinite veins (Figure 5b).

The two-three uppermost meters of the peridotite are marked by the presence of mm- to cm-thick veins of calcite of various orientations (Figure 5c), sometimes showing evidence of crack-seal precipitation (Figure 5e). These veinlets intersect or are injected into serpentine veins. In some place, at the contact with the carbonate rocks, the peridotite is intensively altered by iddingsitization (low T° oxydation and hydratation) (Figure 5f).

3.2.2. Carbonate Veins

Figure 9 shows the microstructure of the carbonate veins cutting through the peridotite. These rocks are mainly composed of mm-sized calcite dusty crystals with a polygonal granoblastic microstructure and triple junctions between calcite grains (Figures 9a and 9b), particularly in the innermost parts of the veins. Other common

Figure 6. Large carbonate veins in the lower part of the Grande Galerie (a–c) and contact between the peridotite and the carbonate cover (d–e) (see Figure 3 for location). (a) General view of the main peridotite/carbonate cover contact, with a large carbonate vein crosscutting the upper part of the lherzolite. (b) Close view of a large carbonate vein crosscutting the lherzolite; note its boudinaged attitude and extensional C' plane crosscutting it. (c) Relationship between two subparallel large carbonate veins within the peridotite; the upper one is less deformed, while the lower one is stretched and boudinaged within a greenish shear zone. (d) Steep west-dipping main peridotite/carbonate cover contact on the southern side of the P11 pit; note the increase in alteration of the ultramafic rocks approaching toward the main contact. (e) Main contact between the peridotite and the microbreccia with peridotite lenses on the southern side of the upper part of the Grande Galerie; note the variable size of the peridotite blocks embedded within the pinkish microbreccia. Photos a-b and d-e by V. Guinot.

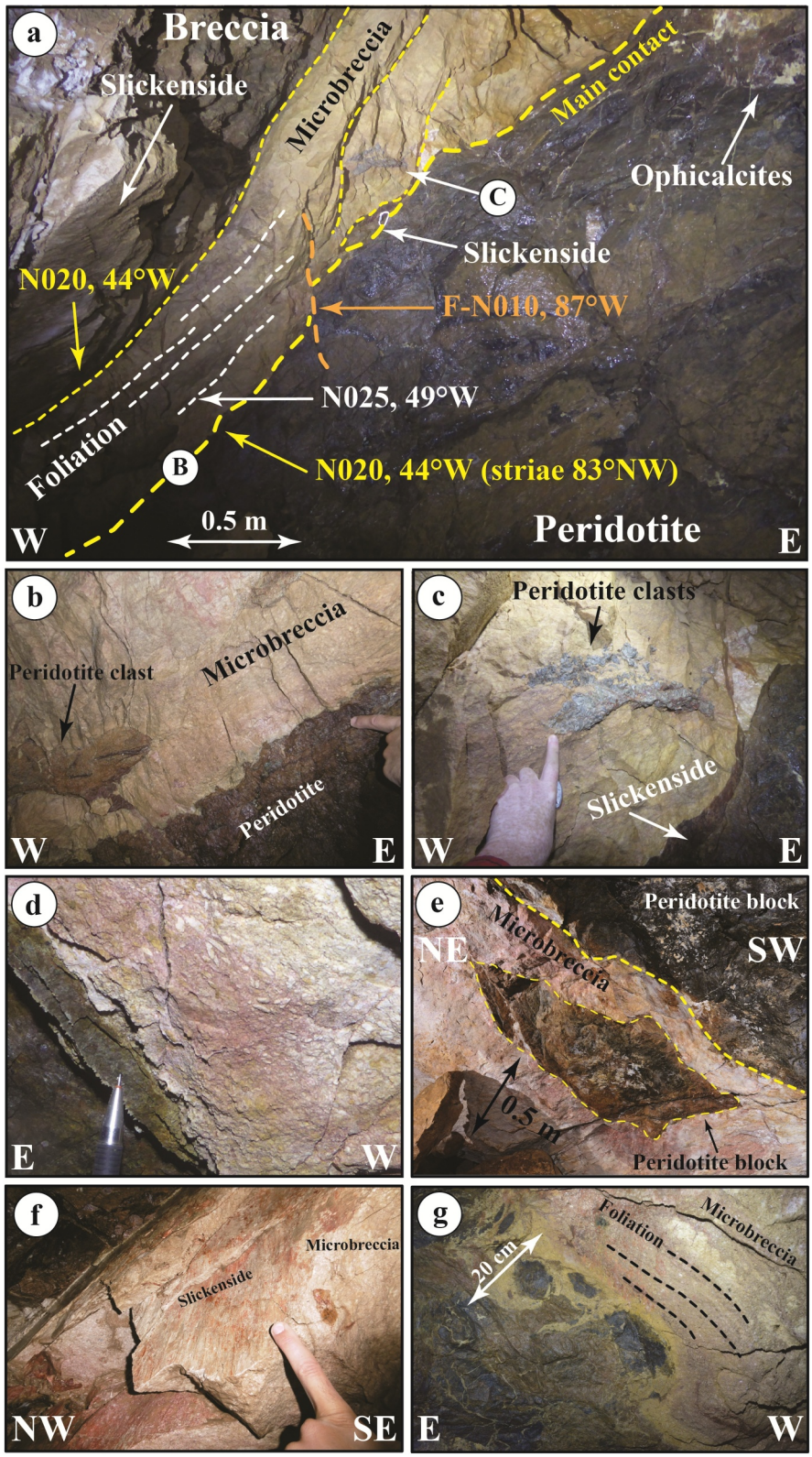

Figure 7.

minerals are isolated colorless micas (phlogopite) (Figure 9c), euhedral colorless amphiboles (pargasite) (Figure 9b) and pyrite. Some rare, altered remnants of clinopyroxene (diopside), likely derived from the ultramafic host rock, are present close to the vein margins. Calcite grains commonly display two sets of thin twins (Figures 9a, 9b, 9c, and 9e), with minor presence of thicker tabular twins (Figures 9d and 9f). A distinct microstructure of these rocks is the presence of small-sized (up to ∼100 μm) dolomite exsolution blebs in spherulae and vermicules developed within and across the larger calcite grains to form myrmekite-like exsolution microstructures (Figures 9b, 9c, 9d, and 9f). Locally, and more frequently toward the most external parts of the veins, calcite shows evidence of different degrees of recrystallization (Figures 9e and 9f). The more or less recrystallized intervals are aligned in a direction sub-parallel with the veins boundaries and is probably the microscopic expression of the weak internal foliation observed in the carbonate veins at the outcrop scale. In some cases, calcite recrystallization is minor and results in clean calcite rims growing around dusty calcite cores (Figure 9e). In other cases, recrystallization is more intense and results in corridors of calcite grains with much more variable grainsize due to progressive sub-grains formation from the larger calcite crystals (Figure 9f). This last microfacies is comparable with the cataclastic microstructure observed in the microbreccia (see following Section 3.2.3).

The microscopic facies of the sheared contacts between the carbonate veins and the peridotite is rather complex (Figure 10). At the sheared outermost boundaries of the calcite veins, large calcite grains appear to be highly fragmented by brittle fracturing (Figure 10a). The finer grained intervals in proximity of the ultramafic host rock often show evidence of non-coaxial shearing and are mainly composed of small calcite grains and fractured remnants of pargasite crystals in association with larger chlorite fishes (Figure 10b). Where the boudinaged elements of the calcite veins are found within the green fine-grained shear bands (see Figure 6c), some domains have a mineralogical assemblage analog to that of the calcite veins, consisting in mostly fine-grained calcite + phlogopite + pargasite (Figure 10e), whereas some other domains belong to the altered peridotite and mainly consist in mosaic-like serpentine domains separated by a complex network of thin calcite veins (Figure 10d). In this context, small tourmaline crystals can be found in association with calcite and chlorite (Figure 10c). In the portions of the fine-grained shear bands where macroscopic elements of the white carbonate veins are lacking (see for example the lower part of Figure 6c), large calcite crystals are absent at the microscopic scale (Figures 10f–10h). Here, some poorly preserved minerals of the original assemblage of the peridotite can be locally observed and consist in dark-green Cr-spinel (Figure 10g) and clinopyroxene (diopside) porphyroclasts (Figure 10h). Fine-grained tremolite fibers can be found in the weathered remnants of ultramafic clasts (Figure 10g). These domains are characterized by the presence of large chlorite crystals (Figures 10f–10h) and by fractured (cataclastic) pargasite, calcite and dolomite grains (Figures 10f and 10g).

3.2.3. Microbreccia

In thin sections, the microbreccia is composed of a sub-millimetric calcite matrix, with grains showing variable grainsize and sharp straight boundaries, that support larger (mm-sized) calcite grains and large (mm- to cm-sized) peridotite clasts (Figures 11 and 12). Stylolites are common in the microbreccia (e.g., Figure 11d). Larger carbonate clasts (few mm to cm) are typically elongated (ovoid), with their long axis parallel to the foliation. They often consist of remnants of single large calcite crystals or aggregates of these crystals (Figures 11a and 11b). They have overall irregular boundaries, but with angular outlines and straight sharp contacts with the finer grains of the matrix (Figures 11b–11e). The larger calcite grains of the matrix (∼200–300 μm) usually display a dusty core surrounded by a x10 μm thick clear rim (Figures 11f and 11g). Some of these large calcite grains preserve

Figure 7. Some characteristic features of the microbreccia and the outcrop scale and of its relationships with the peridotite (see Figure 3 for location). (a) Main contact between peridotite (below) and a carbonate microbreccia bearing large peridotite blocks (above) with representation of the main structural features. Note that both the contacts between the peridotite and the microbreccia and between the microbreccia are mainly represented by sharp fault planes with dip-slip striae, and are cut by steeper normal faults. Note also ophicalcites below the main peridorite/carbonate cover contact (upper right corner) and serpentinization of the ultramafic rocks close to the contact. (b) Detail of the main peridotite/cover contact (see location in panel a) where it appears as slightly irregular with a lobate shape. (c) Detail of the main peridotite/cover contact (see location in panel a) where it appears as a sharp fault plane with dip-slip slickenside lineation. (d) Typical facies of the microbreccia with mm-sized ovoidal white marble clasts. (e) Metric peridotite block embedded within the foliated microbreccia below a decametric peridotite lens. (f) Detail of a striated fault plain in the microbreccia with dip-slip slickenside lineation (top-to-the-WNW). (g) Detail of the main contact between the main peridotite body and the overlying carbonate microbreccia with a lobate geometry; note the shape of the characteristic yellowish/greenish altered zone of the underlying peridotite suggesting some kind of percolation/infiltration.

10.1029/2024TC008757

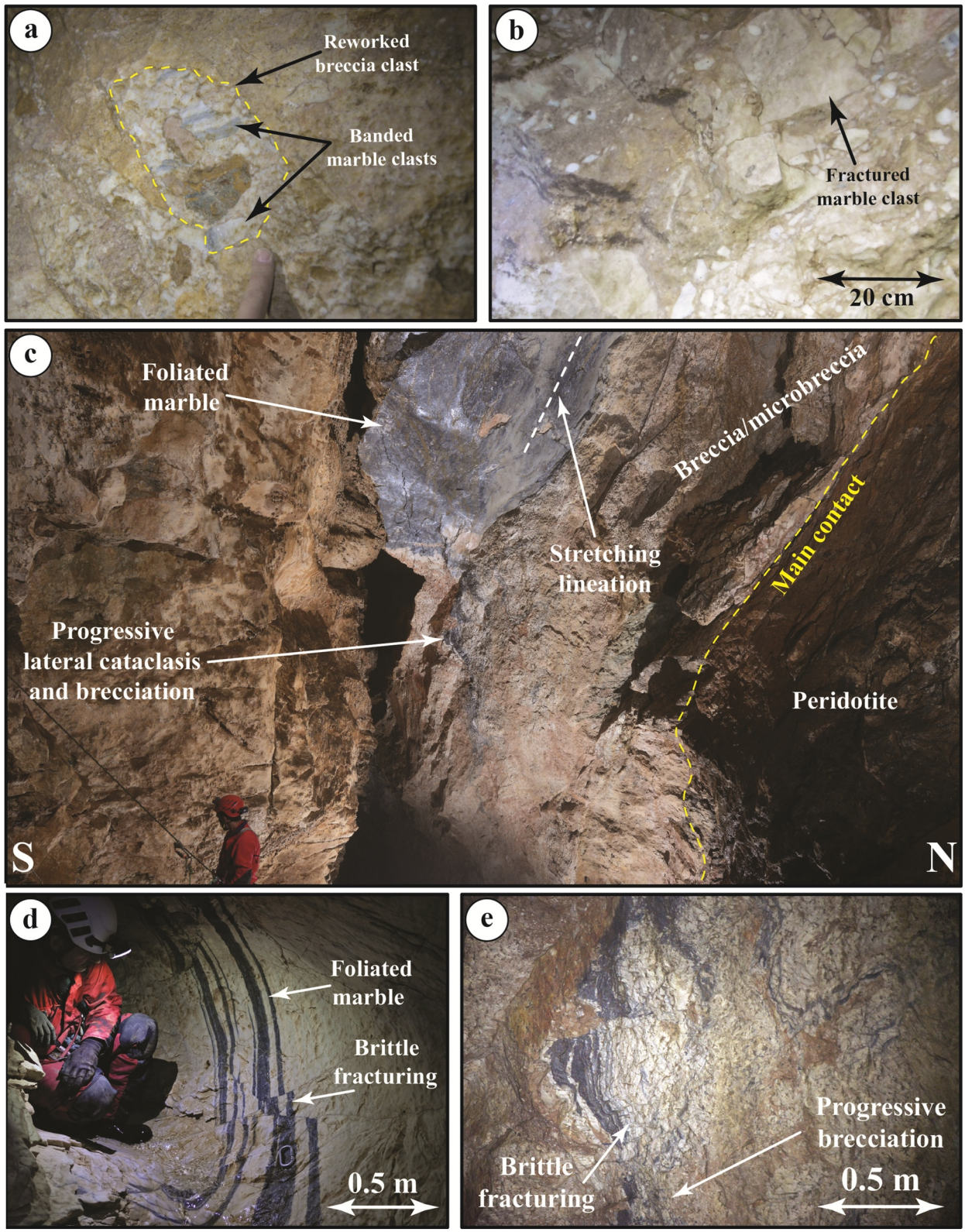

Figure 8.

traces of dolomite exsolution blebs in spherulae and vermicules, such as those observed in the large carbonate veins (see Section 3.2.2; Figure 9d).

In general, at the microscopic scale, these rocks seem to display an overall cataclastic fabric, with the progressive development of a cataclastic matrix formed by calcite subgrains progressively crushed at the expense of larger calcite porphyroclasts (Figures 11a–11e). A cataclastic foliation is defined by alignments of boudinaged large (mm-sized) ovoidal calcite grains surrounded by a fine-grained cataclastic calcite matrix (Figures 11a–11c). Progressive cataclastic disruption of the larger calcite crystals by grain border comminution to produce fine-grained matrix is testified by: (a) their jigsaw boundaries, with the cataclastic subgrains alimenting the inter-boudins (Figure 11b); (b) brittle fracturing crosscutting and offsetting sets of twins (Figures 11b-11c, and 11e); (c) crumbled brittle texture preserved in some of the larger grains (Figure 11e). In the larger polycrystalline calcite aggregates, incipient subgrain formation at grain boundaries is testified by jigsaw irregular contacts between the crystals (Figure 11d). Locally, and particularly where the cataclastic matrix is less abundant, large calcite crystals show evidence for pre-brittle deformation recrystallization resulting in dusty cored grains surrounded by thin clear calcite rims (Figures 11f and 11g), as locally observed also in the large carbonate veins (see Section 3.2.2; Figure 9e). In general, twin sets in the large calcite grains vary from thin to thick tabular twins (Figures 11c–11e). Other components of the mineralogical assemblage are rare, altered remnants of euhedral colorless amphibole (pargasite) (Figure 11g) and fragmented remnants of light green/blue (Cr-free, Al-rich) spinel surrounded by clear calcite rims (Figures 11e and 11g).

The peridotite clasts within the microbreccia are almost completely altered and are composed of scarce remnants of clinopyroxene (Cr-diopside), orthopyroxene (bronzite?) and dark green Cr-spinel surrounded by a complex fine-grained matrix mainly made of calcite, serpentine, chlorite and Fe-oxide, with minor fibrous tremolite (Figure 12a). The calcite/serpentine matrix locally shows a mesh texture that is often sheared to form bright sigmoidal calcite domains surrounded by thin wraps of dark fine-grained serpentine (Figure 12a). The transition between the larger peridotite clasts and the calcite matrix of the microbreccia is often characterized by relatively large fibers of tremolite and smaller grains of calcite and chlorite (Figure 12b). Peridotite clasts may be cut by millimetric calcite veins to form ophicalcites. Such veins have polycrystalline texture, with relatively well-preserved remnants of mafic minerals (such as pyroxene or dark-green Cr-spinel) surrounded by a cement of calcite with polygonal granoblastic texture (Figures 12c and 12d).

3.2.4. Coarse Marble Breccia

At the thin section scale, the coarse marble breccia perfectly matches its aspect at the outcrop scale (Figure 13). The breccia appears to be composed of large (mm- to cm-sized) clasts supported by a finer grained matrix (Figures 13a–13d). There are three main types of large clasts: (a) ductilely stretched marbles showing evidence for non-coaxial shearing (Figures 13b and 13c), which are akin to the Liassic banded marbles known at the base of the Jurassic series in the region (*marbres rubanés*; Ternet et al., 1997); (b) crumbled marble clasts (Figures 13a and 13d), which might be derived either from the marbles or the microbreccia/carbonate veins; (c) carbonate breccia clasts (Figure 13a), which might be either derived from reworking of the microbreccia commonly exposed above the main contact with the peridotite or from polyphase tectonic brecciation leading to tectonic reworking of the marble breccia. In general, alike at the outcrop scale, no clear evidence of peridotite clasts has been observed in the coarse marble breccia in thin section.

Alike at the outcrop scale, ductilely stretched marbles show evidence for a progressive transition from ductile to brittle regime during stretching, as suggested by crack-filling cataclastic matrix within the fractured marble clasts (Figure 13c). Locally, where the matrix is particularly fine grained, the marble breccia shows evidence for cataclastic flow (Figure 13d). Dispersed within the fine-grained matrix, some inclusion-rich bipyramidal quartz crystals occur (Figures 13e and 13f). In the Pyrenean region, similar quartz grains are commonly

Figure 8. Some characteristic features of the coarse marble breccia and of the pre-rift HT/LP marbles outcropping in the Gouffre Georges. (a) Marble breccia clast reworked and cannibalized in the coarse breccia. (b) Coarse marble breccia displaying high variability of the matrix/clasts ratio. (c) View toward the roof of the Grande Galerie near the P11 pit. Note the gray banded marbles with well-marked stretching lineation (white dashed line), and their progressive cataclasis and brecciation toward the main contact. Photo by V. Guinot. (d) The banded marbles in the deep part of the cave. Photo by P. Baby. (e) Progressive transition from fractured/faulted banded marbles and brecciated marbles to form the coarse marble breccia.

10.1029/2024TC008757

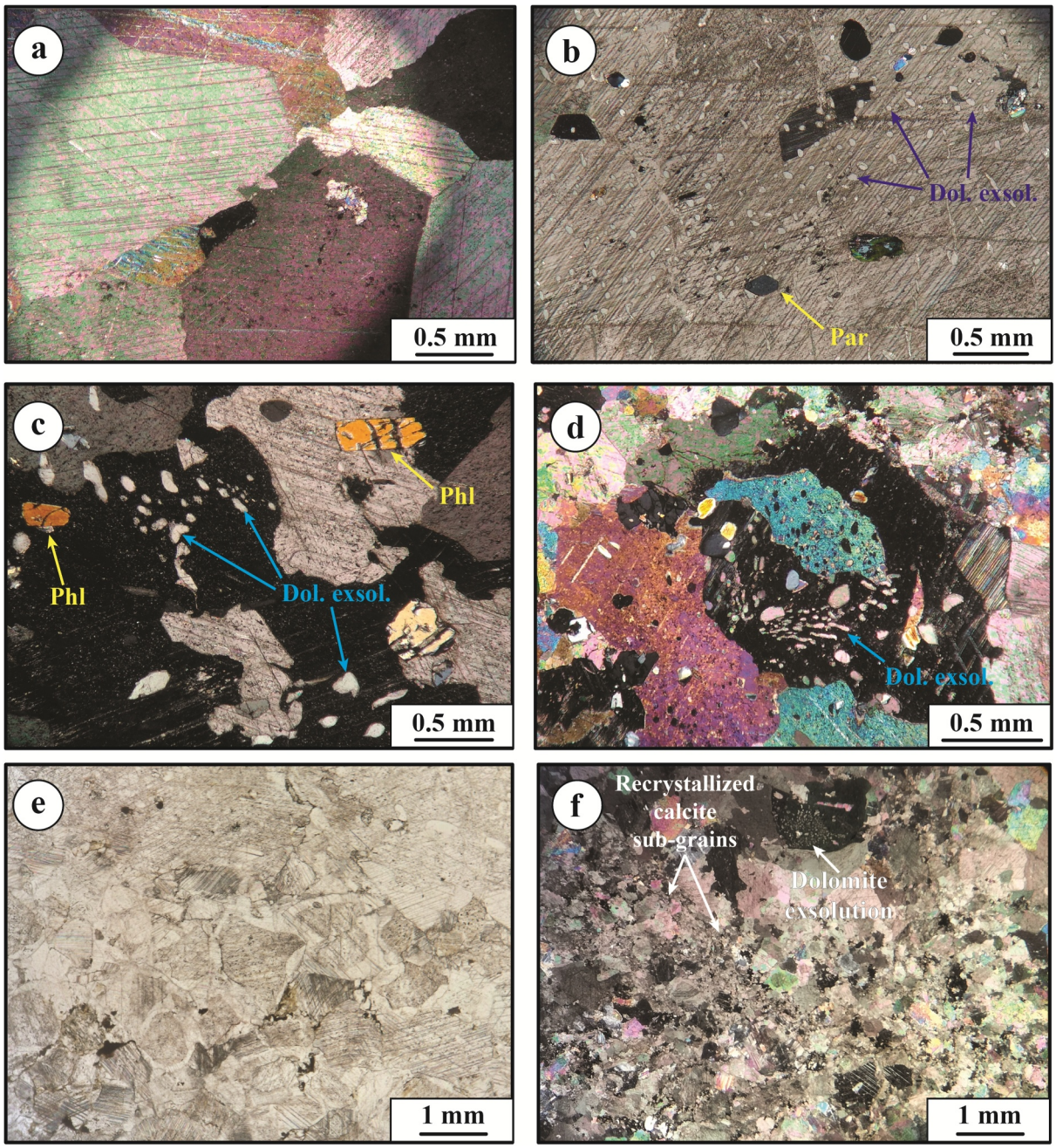

Figure 9. Microscopic facies of the large carbonate veins intruding the serpentinized peridotite. (a) Large calcite with polygonal granoblastic texture, triple junctions between grains and displaying two sets of thin twins (crossed polars). (b) Large calcite grains displaying two sets of clearly visible thin twins with small-sized dolomite exsolution blebs in spherulae; note also an euhedral pargasite crystal in the lower part of the picture (plane-polarized light). (c) Large calcite crystals with small-sized dolomite exsolution blebs in spherulae and phlogopite crystals (crossed polars). (d) Typical myrmekite-like texture of small-sized dolomite exsolution blebs in spherulae and vermicules developing in larger calcite grains; note the coexistence of both thin twins and thicker tabular twins in calcite (crossed polars). (e) Evidence for recrystallization in calcite consisting in clean calcite rims growing around dusty calcite cores (plane-polarized light). (f) More pronounced recrystallization in calcite resulting in corridors of calcite grains with very variable grainsize due to progressive sub-grains formation from the larger calcite crystals; note myrmekite-like texture of small-sized dolomite exsolution blebs in a large calcite crystal in the upper part of the picture (crossed polars).

observed in Upper Triassic-Lower Liassic evaporites, at the very base of the Jurassic pre-rift sedimentary cover (e.g., Beaugey, 1889; Calvet & Lucas, 2001). In general, the matrix of the coarse breccia shows no micro-structural evidence for recrystallization.

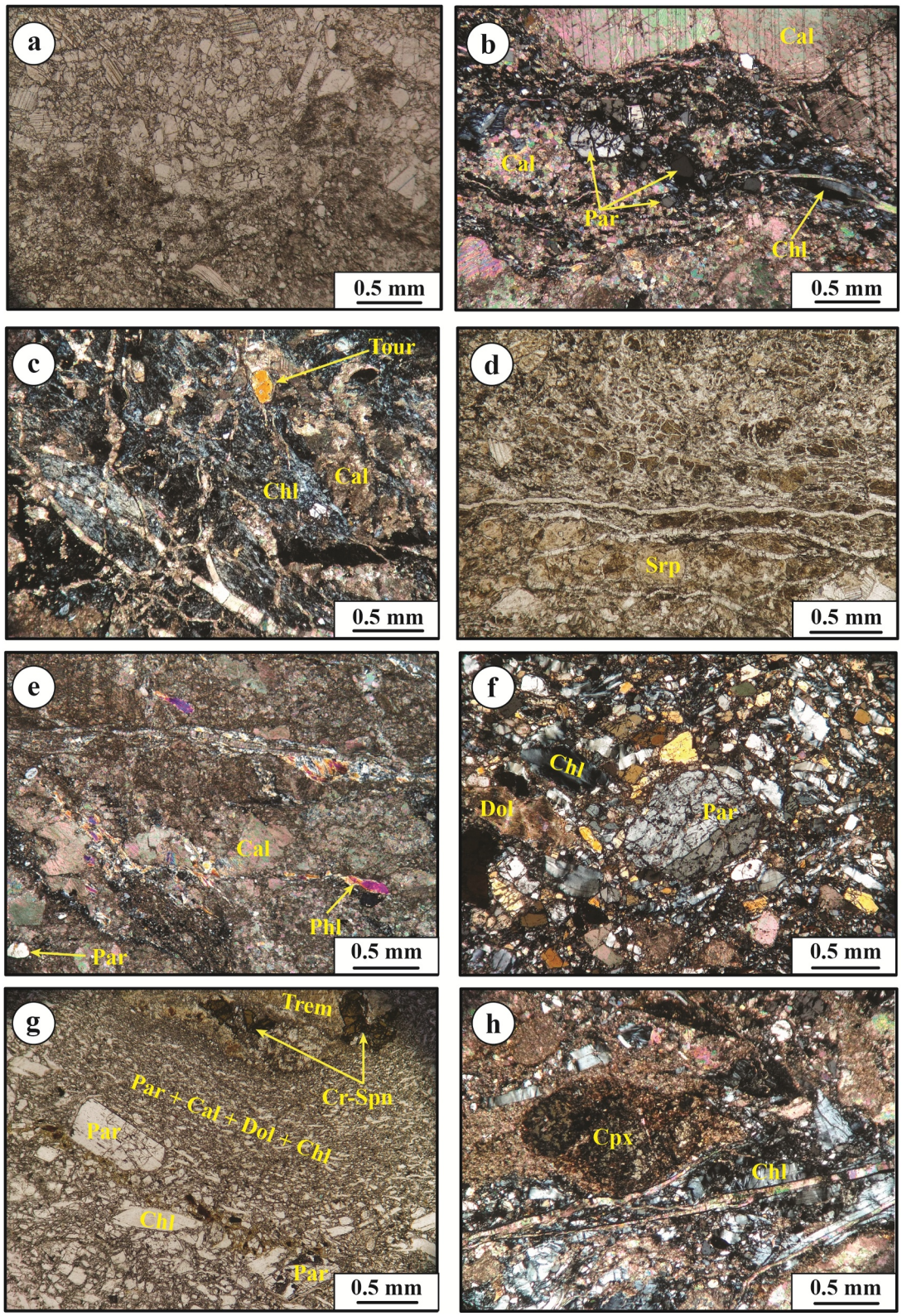

Figure 10.

4. Data Analysis

4.1. Lithofacies Interpretation

In the following section, we discuss the origin of the large carbonate veins, the microbreccia and the coarse marble breccia. Unraveling their genesis and significance is crucial to propose a tectonic model for the Gouffre Georges peridotite/marble sheared contact.

4.1.1. Large Carbonate Veins

The veins are characterized by five main characteristics: (a) up to decimetric thickness and decametric length; (b) planar geometry and contacts suggesting formation associated to brittle fracturing in the host-rock (dike and dikelet geometry); (c) layered internal structure; (d) HT metamorphic mineralogy (phlogopite, pargasite); (e) HT microstructure, with dolomite exsolution in calcite (similar to those described in high-grade marbles and carbonatites; Puustinen, 1974; Zaitsev and Polezhaeva, 1994; Letargo et al., 1995; Mizuochi et al., 2010; Chakhmouradian et al., 2016 and references therein), and variable calcite recrystallization.

Considered together, these features strongly suggest injection of a hot and low viscosity material in the very upper part of the peridotite. Based on these features, we propose three alternative hypotheses:

1. These veins formed from crystallized melts produced by partial melting at the base of the pre-rift carbonates during mantle exhumation. These melts could have flowed in the brittle extensional structures affecting the peridotite due to the extremely low viscosity of carbonate melts (Dobson et al., 1996). Thus, according to this interpretation, the large carbonate veins would represent pseudo-carbonatite dikes (*sensu* Mitchell, 2005).

Partial melting temperature of carbonates at low crustal pressure conditions may occur at temperatures as low as ~600–675°C (Durand et al., 2015; Floess et al., 2015; Gittins & Tuttle, 1964; Wyllie and Tuttle, 1960). These values are similar to the maximum temperatures reached at the base of the pre-rift cover during the Cretaceous syn-rift episode (e.g., Clerc et al., 2015; Golberg & Leyreloup, 1990). Indeed, the base of the Early Cretaceous sedimentary basin reached temperatures from 200 to 630°C in the Basque-Cantabrian Basin (i.e., *Nappes des Marbres* unit; Lamare, 1936; Martínez-Torres, 1989; Mendia and Ibarguchi, 1991; Ducoux et al., 2019), to 350–600°C in the Mauléon Basin core (Corre, 2017; Saspiturry et al., 2020b), to 400–630°C in the Internal Metamorphic Zone (Chelalou et al., 2016; Ducoux et al., 2021; Lagabrielle et al., 2016) including the Aulus (Clerc, 2012; Clerc et al., 2015) and Boucheville basin (Boulvais, 2016; Chelalou et al., 2016). Additionally, impurities found in carbonates, along with the presence of elements like fluorine and others commonly found in evaporites (such as phosphorus or chlorine), can lower the melting point of carbonates. This makes the melting process easier and occurs at lower temperatures (Lentz, 1999). The lower part of the Mesozoic sedimentary series of the Aulus Basin is known to be composed of impure carbonates, with some metapelite interlayers (Ternet et al., 1997), and the base of this series is composed of the originally thick Upper Triassic-Lower Liassic evaporitic series (Keuper; Biteau et al., 2006; Calvet & Lucas, 2001; Canérot et al., 2005; Curnelle, 1983). The implication of hyper-saline brines derived from the Keuper evaporitic series in the chemical reactions occurring along the mantle/cover detachment during the Cretaceous rifting has been largely demonstrated in close proximity with the Lherz ultramafic body (Uzel et al., 2020) and in other areas of the North Pyrenean Zone and of the Basque-Cantabrian region (Corre et al., 2018; DeFelipe et al., 2017; Lagabrielle et al., 2019a, 2019b; Salardon et al., 2017; Nteme Mukonzo et al., 2021). The presence of evaporite-derived fluids circulating within the

Figure 10. Microscopic facies of the sheared contacts between the large carbonate veins and the ultramafic host rock. (a) At the sheared outermost boundary of a large calcite vein, large calcite grains appear to be highly crumbled by brittle fracturing (plane-polarized light). (b) Finer grained interval of a large calcite vein, in proximity of the ultramafic host rock, mainly composed of small calcite grains and fractured remnants of pargasite crystals in association with larger chlorite fishes (crossed polars). (c) Small tourmaline crystal (in yellow) found in association with calcite and chlorite at the transition between a boudinaged calcite vein and the sheared green/gray fine-grained matrix of a shear zone in the ultramafic rocks (crossed polars). (d) Mosaic-like serpentine domains separated by a complex network of thin calcite veins in the green/gray fine-grained matrix of a shear zone in the ultramafic rocks hosting boudinaged remnants of a large calcite vein (plane-polarized light). (e) Mineralogical assemblage of a boudinaged remnant of a large calcite vein within a shear zone composed by polysized calcite grains, phlogopite and pargasite (crossed polars). (f) Portion of the green fine-grained matrix of a shear zone within the ultramafic rocks composed by large chlorite grains and polysized fractured remnants of pargasite and dolomite (crossed polars). (g) Portion of the green fine-grained matrix of a shear zone within the ultramafic rocks composed of polysized pargasite, chlorite, dolomite and calcite and with remnants of dark-green Cr-spinel surrounded by fine-grained tremolite (plane-polarized light). (h) Portion of the green fine-grained matrix of a shear zone within the ultramafic rocks mainly composed of carbonate and large chlorite crystals and with a large weathered clinopyroxene (diopside) porphyroclast (crossed polars).

10.1029/2024TC008757

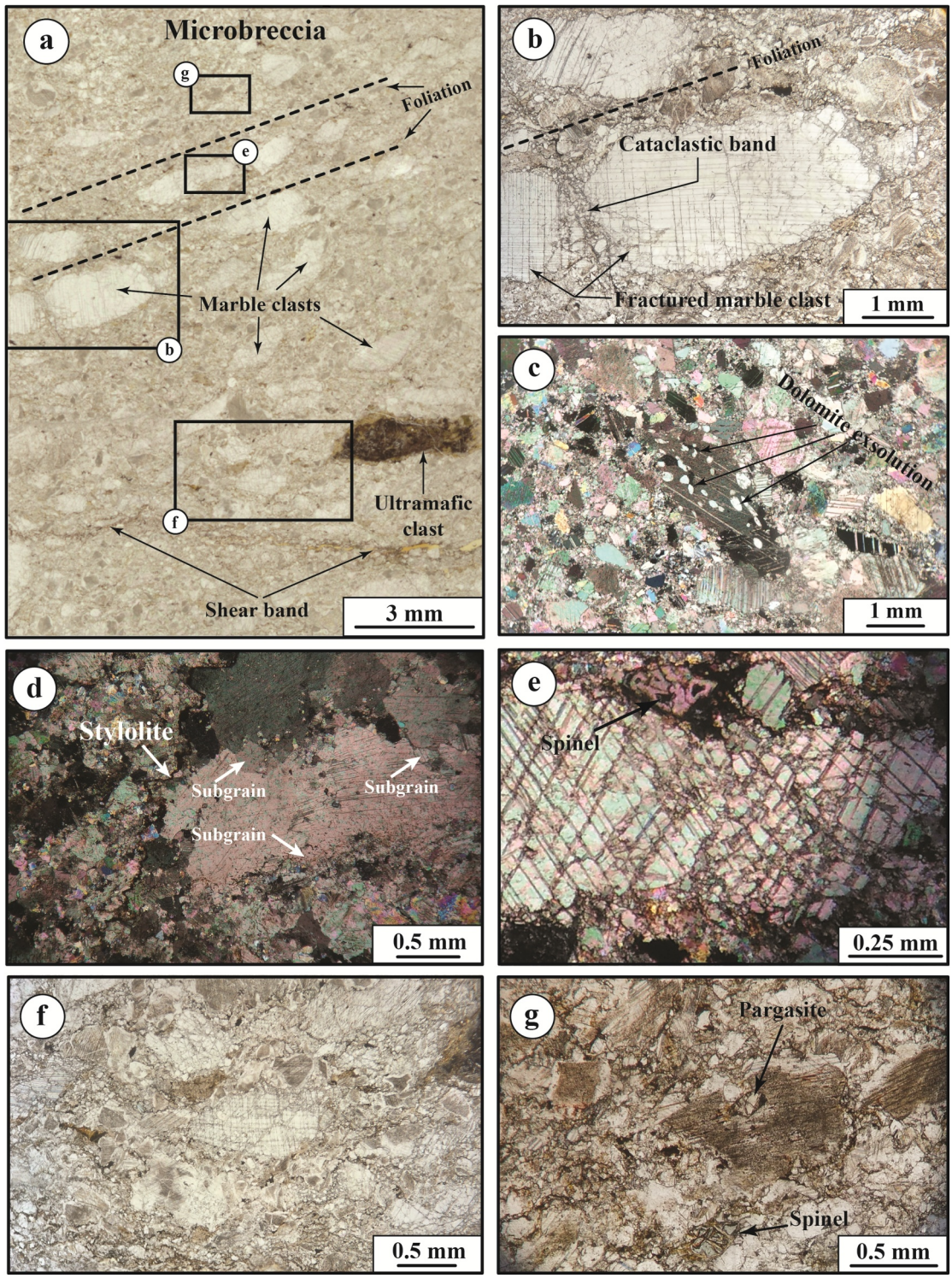

Figure 11.

mantle/cover detachment is also suggested by the occurrence of boron-bearing minerals such as tourmaline in the metasomatized sheared contacts between the large carbonate veins and the ultramafic host rock documented in this study (see Figures 10c and Section 3.2.2). Thus, the pre-rift salt could have acted as a catalyst allowing to achieve the thermal and chemical conditions required for melting at the base of the pre-rift carbonate cover.

Carbonate melts are thought to be very corrosive for silicate host rocks and might digest some silicate minerals (e.g., Hode Vuorinen & Skelton, 2004; Kruk & Sokol, 2022). This would result in a mixed silicate-carbonate magma, which could produce during crystallization minerals such as phlogopite or pargasite, in addition to carbonate minerals. The fact that the observed pargasite crystals are generally euhedral and often bear calcite inclusions is suggestive for rapid crystal growth in a very low viscosity medium, as it would be the case for pseudo-carbonatitic melts.

Carbonate partial melting is thought to liberate large amounts of CO_2 by decarbonation of carbonate minerals (e.g., Persikov and Bukhtiyarov, 2004; Ganino & Arndt, 2009; Ganino et al., 2013; Durand et al., 2015). Interaction of such fluids with ultramafic rocks can result in carbonation of mafic minerals such as olivine or clinopyroxene (e.g., Kelemen & Matter, 2008; Kelemen et al., 2018; Menzel et al., 2018). This would be consistent with observation of carbonated mesh textures in the sheared ultramafic rocks at the boundaries of the large carbonate veins (see Figures 12a and Section 3.2.3). The migration of such fluids within the overlying carbonates/marbles might have produced intense hydraulic fracturing, and thus be responsible for the formation of at least some of the marble breccia largely known in outcrop in the Aulus Basin (and in the North Pyrenean Zone in general), as suggested by previous studies (Dauteuil et al., 1987; Golberg, 1987; Minnigh et al., 1980; Ternet et al., 1997).

2. a second interpretation is that the formation of the veins resulted from carbonate-rich metamorphic fluids produced during an HT hydrothermal event associated to the HT-LP North-Pyrenean metamorphism. However, in a carbonate dominated environment that experienced HT conditions, it is not easy to distinguish between fluids derived from partial melting of carbonate rocks and carbonate-rich hydrothermal fluids extracted during HT metasomatic processes (see for example Durand et al., 2015; Yaxley et al., 2022 and references therein). For this reason, this kind of carbonate rocks are often referred to in the literature as vein/dikes.
3. one last alternative interpretation could be that these carbonate veins are the result of hyper-ductile marble flow within the extensional structures due to the extreme plasticity of calcite at high thermal conditions, such as those known in the region for the syn-rift HT-LP North Pyrenean metamorphism (Albarede & Michard-Vitrac, 1978; Golberg & Leyreloup, 1990; Golberg & Maluski, 1988; Montigny et al., 1986). However, the carbonate veins are clearly distinct from the HT-LP marbles laying above the contact with the peridotite, both from a macroscopic and microscopic point of view.

In summary, the emplacement of the large carbonate veins (dikes?) within the brittle extensional structures of the Lherz peridotite most likely represents a phase of high temperature at the base of the pre-rift sedimentary cover during Cretaceous extension.

4.1.2. Microbreccia

The mineralogical composition of the microbreccia is broadly analog to that of the large carbonate veins, which mainly consists in calcite, phlogopite, pargasite and altered peridotite clasts. The only notable difference is the

Figure 11. Microscopic facies of the microbreccia. (a) General aspect of the microbreccia in thin section. Note the overall cataclastic fabric, with the progressive development of a cataclastic matrix formed by calcite subgrains progressively crushed after larger calcite porphyroclasts (natural light). (b) Detail of large calcite grains affected by boudinage and cataclasis. The large calcite grains have overall irregular boundaries, with angular outlines and straight sharp contacts with the finer grains of the matrix. Note the jigsaw boundaries of the large calcite grains, with the cataclastic subgrains filling inter-boudin space and brittle fracturing crosscutting and offsetting sets of twins (plane-polarized light). (c) Example of a large calcite grain displaying dolomite exsolution blebs in spherulae and vericules such as those observed in the large carbonate veins (see Figure 9; crossed polars). (d) Example of a large polycrystalline calcite aggregate (right side of the picture), with incipient subgrain formation at grain boundaries testified by jigsaw irregular contacts between the crystals (crossed polars). (e) Example of crumbled brittle texture preserved in a large calcite grain. Note also the presence of small, fragmented remnants of Cr-free Al-rich blue spinel surrounded by a clear calcite rim (crossed polars). (f) Example of a portion of the microbreccia where the cataclastic matrix is less abundant. Large calcite crystals show evidence for pre-brittle recrystallization resulting in dusty cored grains surrounded by thin clear calcite rims (plane-polarized light). (g) Example of other components of the mineralogical assemblage, such as altered remnants of euhedral colorless amphibole (pargasite) and fragmented remnants of light green/blue (Cr-free, Al-rich) spinel surrounded by a clear calcite rim (plane-polarized light).

10.1029/2024TC008757

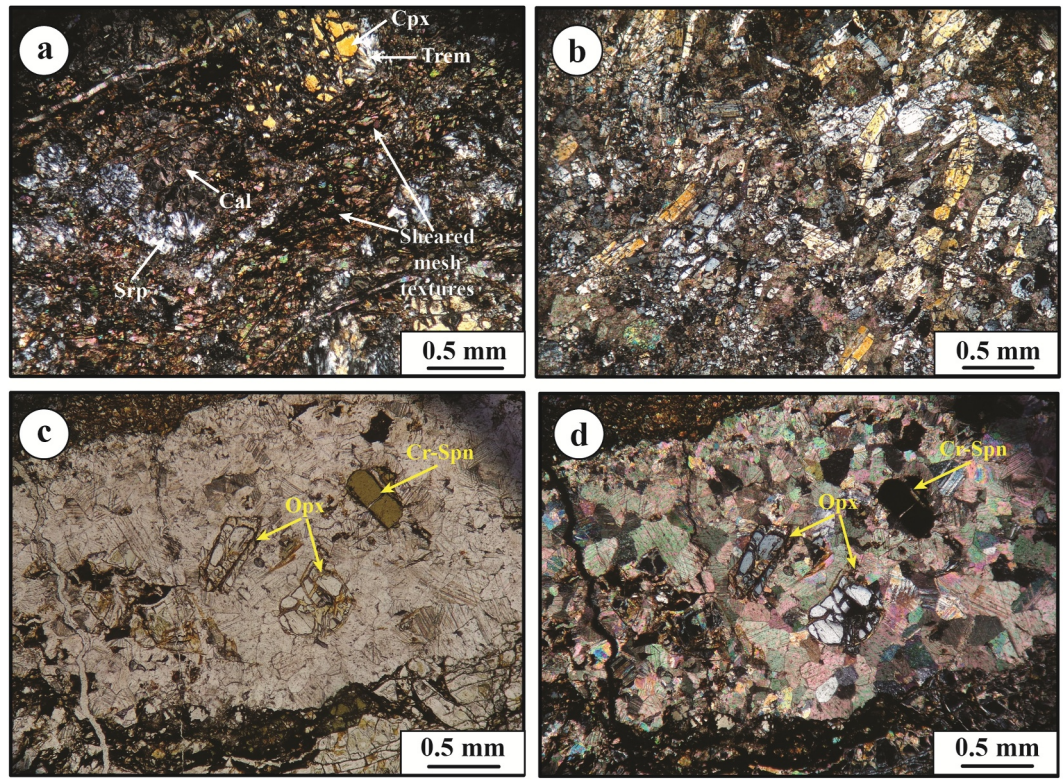

Figure 12. Some characteristic features in thin section of the ultramafic clasts preserved within the microbreccia. (a) Example of a weathered ultramafic clast mainly composed by a complex fine-grained matrix primarily made of calcite, serpentine, chlorite and Fe-oxide, with minor fibrous tremolite and showing remnants of a clinopyroxene porphyroclast (yellow grains, on the upper right corner of the picture). Note the sheared mesh texture of the fine-grained (carbonated?) calcite/serpentine matrix (crossed polars). (b) Transition between a large ultramafic clast and the calcite matrix of the microbreccia characterized by relatively large fibers of tremolite (yellow elongated crystals) and smaller grains of calcite and chlorite (crossed polars). (c and d) Example of a millimetric calcite veins cutting through an ultramafic clast to form ophicalcite. The vein has polycrystalline texture, with relatively well-preserved remnants of mafic minerals (such as pyroxene or dark-green Cr-spinel) floating in a cement of calcite with polygonal granoblastic texture (c is in plane-polarized light; d is in crossed polars).

presence of light green/blue Al-spinel (Figures 11e and 11g), which has not been observed in the large carbonate veins. This observation, together with the general cataclastic texture of the microbreccia and its structural position between the main contact with the Lherz peridotite body, isolated large blocks of peridotite and the coarse breccia, suggests that this lithofacies might have resulted from progressive cataclastic brecciation of a material analog to that of the large carbonate vein/dikes. Such veins intruded in the upper part of the Lherz peridotite body along the main detachment fault, wrapping around and progressively isolating amygdale-shaped lenses of peridotite in the uppermost part of the footwall of the detachment. Thus, the foliation observed in the microbreccia at the outcrop scale, which is sub-parallel to the main contacts with the underlying peridotite and wraps around isolated lenses of peridotite (see for example Figure 7a), can be interpreted as a tectonic cataclastic foliation. This foliation could be the result of micro-scale brittle boudinage of the large calcite grains in a cataclastic calcite matrix (as suggested by the microfabric shown in Figure 11). This general interpretation is also consistent with observations made along the contacts between the microbreccia and the peridotite. Where such contacts are not clearly marked by normal faults, they display a lobate geometry (see Figures 7b and 7g), with the shape of the alteration zone of the underlying peridotite recalling some kind of percolation/infiltration (see Figure 7g). Such kind of features might result from chemical etching of the peridotite, since carbonate melts are thought to be very corrosive for silicate host-rocks (e.g., Hode Vuorinen & Skelton, 2004; Kruk & Sokol, 2022). Consistently, the mineral composition of the observed alteration zones includes tremolite ($Ca_2Mg_5Si_8O_{22}(OH)_2$), which might be the result of interaction between ultramafic minerals such as forsterite (Mg_2SiO_4) and a carbonate melt ($CaO + CO_2 + H_2O$).

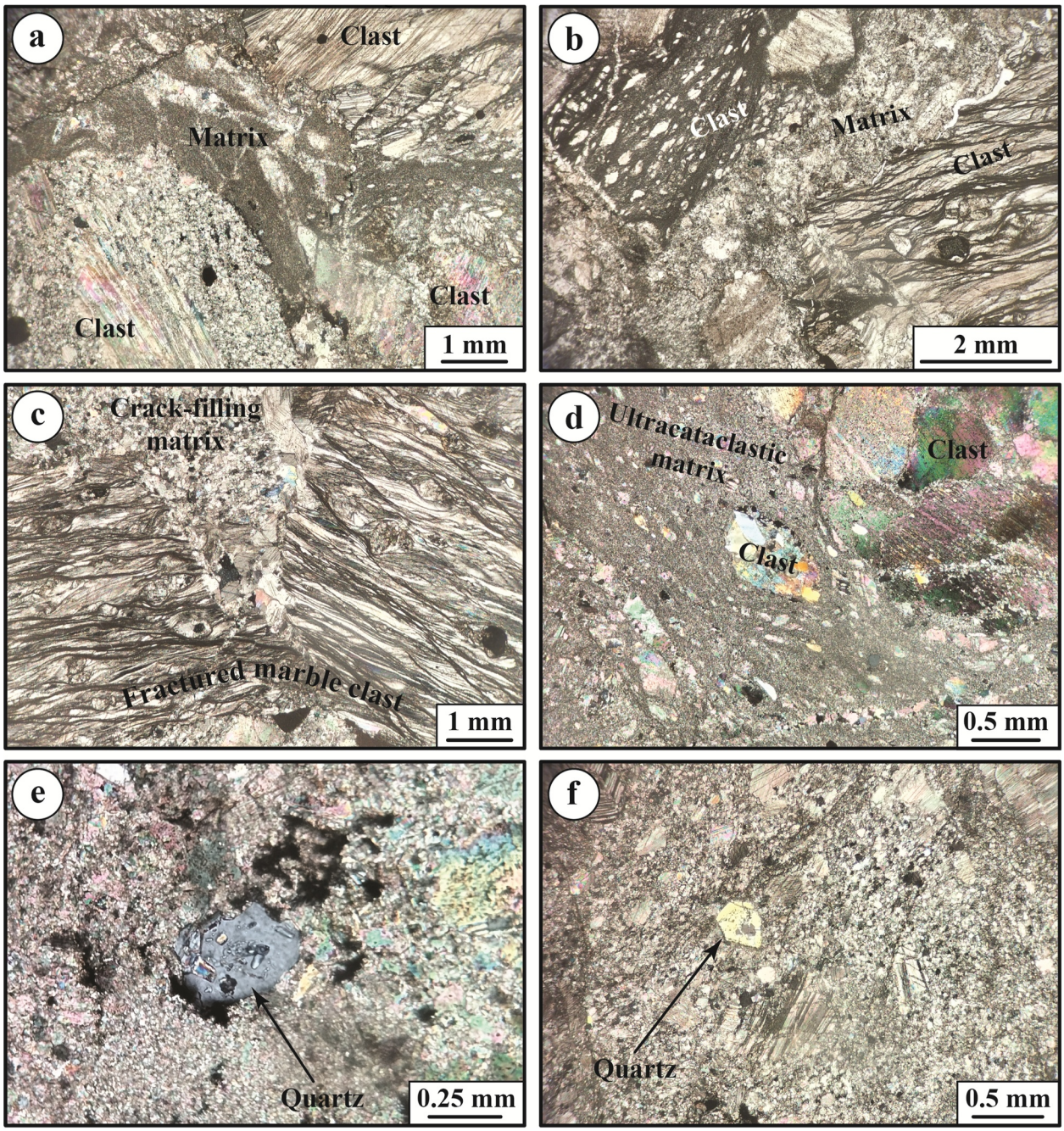

Figure 13. Microscopic facies of the coarse marble breccia as observed in samples from the Salle the la Famine. (a) Example of a crumbled marble clast (upper right corner) and a carbonate microbreccia breccia clast (lower left corner) separated by a fine-grained calcite matrix (crossed polars). (b) Ductilely stretched marble clasts showing evidence for non-coaxial shearing (upper left and lower right corners; plane-polarized light). (c) Crack-filling calcite matrix in a fracture developed within a ductilely stretched marble clast with (crossed polars). (d) Example of cataclastic flow in the very fine-grained calcite matrix wrapping around polycrystalline marble clasts (crossed polars). (e and f) Inclusion-rich euhedral (bipyramidal) quartz grains dispersed within the fine-grained calcite matrix (crossed polars).

The presence of Al-spinel in the microbreccia further support the hypothesis that evaporite-derived fluids circulated along the Lherz detachment and had a role in the partial melting (or extraction of HT metamorphic fluids) at the base of the pre-rift carbonates. In fact, this mineral has been previously observed in the region only in the sapphirine-bearing rocks outcropping on the northern flank of the Lherz Massif (Uzel et al., 2020). These authors claim that the mineralogical assemblage of those rocks formed from the metamorphic transformation of Triassic (Keuper) evaporites under high T and low P conditions during the Cretaceous rifting.

The formation of this tectonic microbreccia likely represents the result of progressive cooling during lithospheric stretching and mantle exhumation. This facies could in fact witness the syn-rift transition from the high temperature/ductile regime represented by syn-extensional HT-LP metamorphism (and partial melting?) of the pre-rift sedimentary cover, to the low temperature/brittle regime resulting in cataclastic deformation of the carbonate vein/dikes injected along the main mantle-exhuming detachment fault. This progressive cooling during extensional deformation is also witnessed by the presence of thick tabular twins in the larger calcite grains preserved in the microbreccia (see Figures 11c and 11e). In fact, this mechanical twinning morphology in calcite typically develops at temperatures between 150°C and 300°C (e.g., Burkhard, 1993; Ferrill, 1991), thus testifying a relevant temperature drop during deformation compared to the temperatures required for partial melting of carbonates and/or recorded by the metamorphosed sedimentary pile (up to ∼600°C).

More in general, it is important to highlight the fundamental contribution of microscopic observations for the interpretation of the microbreccia. In fact, the aspect of this lithofacies in outcrop might be extremely misleading. Its penetrative foliation characterized in outcrop by the alignment of elongated calcite grains might be in fact misinterpreted as a sedimentary layering. However, microscopic observation allows to show that this feature results from progressive brittle fracturing and is indeed a tectonic feature (Figure 11).

4.1.3. Coarse Marble Breccia

Progressive temperature decrease during rifting as suggested by the formation process of the above described microbreccia is also testified by the formation of the coarse marble breccia. In fact, this breccia reworks clasts of the Mesozoic marbles which were previously stretched under HT-LP metamorphic conditions (Clerc et al., 2015). As suggested by previous studies focused on the surroundings of the Lherz Massif, this breccia likely formed by in situ tectonic and/or hydraulic fracturing and limited mixing of meta-sediments of the Jurassic cover in the brittle regime (Dauteuil et al., 1987; Golberg, 1987; Lagabrielle et al., 2016; Ternet et al., 1997). This process followed in time the ductile HT stretching of the Jurassic sediments in a continuum of deformation, thus testifying a progressive cooling (and exhumation) of the base of the pre-rift cover during crustal stretching and mantle exhumation.

4.2. Kinematic Evolution and Implications for the Cretaceous Rifting

The structural data set presented in this work brings new important constraints concerning the kinematic evolution of the NPZ during the Cretaceous syn-rift episode. In fact, since the discovery of inverted Cretaceous rift basins in the North Pyrenean Zone, the kinematic evolution of this rift system has been matter of keen debate (see Asti et al., 2022 for a review). The end members of the main kinematic models that have been proposed span from orthogonal rifting with a ∼NNE-SSW direction of extension (e.g., Jammes et al., 2009; Lescoutre et al., 2019; Masini et al., 2014; Tugend et al., 2014; Saspiturry et al., 2019a) to transtensional or pull-apart left-lateral tectonics following a ∼WNW-ESE stretching direction (e.g., Choukroune & Mattauer, 1978; Debroas, 1978, 1987, 1995; Oliva-Urcia et al., 2010; Saint-Blanquat et al., 2016, 2017). Along the section of the Gouffre Georges described in this work, the main extensional tectonic contact between the Lherz peridotite body and the Mesozoic sedimentary cover, as well as the other associated extensional structures (minor normal faults, slickenlines, S-C structures, R shear planes), clearly point to a direction of extension trending between W-E to WNW-ESE along an overall ∼N-S trending and W-dipping detachment contact. This means that, at least in the final stages of the Cretaceous rifting which culminated with mantle exhumation at the base of the pre-rift cover, in the Aulus Basin the extensional regime was clearly associated to an oblique ∼WNW-ESE trending stretching component. This observation is much more in line with a left-lateral transtensional regime rather than with an orthogonal rifting mode.

Equivalent ∼N-S lithospheric tectonic features have been recently documented within the West Pyrenean orogen. For example, the Maupasacq passive seismic acquisition demonstrated that in the Mauléon basin three major N20-trending structures (namely the Iholdy, Saison and Barlanès lineaments) are currently rooting at depth in the upper lithospheric mantle (Lehujeur et al., 2021; Saspiturry et al., 2022). These tectonic features, defined as syn-collisional upper lithospheric transfer zones at the origin of the non-cylindrical shape of the West-Pyrenean belt (Saspiturry et al., 2022), seem to have also played a fundamental role during the Cretaceous syn-rift episode. For instance, the Barlanès structure is punctuated by outcrops where sub-continental mantle (Fabriès et al., 1991, 1998) was reworked into the Albian-Cenomanian Urdach syn-rift sedimentary breccia (Debroas et al., 2010; Fortané et al., 1986; Jammes et al., 2009; Lagabrielle et al., 2010; Roux, 1983). This spatial correlation suggests

that the Barlanès structure was prominent in the Cretaceous syn-rift denudation of mantle material. As the ~N-S detachment recognized in the Gouffre Georges, it necessarily implies that the Barlanès structure was rooted at depth in the upper lithospheric mantle at the end of the Cretaceous hyperextension (Saspiturry et al., 2021b). Thus, the final exhumation and denudation of sub-continental mantle during the Early Cretaceous syn-rift along the N0-20° Barlanès and Gouffre Georges lithospheric structures could reflect the complex kinematic history of the Iberia/Eurasia plate boundary suffering an evolution from NNE-SSW orthogonal rifting (Late Jurassic to Early Albian time) to a transtensional WNW-ESE rift opening during the Late Albian to Early Cenomanian (Asti et al., 2022).

5. Discussion

5.1. Tectonic Evolution of the Mantle/Cover Tectonic Contact

Our data clearly show that the contact exposed along the above-described section of the Gouffre Georges juxtaposing the Lherz peridotite (in the footwall) and the pre-rift Mesozoic carbonate cover (in the hanging wall) is tectonic. Crustal basement rocks are completely lacking between these two main tectonic units, nor are found as clast in tectonic breccias exposed in the cave. These observations imply that the tectonic features described in this work are related to advanced stage of the Cretaceous North Pyrenean rifting. Indeed, the tectono-thermal processes recorded in the Gouffre Georges followed the complete lateral extraction of the continental crust in the distal part of the hyperextended domain of the Pyrenean paleo-passive margin. Early Cretaceous continental crust extraction occurred between the cover décollement (*sensu* Lagabrielle et al., 2019a, 2019b), consisting in the Keuper evaporites, and the crust-mantle detachment (*sensu* Lagabrielle et al., 2019a, 2019b), thus allowing the syn-extensional tectonic juxtaposition between mantle peridotites and pre-rift sedimentary rocks (e.g., Asti, Lagabrielle, et al., 2019; Clerc & Lagabrielle, 2014; Clerc et al., 2016; Duretz et al., 2020). Figure 14 schematically represents the conceptual model envisaged for the evolution of the tectonic contact between the mantle rocks and the overlying carbonate cover described in this work. It shows only the processes that occurred in proximity of the detachment surface and whose expression can be seen in the rock exposures within the Gouffre Georges. This figure does not represent the whole deformation accommodated in the hanging wall and in the footwall several tens to several hundreds of meters away from the detachment surface since it cannot be observed in the cave (see Section 5.2).

After the complete lateral extraction of the continental crust, the Mesozoic pre-rift sedimentary cover is put directly in contact with the exhumed mantle. At the beginning of this stage, the Jurassic carbonate rocks and the mantle rocks are likely still decoupled thanks to the presence of an intervening residual layer of Keuper evaporites (Figure 14b). With the proceeding of rifting, the combination of asthenosphere rise (i.e., rise of the isotherms) and accumulation of relevant thickness (x1,000 m) of syn-rift sediments (burial) lead to considerable temperature rise in the pre-rift sedimentary cover (Figure 14b). This process is thought to be responsible for the syn-rift HT-LP North Pyrenean metamorphism (e.g., Duretz et al., 2020; Saspiturry et al., 2021a and references therein). Syn-rift paleo-thermal gradients have been estimated at around 60–80°C/Km (Corre, 2017; Hart et al., 2017; Saspiturry et al., 2020b; Vacherat et al., 2014). At the very base of the pre-rift sedimentary pile of the Aulus Basin, maximum temperatures were in the order of ~600°C (Clerc et al., 2015). At these temperatures, carbonates are thought to be extremely ductile (Dobson et al., 1996). Moreover, as discussed above, the presence of evaporites (Keuper) at the base of the Jurassic series might have also favored partial melting of the pre-rift carbonate cover. In fact, the presence of elements such as Cl, F and P which are commonly abundant in evaporites can significantly drop the melting temperature of carbonates (Lentz, 1999). By contrast, at these temperature conditions, the ultramafic mantle rocks are brittle and likely develop brittle fault planes during extension. Typically, the uppermost lithospheric mantle layer below the crust/mantle detachment (*sensu* Lagabrielle et al., 2019a, 2019b) develops anastomosed low-angle shear planes individualizing amygdale-shaped peridotite/serpentinite lenses (see "lenticular layer" in Lagabrielle et al., 2019a, 2019b). The extreme rheological contrast between the brittle exhuming peridotite and the overlying hyper-ductile/molten (?) pre-rift cover allows flowing of the potentially generated pseudo-carbonatitic melts/HT hydrothermal fluids or of the hyper-ductile marbles within the brittle extensional structures of the underlying peridotite to form the large carbonate vein/dikes (Figure 14b). This process can lead to a progressive incorporation of large mantle lenses within the carbonate fluid/melt, as those commonly observed within the microbreccia above the main peridotite/cover contact (Figures 6e and 7e). During this stage, liberation of overpressured fluids due to decarbonation of the pre-rift carbonates exposed to the HT

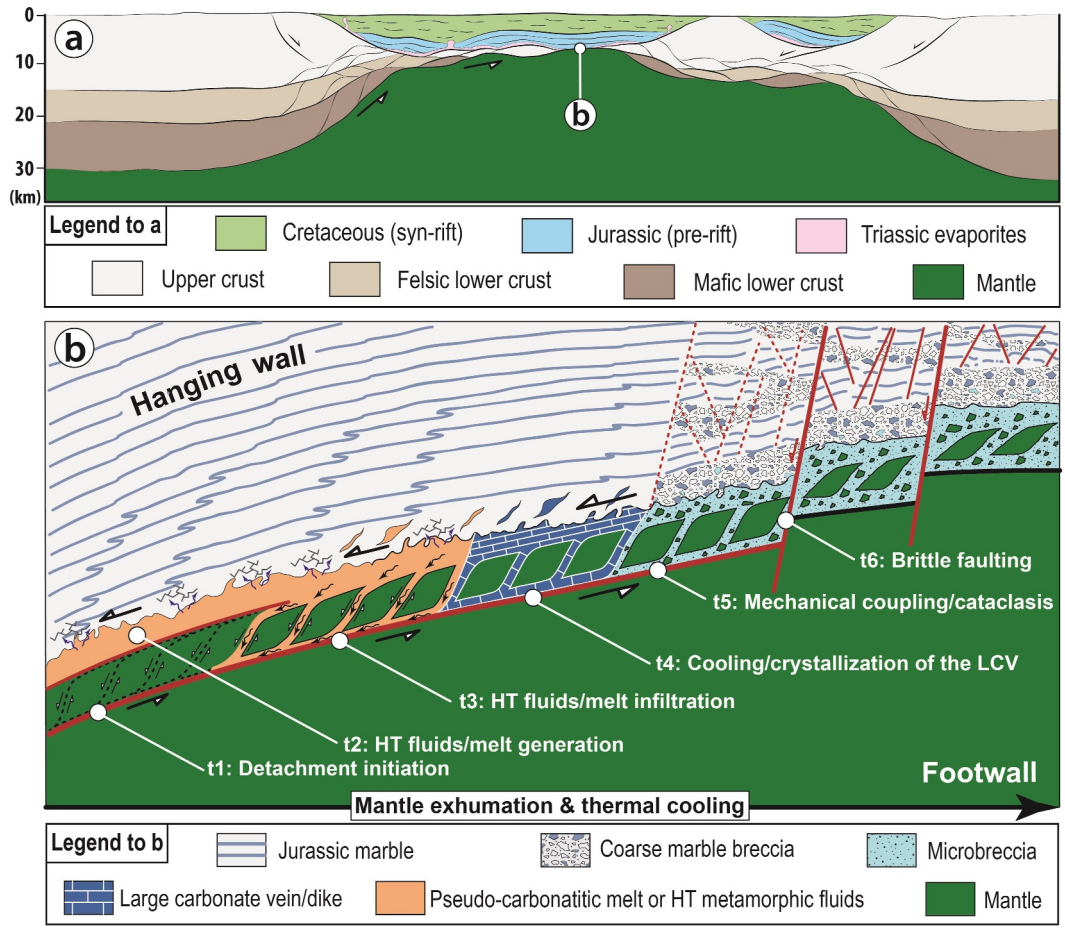

Figure 14. (a) Schematic cross-section of the North Pyrenean rift system with potential location of the features presented in this work and where takes place the evolution exposed in panel (b) (white dot; redrawn and modified after Asti et al. (2021) and inspired from Clerc et al. (2015, 2016)). (b) Schematic conceptual model (not to scale) for the evolution of the extensional tectonic contact between the peridotite (sub-continental mantle) and the overlying carbonate cover during the Cretaceous rifting as reconstructed from observations in the Gouffre Georges. At stage t1, the pre-rift carbonate cover and the exhuming lithospheric mantle are mechanically decoupled thanks to the presence of an intervening residual layer of evaporites. Temperature rise produce syn-extensional HT-LP metamorphism in the pre-rift cover while incipient brittle extensional faults develop in the peridotite. During stage t2, progressive temperature increase, together with the influence of evaporite-derived fluids, lead to partial melting at the base of the pre-rift carbonate cover (or liberation of HT carbonate-rich metamorphic fluids). During stage t3, the pseudo-carbonatitic melts (or HT metamorphic fluids) intrude within the brittle extensional faults developed within the upper part of the exhuming peridotite. Overpressured fluids produced by decarbonation of the pre-rift carbonates generate a first generation of hydraulic breccia in the pre-rift cover. During stage t4, progressive syn-extensional cooling leads to crystallization of the large carbonate vein/dikes. (e) Syn-extensional cooling leads to progressive embrittlement of the pre-rift cover and mechanical coupling between the carbonate cover and the brittle exhuming peridotite. The whole contact undergoes brittle deformation leading to the formation of the carbonate microbreccia and of the coarse marble breccia by cataclastic mechanisms (stage t5). Finally, during stage t6, high-angle brittle normal faults crosscut and offset the main peridotite/cover contact to form the topographic steps forming the main pits (P5 and P11). L.C.V.: large carbonate veins.

thermal regime can result in early hydraulic brecciation at the base of the pre-rift cover, as suggested by previous studies (Dauteuil et al., 1987; Golberg, 1987; Minnigh et al., 1980; Ternet et al., 1997).

With the proceeding of lithospheric stretching, progressive temperature drop might have occurred, leading to crystallization of the large carbonate vein/dikes and embrittlement of the metamorphosed pre-rift carbonate cover (Figure 14b). This cooling might be due to progressive tectonic removal of the overlying syn-rift sedimentary cover during rifting, thus reducing the effect of sedimentary burial on the overall thermal regime. Another possible explanation for the cooling of the system might be a quenching process, as suggested by previous studies in the Lherz Massif (Minnigh et al., 1980). In fact, the CO_2 gas liberated by decarbonation due to HT

metamorphism and/or partial melting of the pre-rift carbonates and migrating upwards might have acted as an efficient way for heat transport and cooling of system. A notable difference between these two possible explanations is that in the first case heat transfer is dominated by conduction and is much more progressive, while in the second case it occurs by convection and is thus much more efficient and rapid, leading to a quick cooling of the system.

Progressive cooling of the system favored mechanical coupling along the main mantle/cover extensional contact. This allowed progressive tectonic brecciation in most of the crystalized large carbonate vein/dikes (to produce the carbonate microbreccia) and of the marbles (to produce the coarse marble breccia) (Figure 14b). This process of tectonic breccia formation is similar to what have been proposed for the evolution of the Agly massif area in the eastern NPZ at the base of the Jurassic pre-rift cover during advanced stages of the Cretaceous extension (Motus et al., 2022). Brittle deformation in the crystallized pseudo-carbonatitic dikes/hydrothermal veins preferentially affected the thicker (m-sized) vein/dikes at the top of the lenticular layer, thus allowing the preservation of thinner (dm-sized) poorly deformed carbonate vein/dikes in deeper parts of the lenticular layer. Paroxysm of this syn-extensional cooling stage is accompanied by the development of westward dipping steep normal faults (70°) crosscutting both the cataclastic cover and the mantle (Figure 14b). These faults are responsible for the current morphology of the Gouffre Georges insofar as they are directly located right upon the P5 and P11 pits (Figure 4).

The exposed tectonic model is able to account for the presence of large mantle lenses embedded within the carbonate microbreccia above de main mantle/cover tectonic contact. Moreover, the presence of an intervening layer of crystallized pseudo-carbonatitic melts/HT hydrothermal fluids between the marbles and the peridotite prevents tectonic mixing of mantle clasts and marble clasts during the formation of the coarse marble breccia.

Uplift and exhumation of the Lherz peridotite in a solid state was proposed long ago (Avé Lallemand, 1967; Minnigh et al., 1980; Vielzeuf and Kornprobst, 1984). However, the concept of mantle exhumation by detachment faulting at distal passive margins during the Cretaceous rifting was proposed for the first time much more recently (Lagabrielle and Bodinier, 2008). Our observations definitely confirm the model of detachment faulting accounting for the emplacement of the Lherz mantle body, as already supported by other studies on other peridotite massifs of the NPZ (e.g., Asti, Lagabrielle, et al., 2019; Jammes et al., 2009; Lagabrielle et al., 2019a, 2019b; Lescoutre et al., 2019; Saspiturry et al., 2019a). Moreover, our study definitely identified the detachment fault responsible for the exhumation of the Lherz Massif, whose existence was often inferred (e.g., Clerc et al., 2012; Lagabrielle and Bodinier, 2008; Uzel et al., 2020), but which was never identified before in the field. These findings give an extraordinary opportunity to study and unravel the rheological, thermal and metasomatic processes that occur when the subcontinental mantle meets a carbonate- and evaporite-rich sedimentary cover during its exhumation, and that are here only presented as preliminary observations.

5.2. Considerations on the Thickness of the Lherz Detachment Fault

What can be observed in the cave is only one part of the detachment zone affecting the top of the Lherz ultramafic body. In fact, the cave runs along the detachment surface separating the hanging wall from the footwall and does not crosscut the whole shear zone (or damage zone, once in the brittle regime). For this reason, establishing the overall thickness of the whole detachment zone is complex. However, there are some aspects that should be considered to constrain the thickness of the Lherz detachment:

1. The thickness of the shear zone in the footwall is difficult to determine, since the temperature regime under which mantle exhumation occurred was too low to produce diffuse ductile deformation in the ultramafic rock. In fact, among the 40 lherzolite outcrops in the whole NPZ there is only one report of a (small) mylonitic band developed during the Cretaceous extension event in a peridotite massif (see Vissers et al., 1997). The geometry of the Gouffre Georges does not allow to crosscut the whole footwall of the detachment. However, considering the distance between the detachment surface exposed in the cave and lenticular serpentinites outcropping in the western part of the Lherz Massif (similar to those observed in the cave in the detachment footwall), the thickness of the lenticular layer (*sensu* Lagabrielle et al., 2019a, 2019b) can be estimated to at least a couple of hundred meters. This is just a qualitative estimation and of course considers only a late part of the deformation (once water could impregnate the footwall to produce serpentinization). Nonetheless, it shows that the deformation associated to the detachment footwall is not affecting only the portion of the Lherz Massif exposed in the cave.

2. There is very little evidence of non-coaxial ductile deformation in the HT/LP Jurassic marble in the hanging wall of the detachment and markers of the extensional deformation (other than flattening) are substantially lacking. Accordingly, calcite Crystallographic Preferred Orientation (CPO) measured by Electron Back Scattering Diffraction (EBSD) in the marbles surrounding the Lherz Massif (see Lagabrielle et al., 2016) is weak and the dominant crystallographic fabric is planar (oblate ellipsoid). This might depend on the fact that most of the ductile deformation in the Mesozoic cover in the hanging wall have been taken over by the upper Triassic evaporites that were at the base of the Jurassic carbonates prior to crustal breakup. This major decoupling layer between the exhuming mantle and the sedimentary cover is now gone due to its extreme physical and geochemical mobility during HT/LP metamorphism (see Sections 4.1 and 5.1). Ductile deformation in the detachment hanging wall also extensively affected the crustal bedrock during the Cretaceous extension. This is witnessed by non-coaxial ductile shear documented in the crustal lenses at the margins of the Aulus Basin (Asti et al., 2021) and in other parts of the NPZ (Asti, Lagabrielle, et al., 2019; Aumar et al., 2022). This process is well illustrated in the thermo-mechanical models of Duretz et al. (2020). These models show that ductile deformation affects the pre-rift carbonate cover only once the evaporite decoupling layer have been removed and the pre-rift cover end up in tectonic contact with the exhumed mantle after crustal breakup. This would imply that most of the rock volume that have been affected by ductile deformation in the detachment hanging wall during extension is not preserved close to the contact between the exhumed mantle and the sedimentary cover because it has been laterally extracted via ductile flow. Hanging wall thinning and its progressive lateral extraction by ductile flow has been proposed as an important mechanism allowing exhumation associated to detachment faulting in the NPZ (e.g., Clerc & Lagabrielle, 2014) and in many other extensional contexts (e.g., Asti, Faccenna, et al., 2019; Bartley & Wernicke, 1984; Cooper et al., 2010; Lister and Davis, 1989; Miller et al., 1983; Platt et al., 2015; Ring et al., 1999).
3. Brecciation of the Jurassic marbles in the detachment hanging wall is not limited to the few meters of thickness that are exposed in the Gouffre Georges. These brecciated marbles crop out extensively in the Mont Béas peak (see Sections 2 and 3.1). This mountain, in which the Gouffre Georges is excavated, is entirely composed of marble breccia and intervening marble lenses of very variable size (see geological maps by Ternet et al., 1997 and by Lagabrielle et al., 2016) over a thickness of about 500 m. The origin of this breccia is still matter of debate since there are probably several overlapping generations of breccias with different significations (see Section 2). However, it is very likely that most of these breccias are related to the activity of the detachment during mantle exhumation and were formed by tectonic and/or hydraulic fracturing processes. Such processes have also been documented in the Agly massif area in the eastern NPZ during the Cretaceous extension (Motus et al., 2022).

Combining all these considerations together, reveals that the deformation recorded along this Early Cretaceous detachment is marked by a several hundreds of meters thick rock volume on both sides of the structure. The damage zone of this tectonic contact responsible for continental breakup and undercover mantle exhumation is therefore significant. It is also the first example of mantle-exhuming detachment described to date in the Pyrenean inverted rifted margin system with such spectacular continuity, although many recent articles deal with the hyperextension of the continental crust in the Pyrenees.

5.3. Considerations on the Presence of Ultramafic Clasts-Bearing Breccias

The age (Cretaceous vs. Cenozoic) of the final mixing and the formation of the polymictic (ultramafic + marble clasts) sedimentary breccia around the Lherz body, as well as its depositional environment (marine vs. continental), remain debated. These sedimentary breccias represent ophicalcites type 2 of Lemoine et al. (1987) or *sedimentary ophicalcites* of Clerc et al. (2014).

The polygenic character of the microbreccia exposed in the Gouffre Georges cannot be explained via sedimentary processes. Indeed, as explained in Section 4.1.2, it seems to result from a complex interaction between thermal and tectonic processes during the final stages of lithospheric mantle exhumation. Thus, contrastingly with what has been proposed for other localities in the Aulus Basin (Clerc et al., 2012; Lagabrielle and Bodinier, 2008; Lagabrielle et al., 2016; Uzel et al., 2020), this (micro)breccia did not form from sedimentary mixing after mantle denudation to the seafloor. Instead, the above described cataclastic facies (microbreccia and coarse breccia) developed under the pre-rift cover. As discussed later in Section 5.6, this interpretation therefore requires that part of the Pyrenean ophicalcites, as those exposed in the Gouffre George mantle, might locally have developed under cover and did not result from direct interaction with seawater at the sea floor as proposed elsewhere in the

Pyrenees (e.g., Clerc et al., 2014; Jammes et al., 2009; Masini et al., 2014). This interpretation also questions the co-existence of tectonic breccia and sedimentary mixed breccia on the bottom of the Cretaceous Aulus Basin.

Since the concept of mantle exhumation by detachment faulting at distal passive margins was applied to the North Pyrenean rift system in the 2000's (Jammes et al., 2009; Lagabrielle and Bodinier, 2008), several studies have proposed that the sedimentary polymictic breccia around the Lherz Massif (Lacroix, 1895) was a syn-rift unit and was witness for mantle exposure to the seafloor during the Cretaceous rifting (Clerc et al., 2012; Lagabrielle and Bodinier, 2008; Lagabrielle et al., 2016; Uzel et al., 2020). These authors applied the concept of tectono-sedimentary breccia formation by sedimentary reworking of tectonic breccias that are continuously extracted and submitted to erosion along detachment faults, that have been also proposed along other mantle-exhuming detachment faults preserved in the Alps (e.g., Masini et al., 2012) and documented at OCCs detachments (Escartin et al., 2017). However, while there is general consensus on syn-rift sedimentary reworking of mantle rocks in the western NPZ (Urdach massif) (e.g., Asti, Lagabrielle, et al., 2019; Canérot, 2017; Debroas et al., 2010; Jammes et al., 2009; Lagabrielle et al., 2010, 2019a), our observations clearly show that it is not possible to apply this model to the Gouffre Georges breccia. Whether these observations can be extrapolated to the whole Lherz Massif and have an impact on the interpretation of the polymictic breccias surrounding it remains an open question which is beyond the scope of this paper.

5.4. Implications for the Thermal Regime at the Base of the Sedimentary Cover During the Cretaceous Extension

The presence of crystallized pseudo-carbonatitic dikes/HT hydrothermal veins questions the existing estimations of paleo-temperatures reached at the base of the sedimentary cover during the Cretaceous rifting. In the North Pyrenean Zone, these temperatures have been mostly estimated by Raman spectroscopy of carbonaceous material (RSCM) thermometry, particularly in the last decade (e.g., Chelalou et al., 2016; Clerc et al., 2015; Ducoux et al., 2021; Saspiturry et al., 2020b). The highest maximum paleo-temperatures have often been found at the base of the pre-rift meta-sediments series, often associated to the presence of ultramafic bodies in the surroundings, and are in the order of ∼600°C. However, these temperatures are very close to and overlap with the upper limit for the calibration of RSCM thermometry (Beyssac et al., 2002; Rahl et al., 2005). Thus, these thermal estimations might be imprecise and underestimate the maximum paleo-temperatures reached by the sedimentary cover during the final steps of mantle exhumation. In this regard, the presence of crystallized pseudo-carbonatitic melts/HT hydrothermal fluids at the base of the pre-rift sedimentary series, as documented in this study, might be very useful to improve our knowledge on the thermal conditions of the Cretaceaous North Pyrenean rifting. In fact, the application to the large carbonate vein/dikes crosscutting the upper part of the Lherz body of other geo-thermometers more adequate to high thermal conditions (>600°C) than RSCM thermometry might bear new and more accurate estimations on the highest paleo-temperatures reached by the sedimentary cover during rifting. Our results suggest that the Gouffre Georges cave might have recorded one of the highest syn-rift temperature ever identified along the Pyrenean passive margins to date. Insofar, as this thermal regime is directly linked to the continental lithosphere deformation state, this latter has certainly reached its minimum effective thickness in the Gouffre Georges locality. Here, early Cretaceous lithosphere thinning being more pronounced than elsewhere in the Pyrenees, the paleo-thermal gradient may have reached values higher than the 60–80°C/km estimated along the western Pyrenean passive margin (Hart et al., 2017; Saspiturry et al., 2020b; Vacherat et al., 2014).

5.5. Differences Amongst Exhumed Peridotites in the Western and Eastern Pyrenees

Substantial differences exist between the mantle peridotites exposed in the western and eastern part of the NPZ which have been highlighted by several studies in the past. These differences include the intensity of their serpentinization (e.g., Clerc et al., 2014; Lagabrielle et al., 2010; Monchoux, 1970), the maximum temperatures reached by the HT-LP metamorphism of the sedimentary cover in the surroundings of the ultramafic massifs (Clerc et al., 2015; Ducoux et al., 2021), the interpretation of the ultramafic-bearing breccias associated to the exhumed massifs (e.g., Clerc et al., 2012; Debroas & Azambre, 2012; Debroas et al., 2010, 2013; Jammes et al., 2009; Lagabrielle and Bodinier, 2008; Lagabrielle et al., 2010, 2016) and the long-term exhumation history of the mantle rocks suggested by their petrologic evolution (Fabriès et al., 1991, 1998; Henry et al., 1998; Vissers et al., 1997).

Peak temperatures of the HT-LP metamorphism reach temperatures of ~400°C in the western NPZ, while they reach ~600°C in the east (Clerc et al., 2015; Ducoux et al., 2021; Golberg & Leyreloup, 1990). These temperature differences are consistent with those estimated along mantle-exhuming detachment faults in the two portions of the belt. In fact, peak temperatures estimated along the detachment faults exposed in the Urdach and Saraillé massifs (western NPZ) during mantle exhumation point greenschist facies conditions, not exceeding 450°C (Asti, Lagabrielle, et al., 2019; Lagabrielle et al., 2019a, 2019b). By contrast, peak temperatures on the Lherz detachment (eastern NPZ) are in the order of 600°C or possibly more (Uzel et al., 2020; this study). This difference might be due to a differential thickness of the sedimentary cover between the western and eastern NPZ, thus producing a differential burial effect between the two portions of the rift system during HT-LP metamorphism and mantle exhumation. This explanation is consistent with the metasomatic and tectono-sedimentary evolution of the different mantle exhuming systems. In fact, as discussed in Sections 5.4 and 5.6, proofs of mantle exposure to the seafloor exist in the western NPZ, where the peridotite massifs are often completely serpentinized and mantle rocks have been reworked in syn-rift sediments. By contrast, the eastern NPZ peridotite bodies are generally serpentinized only along detachment faults which controlled the plumbing system and have preserved a relatively thick cover of sediments at the end of rifting, which prevented pervasive serpentinization and syn-rift sedimentary reworking. A thinner sedimentary pile in the west would have ease mantle unroofing in the western rather than in eastern NPZ, with a same amount of extension along the whole rift system.

5.6. Insights From the Lherz Detachment Into Mantle Exhumation Processes

5.6.1. Structural and Metasomatic Evolution: Comparisons With Modern and Fossil Analogs

As outlined in Section 3.1, the uppermost portion of the peridotite beneath the main peridotite/carbonate cover contact features an anastomosing network of shear planes isolating sigmoidal lenses of serpentinized peridotite, and defining an overall phacoidal fabric. This feature, referred to as "lenticular layer" by Lagabrielle et al. (2019a, 2019b), has been documented in other mantle-exhuming detachments within the NPZ, such as the Urdach and Saraillé massifs in the western NPZ (Asti, Lagabrielle, et al., 2019; Lagabrielle et al., 2019a, 2019b), the Moncaup peridotite in the central NPZ (Lagabrielle et al., 2010), and the Bestiac peridotite(s) in the eastern NPZ (de Saint Blanquat et al., 2016). This layer represents a shear zone within the uppermost section of the exhuming mantle, a feature that is commonly observed throughout the NPZ (Lagabrielle et al., 2010, 2019a, 2019b). Similar tectonic features have been identified in oceanic core complexes (OCCs) along the slow-spreading Mid-Atlantic Ridge, where mantle exhumation is currently active (e.g., Karson et al., 2006; Escartin et al., 2017). Additionally, similar sigmoidal lenses have been described in the Ronda peridotite massif (Betic Cordillera, Spain) in the footwall of a mantle-exhuming detachment zone formed during continental extension (e.g., Precigout et al., 2013; Bessière et al., 2021).

Thus, the lenticular layer appears to be a tectonic feature that forms relatively early in the exhumation history of mantle peridotites within extensional systems. It has been observed both in areas where the mantle was fully exhumed and exposed at the seafloor, such as in the Urdach massif of the western NPZ (Lagabrielle et al., 2019a) or in present-day oceanic environments (Escartin et al., 2017; Karson et al., 2006), as well as in domains where mantle peridotites were only partially exhumed, retaining a thicker crustal basement or pre-rift sedimentary cover, as seen in the Saraillé massif of the western NPZ (Corre et al., 2016; Lagabrielle et al., 2019b), the Lherz Massif (this study), or the Ronda Massif (Bessière et al., 2021 and references therein).

Along the contact with the overlying carbonate cover exposed in the cave, the peridotite appears intensely transformed by different types of reactions. In contrast, the Lherz peridotite body, outside the cave, remains mostly well-preserved and relatively unaltered, except along late faults. This difference suggests that fluid circulation during mantle exhumation was structurally controlled, occurring primarily along the detachment where fluid-rock interactions were promoted by deformation processes. In places where mantle rocks have been exhumed to the seafloor during rifting, such as present-day OCCs at slow-spreading ridges (e.g., Andreani et al., 2007; Boschi et al., 2006; Rouméjon et al., 2015, 2018), distal passive margins (e.g., Agrinier et al., 1996; Boillot et al., 1987; Sallarès et al., 2013), or fossil hyperextended margins in ophiolitic suites in the Alps (e.g., Froitzheim & Manatschal, 1996; Desmurs et al., 2001; Picazo et al., 2013) or in the western Pyrenees (e.g., Lagabrielle et al., 2010, 2019a; Saspiturry et al., 2024; Tichadou et al., 2021), peridotites are often intensely serpentinized, not only along the detachment faults, but also for several hundred meters (to a few kilometers) in their footwall. This pattern suggests extensive fluid infiltration during and after the late stages of mantle

exhumation. The limited serpentinization observed in the rest of the Lherz body outside the cave indicates that it was not fully exposed to the seafloor and was instead shielded by a relatively thick layer of pre- and syn-rift sediments. This cover likely sheltered the peridotite in the detachment footwall from pervasive fluid infiltration and fluid-rock interactions. Similar observations are reported from the Ronda Massif in Spain, where mantle peridotites preserved a cover of thinned crustal rocks and/or pre-rift sedimentary layers at the end of rifting, preventing exposure to the seafloor (e.g., Bessière et al., 2021). The Ronda Massif also shares a key similarity with the Lherz Massif, in that its allochthonous pre-rift sedimentary cover underwent HT-LP metamorphism during rift-related mantle exhumation (Bessière et al., 2021; Mazzoli et al., 2013), as observed in the NPZ.

As described in Sections 3.2.1 and 3.2.2, alteration processes affecting the peridotite in the Gouffre Georges include carbonation, tremolitization, chloritization, serpentinization (pervasive and in veins) and iddingsitization. Unfortunately, our observations lack the resolution needed to establish a detailed relative chronology for these processes. However, several observations suggest that serpentinization and carbonation of the peridotite occurred syn-tectonically. Specifically, the presence of sheared carbonated mesh-textures occurring together with botryoidal serpentine overgrowth over clino-pyroxene (Figure 12a) points to carbonation reactions occurring concurrently with shearing. Additionally, the fact that serpentine occurs both as pervasive replacement of the ultramafic minerals and in syn-tectonic anastomosed shear veins suggests serpentinization mechanisms like those described by Andreani et al. (2007) on mantle-exhuming detachment faults at OCCs. These authors proposed that this kind of serpentinization along detachment faults can occur at depths of approximately 3–4 km below the seafloor, thus much before exposure of mantle to the seafloor.

Thin calcite veins crosscutting the serpentinized peridotite just below the contact with the carbonate cover clearly postdate serpentinization. In fact, these veins form a network that crosscuts and/or reactivates pre-existing serpentinite veins. The resulting ophicalcite corresponds to the first type of ophicalcites (OC1) described by Lemoine et al. (1987) or to the tectonically controlled type of ophicalcites described by Clerc et al. (2014) in Alpine and Pyrenean exposed mantle units, respectively. Although this type of rocks is found in settings where mantle rocks have been exhumed to the seafloor at present-day slow-spreading ridges (e.g., Picazo et al., 2012) or OCTs (e.g., Schwarzenbach et al., 2013), its formation is linked to seawater circulation within fractured serpentinite during exhumation, which can occur several kilometers below the seafloor before mantle rocks are fully exposed to the seabed (e.g., Andreani et al., 2007; Cannat et al., 2010). Therefore, the presence of this type of ophicalcites along the detachment fault that exhumed the peridotites of the Lherz Massif does not imply their exposure to the seafloor during rifting.

5.6.2. Comparative Analysis of Mantle Exhumation Models at Distal Passive Margins

A key observation in the Gouffre Georges is that Jurassic marbles, representing the pre-rift sedimentary cover, are found in direct contact with the Lherz peridotite along the detachment fault. In the Aulus Basin, and more broadly throughout the Internal Metamorphic Zone, the syn-extensional HT-LP metamorphic foliation (S_1) in the Jurassic cover overprints and parallels the primary sedimentary bedding (S_0) to form a S_0/S_1 foliation (e.g., Clerc & Lagabrielle, 2014; Clerc et al., 2016; Lagabrielle et al., 2016). Notably, this foliation in the hanging wall is subparallel to the detachment surface. Similar observations have been reported from other peridotite massifs in the western NPZ (Asti, Lagabrielle, et al., 2019; Corre et al., 2016; Lagabrielle et al., 2019a, 2019b), suggesting that the pre-rift cover did not experience significant tilting during rifting and crustal breakup.

Several models developed over the past few decades regarding the evolution of the so-called "magma-poor passive margins" suggest that, in the late stages of rifted margins development, pre-rift sedimentary units may locally come into tectonic contact with exhumed sub-continental mantle. For instance, interpretations of seismic sections from the north-western Iberian margin (e.g., Alves et al., 2006, 2009; Péron-Pinvidic and Manatschal, 2009; Whitmarsh et al., 2001) and field observations from fossil passive margins preserved in the Alps (e.g., Manatschal, 2004; Manatschal and Nievergelt, 1997; Mohn et al., 2012; Masini et al., 2013), indicate that pre-rift cover can be found in contact with the exhumed mantle (Figure 15a). In such cases pre-rift units are welded on their crustal basement on top of extensional allochthonous in the hanging wall of major detachment faults. However, these models cannot be directly applied to the Lherz detachment, as they imply tilting of the pre-rift sedimentary units whose bedding is at high angle to the detachment faults. This is in contrast to the subparallel attitude of the S_0/S_1 foliation in the sedimentary cover and the mantle-exhuming detachments observed in the NPZ.

10.1029/2024TC008757

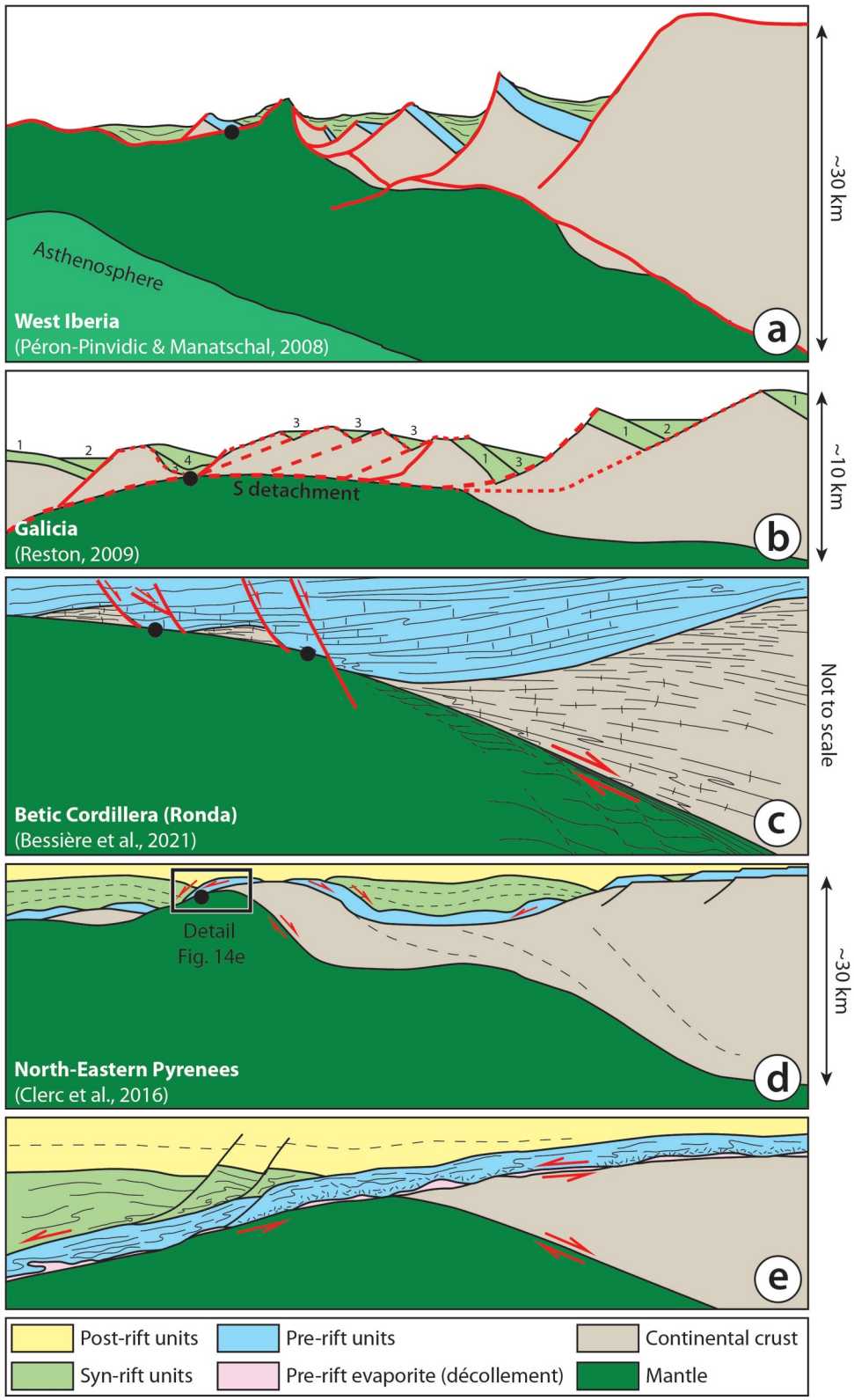

Figure 15.

A similar parallel attitude has been reported in seismic sections from the West Galicia margin and the Porcupine Basin (Figure 15b; Reston, 2005, 2009; Reston et al., 2001, 2007; Péron-Pindivic et al., 2007). In these areas, sedimentary units between faulted and tilted crustal blocks are found in tectonic contact with exhumed mantle in the hanging wall of serpentine detachment faults (referred to as P or S reflectors; Reston, 2009 and references therein). These sedimentary units exhibit internal reflectors (i.e., bedding) that are sub-parallel to the detachment fault. However, these sedimentary units are syn-rift or breakup sequences (*sensu* Soares et al., 2012; Alves & Cunha, 2018; Alves et al., 2020), and therefore do not correspond to the decoupled pre-rift units observed in the hanging wall of the Lherz detachment. Moreover, these models suggest a pervasive serpentinization of the exhumed mantle in the footwall of the detachment, which contrasts with the observation that the Lherz peridotite is very little serpentinized.

The tectonic contact between the decoupled pre-rift cover and the sub-continental mantle, along with the parallelism between the S_0/S_1 foliation in the sedimentary cover and the low-angle mantle-exhuming detachment, necessarily imply the lateral extraction of the entire continental crust during hyperextension. Extraction tectonics has been invoked as a crucial mechanism accommodating thinning in a heterogeneous continental lithosphere (e.g., Asti, Lagabrielle, et al., 2019; Clerc & Lagabrielle, 2014; Duretz et al., 2016; Jammes & Lavier, 2016; Mohn et al., 2012; Petri et al., 2019). In these scenarios, weak layers localize most of the deformation, facilitating the progressive tectonic juxtaposition of various stronger boudinaged lithospheric levels through anastomosing multi-detachment systems. Several recent studies have also documented that such kind of boudinage can also occur at upper crustal levels, particularly in cases of basement-cover decoupling along evaporite layers or due to high thermal gradients resulting from significant sedimentary burial (e.g., Clerc & Lagabrielle, 2014; Clerc et al., 2018; Duretz et al., 2020; Lagabrielle et al., 2020; Saspiturry et al., 2021a). This configuration is representative of the North Pyrenean Cretaceous extension, during which mantle exhumation occurred, and it could thus explain the tectonic juxtaposition of non-tilted decoupled pre-rift units and exhumed sub-continental mantle described in this study.

Among the existing models addressing mantle exhumation at distal passive margins, other than those developed in the last decade by studying the North Pyrenean case and highlighting the fundamental role of salt-decoupling at the base of the pre-rift cover (e.g., Asti, Lagabrielle, et al., 2019; Clerc & Lagabrielle, 2014; Clerc et al., 2016; Duretz et al., 2020; Lagabrielle et al., 2010, 2019a, 2019b), the model that aligns most closely with the observations presented in this study is the one proposed by Bessière et al. (2021) for the exhumation of the Ronda peridotite (Figure 15c). As previously mentioned, the Ronda peridotite is locally in contact with pre-rift units (the Nieves Unit Auctt.) that have experienced HT-LP metamorphism, with peak temperatures exceeding 600°C at the contact with the peridotite (Bessière et al., 2021; Lundeen, 1978; Mazzoli et al., 2013; Mazzoli and Martín-Algarra, 2011; Tubía et al., 1997). Between the allochthonous pre-rift cover and the Ronda Massif, some crustal rafts are preserved along the detachment (e.g., Bessière et al., 2021). These units have undergone syn-extensional ductile deformation and have locally reached partial melting conditions (e.g., Balanyá et al., 1997; Platt et al., 2003; Negro et al., 2006). This configuration closely resembles observations from the western NPZ (Asti, Lagabrielle, et al., 2019; Corre et al., 2016; Lagabrielle et al., 2019a, 2019b), the Aulus Basin (Asti et al., 2021) and other peridotite massifs in the NPZ (Lagabrielle et al., 2010). Bessière et al. (2021) interpret the crustal units surrounding the Ronda peridotite as ductile rafts of continental crust that were abandoned along the detachment after lateral extraction of the crust below an allochthonous pre-rift cover. This tectonic model closely matches those developed in the NPZ over the past decade, emphasizing the essential role of salt decoupling at the base of the pre-rift sedimentary cover (e.g., Clerc & Lagabrielle, 2014; Clerc et al., 2015, 2016; Asti, Lagabrielle, et al., 2019; Saspiturry et al., 2019a, 2021a; Duretz et al., 2020; Lagabrielle et al., 2020; Figures 15d and 15e). Similarly, in the Betics, hundreds of meters of Upper Triassic Keuper evaporites are found at the base of the Jurassic units (e.g., Ziegler, 1988; Flinch & Soto, 2017; Ortí et al., 2017). This salt layer likely favored decoupling between the Mesozoic sedimentary cover and its crustal basement.

Figure 15. Comparison between different models for mantle exhumation at distal passive margins locally showing tectonic contact between the exhumed lithospheric mantle and pre-to-syn-rift sedimentary units. Black dots in (a–d) show the potential location of the detachment faults analog to the one observed in the Gouffre Georges and describe in this study (see Section 5.6.2 in the text for further details). The models are redrawn and modified after: (a) Péron-Pinvidic and Manatschal (2009) for the West Iberia passive margin; (b) Reston (2009) for the Galicia passive margin; (c) Bessière et al. (2021) for the Internal Betic Cordillera paleo-passive margin; (d–e) Clerc et al. (2016) for the North-Eastern Pyrenees paleo-passive margin.

As discussed in Sections 5.3 and 5.5, observations from the Gouffre Georges indicate that the lithospheric mantle was not exhumed to the seafloor during the Cretaceous extension in the Aulus Basin. Accordingly, evidence of peridotite reworking within syn-breakup sedimentary units is extremely localized across the entire NPZ, where peridotite bodies are typically enveloped by pre-Cretaceous extension sedimentary units or stretched ductile crustal lenses (e.g., Lagabrielle et al., 2010). Both analog and numerical models suggest that mantle denudation during lithospheric extension can occur only after that the ductile layers within the lithosphere have progressively embrittled and the upper and lower lithosphere have become mechanically coupled (e.g., Brun & Beslier, 1996; Huismans & Beaumont, 2002, 2003, 2008, 2011, 2014; Lavier and Manatschal, 2006; Mohn et al., 2012; Reston and Pérez-Gussinyé, 2007). In these scenarios, detachment faults can cut through the entire lithosphere and eventually lead to mantle exhumation at the seafloor (Mohn et al., 2012; Pérez-Gussinyé and Reston, 2001; Péron-Pinvidic and Osmundsen, 2016; Reston, 2007, 2009; Tugend et al., 2024). By contrast, in cases where the upper crust remains decoupled from the upper lithospheric mantle for thermo-mechanical reasons such as in Type II margins (*sensu* Huismans & Beaumont, 2003, 2008, 2011, 2014) crustal breakup cannot occur during extension (Alves et al., 2020). Therefore, the mantle cannot be fully unroofed during continental extension as long as a ductile layer separates the uppermost crust from the lithospheric mantle. As previously pointed out by Lagabrielle et al. (2020), in cases where thick salt layers are present at the base of a thick pre-rift sedimentary pile, the uppermost layer of the lithosphere remains mechanically decoupled from the exhuming lithospheric mantle throughout the entire extensional history. This is due to the extremely weak rheology of evaporites and to the progressive heating of the base of the decoupled sedimentary cover, which progressively enters the ductile field due to significant sedimentary burial in the distal part of the rifted margins (Duretz et al., 2020; Saspiturry et al., 2021a). This scenario aligns well with the observations from the Lherz Massif presented in this study, where (a) HT ductile pre-rift units are found in the hanging wall of a mantle-exhuming detachment, (b) there is evidence of the former presence of Upper Triassic salt units at the base of the Jurassic cover, and (c) no evidence supports mantle denudation to the seafloor.

6. Conclusions

This work highlights the importance of the outcrops preserved in the Gouffre Georges. In fact, this cave exposes with spectacular continuity a major lithospheric detachment that developed during the Pyrenean Cretaceous rifting, which put in contact the exhumed sub-continental mantle with the pre-rift carbonate sedimentary cover. This type of tectonic structures have been up to now mainly described thanks to indirect geophysical data on present-day passive margins or to observation on other fossil analogs preserved in mountain belts which are however rather discontinuous. The tectonic contact preserved in the Gouffre Georges is exceptional due to its excellent exposure and the lack of tectonic inversion that might have overprinted its primary features during the Pyrenean orogenic phases.

Another major finding is the evidence for partial melting of the pre-rift carbonate cover during the Pyrenean Cretaceous rifting preserved in the Gouffre Georges. This might likely open new interesting perspectives in our understanding of partial melting in carbonate systems. Whatever the petrological interpretation of the large carbonate veins (pseudo-carbonatitic melts derived from partial melting or HT metamorphic fluids of the pre-rift carbonate cover), these represent HT fluids that have been injected in the extensional structures of the main detachment and have then been affected by brittle fracturing and cataclasis once the system underwent progressive cooling. Thus, the outcrops described in this work recorded a complex thermal history in a continuum of extensional deformation during mantle exhumation.

Observations on the extensional structures preserved in the Gouffre Georges have also important implications on the kinematics of the Pyrenean Cretaceous rifting, which is still a very debated subject. In fact, here the kinematic indicators show that, at least during the final stages of mantle exhumation, the main stretching direction was ~WNW-ESE. This is rather consistent with rifting models proposing a transtensional regime operating during the Cretaceous rifting, rather than NNE-SSW orthogonal stretching.

Finally, we have also shown that in the Gouffre Georges there is no evidence for sedimentary reworking of mantle rocks in the syn-rift sedimentary system. This observation implies that all the extensional tectonic history preserved in the cave took place under a blanket of pre- and syn-rift sediments. This means that direct observation of this kind of structures cannot be made on modern passive margins, but can only be made in fossil analogs brought to the surface by post-rifting collisional tectonics. This gives even more importance to the spectacular outcrops

preserved in the Gouffre Georges. These are, to our knowledge, unique in their kind for continuity and amount of preserved geological information. Future studies performed on this spectacular site will definitely increase our knowledge and understanding of evaporite-rich smooth-slope distal passive margins.

Data Availability Statement

The data on which this article is based are available at the following data repository: Asti et al. (2024), https://doi.org/10.6084/m9.figshare.27979907. The data set includes a Stereonet file (Allmendinger et al., 2013; Cardozo & Allmendinger, 2013) with structural data collected in the Gouffre Georges.

Acknowledgments
The following members of Spéléo Club du Haut Sabarthez (SCHS), Robert Guinot, Vincent Guinot, Irène Baîche, Laurent Danière, Michel Segondy and Maryse Guinot, are warmly acknowledged for their speleological expertise during the expedition that led to the success and safety of this scientific-speleological investigation. Vincent Guinot (SCHS) shot high-quality underground photographs during the expedition that were crucial to this work. Michal Gallay and Jozef Šupinsky, from Pavol Jozef Šafárik University in Košice, Slovakia provided their expertise in LiDAR topography. Nicolas Clément, licensed spelunking instructor at Objectif Spéléo (https://www.objectif-speleo.fr) oversaw the safety and progression of the scientific party: without his valuable support, this work would never have been possible. We thank Patrice Baby, Flora Bajolet, Philippe Boulvais, Serge Fourcade, Pierre Labaume, Yves Lagabrielle, Federico Lucci and Robert Martin for stimulating discussions and precious suggestions. Blandine Danière and Philippe de Parseval are thanked for their help on the mineralogy of the Gouffre Georges. This work was supported by the Orogen Program (BRGM + Total + CNRS-INSU; https://convergent-margins.com/orogen), by the CarTOC project (Géoazur BQRI, 2021 Grant to R. Asti), by the TelluS program of the Institut National des Sciences de l'Univers, CNRS (project ODATPyC to M. de Saint-Blanquat) and partially supported by the PE3 RETURN Project (CUP J33C22002840002). The manuscript benefitted from insightful comments and reviews by Tiago M. Alves, two anonymous reviewers and Associate Editor Laurent Jolivet. Open access publishing facilitated by Universita degli Studi di Bologna, as part of the Wiley - CRUI-CARE agreement.

References

Agrinier, P., Cornen, G., & Beslier, M.-O. (1996). Mineralogic and oxygen isotopic features of serpentinites recovered from the ocean/continent transition in the Iberia Abyssal Plain. *Proceedings of the Ocean Drilling Program, Scientific Results*, *149*, 541–552.

Albarede, F., & Michard-Vitrac, A. (1978). Age and significance of the North Pyrenean metamorphism. *Earth and Planetary Science Letters*, *40*(3), 327–332. https://doi.org/10.1016/0012-821x(78)90157-7

Allmendinger, R. W., Cardozo, N. C., & Fisher, D. (2013). *Structural geology algorithms: Vectors and tensors* (p. 289). Cambridge University Press.

Alves, T. M., & Cunha, T. A. (2018). A phase of transient subsidence, sediment bypass and deposition of regressive–transgressive cycles during the breakup of Iberia and Newfoundland. *Earth and Planetary Science Letters*, *484*, 168–183. https://doi.org/10.1016/j.epsl.2017.11.054

Alves, T. M., Fetter, M., Busby, C., Gontijo, R., Cunha, T., & Mattos, N. H. (2020). A tectono-stratigraphic review of continental breakup on intraplate continental margins and its impact on resultant hydrocarbon systems. *Marine and Petroleum Geology*, *117*, 104341. https://doi.org/10.1016/j.marpetgeo.2020.104341

Alves, T. M., Moita, C., Cunha, T., Ullnaess, M., Myklebust, R., Monteiro, J. H., & Manupella, G. (2009). Diachronous evolution of Late Jurassic-Cretaceous continental rifting in the northeast Atlantic (west Iberian margin). *Tectonics*, *28*(4), 1–32. https://doi.org/10.1029/2008TC002337

Alves, T. M., Moita, C., Sandnes, F., Cunha, T., Monteiro, J. H., & Pinheiro, L. M. (2006). Mesozoic-Cenozoic evolution of North Atlantic continental-slope basins: The Peniche basin, western Iberian margin. *AAPG Bulletin*, *90*(1), 31–60. https://doi.org/10.1306/08110504138

Andreani, M., Mével, C., Boullier, A., & Escartin, J. (2007). Dynamic control on serpentine crystallization in veins: Constraints on hydration processes in oceanic peridotites. *Geochemistry, Geophysics, Geosystems*, *8*(2), Q02012. https://doi.org/10.1029/2006gc001373

Arnaud-Vanneau, A., Arnaud, H., Charollais, J., Conrad, M.-A., Cotillon, P., Ferry, S., et al. (1979). Paléogéographie des calcaires urgoniens du sud de la France. *Géobios*, *3*, 363–383.

Asti, R., Faccenna, C., Rossetti, F., Malusà, M. G., Gliozzi, E., Faranda, C., et al. (2019). The Gediz supradetachment system (SW Turkey): Magmatism, tectonics, and sedimentation during crustal extension. *Tectonics*, *38*(4), 1414–1440. https://doi.org/10.1029/2018TC005181

Asti, R., Lagabrielle, Y., Fourcade, S., Corre, B., & Monié, P. (2019). How do continents deform during mantle exhumation? Insights from the Northern Iberia inverted Paleopassive Margin, Western Pyrenees (France). *Tectonics*, *38*(5), 2018TC005428. https://doi.org/10.1029/2018TC005428

Asti, R., Rossetti, F., Lucci, F., Poujol, M., & Lagabrielle, Y. (2021). Polyphase post- Variscan thinning of the North Pyrenean crust: Constraints from the P-T-t-deformation history of the exhumed Variscan lower crust (Saleix Massif, France). *Tectonophysics*, *820*, 229122. https://doi.org/10.1016/j.tecto.2021.229122

Asti, R., Saspiturry, N., & Angrand, P. (2022). The Mesozoic Iberia-Eurasia diffuse plate boundary: A wide domain of distributed transtensional deformation progressively focusing along the North Pyrenean Zone. *Earth-Science Reviews*, *230*, 104040. https://doi.org/10.1016/j.earscirev.2022.104040

Asti, R., Saspiturry, N., de Saint Blanquat, M., Sorriaux, P., & Ferré, E. C. (2024). Structural dataset from the Lherz detachment (Gouffre Georges, Ariège, France) [Dataset]. *FigShare*. https://doi.org/10.6084/m9.figshare.27979907

Aumar, C., Merle, O., Bosse, V., & Monié, P. (2022). Syn-rift Cretaceous deformation in the Variscan Agly Massif (Eastern Pyrenees, France). *BSGF - Earth Sci Bull*, *193*(6), 6. https://doi.org/10.1051/bsgf/2022006

Aurell, M., Fregenal-Martínez, M., Bádenas, B., Muñoz-García, M. B., Élez, J., Meléndez, N., & de Santisteban, C. (2019). Middle Jurassic–Early Cretaceous tectono-sedimentary evolution of the southwestern Iberian Basin (central Spain): Major palaeogeographical changes in the geotectonic framework of the Western Tethys. *Earth-Science Reviews*, *199*, 102983. https://doi.org/10.1016/j.earscirev.2019.102983

Avé Lallemant, H. G. (1967). Structural and petrofabric analysis of an « alpine-type » peridotite: The lherzolite of the French Pyrenees. *Leidse Geologische Mededelingen*, *42*, 1–57.

Azambre, B., & Ravier, J. (1978). Les écailles de gneiss du facies granulite du Port de Saleix et de la région de Lherz (Ariège), nouveaux témoins du socle profond des Pyrénées. *Bulletin de la Societe Geologique de France*, *S7-XX*(3), 221–228. https://doi.org/10.2113/gssgfbull.s7-xx.3.221

Balanyá, J. C., García-Dueñas, V., Azañón, J. M., & Sánchez-Gómez, M. (1997). Alternating contractional and extensional events in the Alpujarride nappes of the Alboran Domain (Betics, Gibraltar Arc). *Tectonics*, *16*(2), 226–238. https://doi.org/10.1029/96tc03871

Bartley, J. M., & Wernicke, B. P. (1984). The Snake Range décollement interpreted as a major extensional shear zone. *Tectonics*, *3*(6), 647–657. https://doi.org/10.1029/TC003i006p00647

Beaugey, M. (1889). Inclusions d'anhydrite dans les quartz bipyramidés des argiles salifères pyrénéennes. *Bulletin de Mineralogie*, *12–6*, 396–398.

Berthé, D., Choukroune, P., & Jégouzo, P. (1979). Orthogneiss, mylonite and non coaxial deformation of granites: The example of the South Armorican Shear Zone. *Journal of Structural Geology*, *1*(1), 31–42. https://doi.org/10.1016/0191-8141(79)90019-1

Bessière, E., Augier, R., Jolivet, L., Précigout, J., & Romagny, A. (2021). Exhumation of the Ronda peridotite during hyper-extension: New structural and thermal constraints from the Nieves Unit (western Betic Cordillera, Spain). *Tectonics*, *40*(10), e2020TC006271. https://doi.org/10.1029/2020TC006271

Beyssac, O., Goffé, B., Chopin, C., & Rouzaud, J. N. (2002). Raman spectra of carbonaceous material in metasediments: A new geothermometer. *Journal of Metamorphic Geology*, *20*(9), 859–871. https://doi.org/10.1046/j.1525-1314.2002.00408.x

Biteau, J. J., Marrec, A. L., Vot, M. L., & Masset, J. M. (2006). The Aquitaine Basin. *Petroleum Geoscience*, *12*, 247–273. https://doi.org/10.1144/1354-079305-674

Boillot, G., Recq, M., Winterer, E. L., Meyer, A., Applegate, J., Baltuck, M., et al. (1987). Tectonic denudation of the upper mantle along passive margins: A model based on drilling results (ODP Leg 103, western Galicia margin, Spain). *Tectonophysics*, *132*(4), 335–342. https://doi.org/10.1016/0040-1951(87)90352-0

Boschi, C., Fruh-Green, G. L., Delacour, A., Karson, J. A., & Kelley, D. S. (2006). Mass transfer and fluid flow during detachment faulting and development of an oceanic core complex, Atlantis Massif (MAR 30°N). *Geochemistry, Geophysics, Geosystems*, *7*(1), Q01004. https://doi.org/10.1029/2005GC001074

Boulvais, P. (2016). Fluid generation in the Boucheville Basin as a consequence of the North Pyrenean metamorphism. *Comptes Rendus Geoscience*, *348*(3–4), 301–311. https://doi.org/10.1016/j.crte.2015.06.013

Brun, J. P., & Beslier, M. O. (1996). Mantle exhumation at passive margin. *Earth and Planetary Science Letters*, *142*(1–2), 161–173. https://doi.org/10.1016/0012-821x(96)00080-5

Brune, S., Heine, C., Clift, P. D., & Pérez-Gussinyé, M. (2017). Rifted margin architecture and crustal rheology: Reviewing Iberia-Newfoundland, Central South Atlantic, and South China Sea. *Marine and Petroleum Geology*, *79*, 257–281. https://doi.org/10.1016/j.marpetgeo.2016.10.018

Brune, S., Heine, C., Pérez-Gussinyé, M., & Sobolev, S. V. (2014). Rift migration explains continental margin asymmetry and crustal hyperextension. *Nature Communications*, *5*(1), 4014. https://doi.org/10.1038/ncomms5014

Brunet, M. F. (1984). Subsidence history of the Aquitaine Basin determined from subsidence curves. *Geological Magazine*, *121*(5), 421–428. https://doi.org/10.1017/s0016756800029952

Brunet, M. F. (1994). Subsidence in the Parentis Basin (Aquitaine, France): Implications of the thermal evolution. In A. MASCLE (Ed.), *Hydrocarbon exploration and underground gas storage in France* (Vol. 4, pp. 187–198). Springer Verlag. https://doi.org/10.1007/978-3-642-78849-9_14

Burkhard, M. (1993). Calcite twins, their geometry, appearance and significance as stress–strain markers and indicators of tectonic regime: A review. *Journal of Structural Geology*, *15*(3–5), 351–368. https://doi.org/10.1016/0191-8141(93)90132-t

Calvet, F., & Lucas, C., (coord.) (2001). Trias. In A. Barnolas & J. C. Chiron (Eds.), *Synthèse géologique et géophysique des Pyrénées* (Vol. 2, pp. 22–73). BRGM - ITGE.

Canérot, J. (1988). Manifestations de l'halocinèse dans les Chaînons Béarnais (Zone Nord-Pyrénéenne) au Crétacé inférieur. *Comptes Rendus De L'académie Des Sciences Paris*, *306*, 1099–1102.

Canérot, J. (1989). Rifting éocrétacé et halocinèse sur la marge ibérique des Pyrénées Occidentales (France). Conséquences structurales. *Bulletin des Centres de Recherches Exploration-Production Elf-Aquitaine*, *13*, 87–99.

Canérot, J., (2008). Les Pyrénées: Histoire géologique: Atlantica-BRGM.

Canérot, J. (2017). The pull apart-type Tardets-Mauléon Basin, a key to understand the formation of the Pyrenees. *Bulletin de la Societe Geologique de France*, *188*(6), 35. https://doi.org/10.1051/bsgf/2017198

Canérot, J., Hudec, M. R., & Rockenbauch, K. (2005). Mesozoic diapirism in the Pyrenean orogen: Salt tectonics on a transform plate boundary. *AAPG Bulletin*, *89*(2), 211–229. https://doi.org/10.1306/09170404007

Canérot, J., & Mediavilla, F. (2023). The Mid-Albian unconformity, a key to understand the geodynamics of the North Pyrenean Trough. *BSGF-Earth-Sciences Bulletin*, *194*, 4. https://doi.org/10.1051/bsgf/2023001

Cannat, M., Fontaine, F., & Escartín, J. (2010). Serpentinization and associated hydrogen and methane fluxes at slow spreading ridges. In P. A. Rona, C. W. Devey, J. Dyment, & B. J. Murton (Eds.), *Geophysical monograph* (pp. 241–264). American Geophysical Union. https://doi.org/10.1029/2008gm000760

Cardozo, N. C., & Allmendinger, R. W. (2013). Spherical projections with OSXStereonet. *Computer & Geosciences*, *51*, 193–205. https://doi.org/10.1016/j.cageo.2012.07.021

Chakhmouradian, A. R., Reguir, E. P., & Zaitsev, A. N. (2016). Calcite and dolomite in intrusive carbonatites. I. Textural variations. *Mineralogy and Petrology*, *110*(2–3), 333–360. https://doi.org/10.1007/s00710-015-0390-6

Chelalou, R., Nalpas, T., Bousquet, R., Prevost, M., Lahfid, A., Poujol, M., et al. (2016). New sedimentological, structural and paleo-thermicity data in the Boucheville Basin (eastern North Pyrenean Zone, France). *Comptes Rendus Geoscience*, *348*(3–4), 312–321. https://doi.org/10.1016/j.crte.2015.11.008

Choukroune, P. (1973). *La brèche de Lherz dite "d'explosion liée à la mise en place des lherzolites" est une brèche sédimentaire d'âge cénozoïque* (Vol. 277, pp. 2621–2624). C. R. Acad. Sci.

Choukroune, P. (1976). Structure et évolution tectonique de la zone Nord-pyrénéenne. Analyse de la déformation dans une portion de chaîne a schistosité sub-verticale. *Mem. Soc. Géol. France*, *55*, 1–116.

Choukroune, P., & Mattauer, M. (1978). Tectonique des plaques et Pyrénées: Sur le fonctionnement de la faille transformante nord-Pyrénéenne; comparaisons avec les modèles actuels. *Bulletin de la Societe Geologique de France*, *20*, 689–700.

Clerc, C. (2012). Evolution du domaine nord-pyrénéen au Crétacé: Amincissement crustal extrême et thermicité élevée: Un analogue pour les marges passives PhD Thesis. Université Paris 6.

Clerc, C., Boulvais, P., Lagabrielle, Y., & de Saint Blanquat, M. (2014). Ophicalcites from the northern Pyrenean belt: A field, petrographic and stable isotope study. *International Journal of Earth Sciences*, *103*(1), 141–163. https://doi.org/10.1007/s00531-013-0927-z

Clerc, C., & Lagabrielle, Y. (2014). Thermal control on the modes of crustal thinning leading to mantle exhumation: Insights from the Cretaceous Pyrenean hot paleomargins. *Tectonics*, *33*(7), 1340–1359. https://doi.org/10.1002/2013TC003471

Clerc, C., Lagabrielle, Y., Labaume, P., Ringenbach, J. C., Vauchez, A., Nalpas, T., et al. (2016). Basement – Cover decoupling and progressive exhumation of metamorphic sediments at hot rifted margin. insights from the Northeastern Pyrenean analog. *Tectonophysics*, *686*, 82–97. https://doi.org/10.1016/j.tecto.2016.07.022

Clerc, C., Lagabrielle, Y., Neumaier, M., Reynaud, J. Y., & de Saint Blanquat, M. (2012). Exhumation of subcontinental mantle rocks: Evidence from ultramafic-bearing clastic deposits nearby the Lherz peridotite body, French Pyrenees. *Bulletin de la Societe Geologique de France*, *183*(5), 443–459. https://doi.org/10.2113/gssgfbull.183.5.443

Clerc, C., Lahfid, A., Monie, P., Lagabrielle, Y., Chopin, C., Poujol, M., et al. (2015). High-temperature metamorphism during extreme thinning of the continental crust: A reappraisal of the North Pyrenean passive paleomargin. *Solid Earth*, *6*(2), 643–668. https://doi.org/10.5194/se-6-643-2015

Clerc, C., Ringenbach, J. C., Jolivet, L., & Ballard, J. F. (2018). Rifted margins: Ductile deformation, boudinage, continentward-dipping normal faults and the role of the weak lower crust. *Gondwana Research*, *53*, 20–40. https://doi.org/10.1016/j.gr.2017.04.030

Cooper, F. J., Platt, J. P., Anczkiewicz, R., & Whitehouse, M. J. (2010). Footwall dip of a core complex detachment fault: Thermobarometric constraints from the northern Snake Range (Basin and Range, USA). *Journal of Metamorphic Geology*, *28*(9), 997–1020. https://doi.org/10.1111/j.1525-1314.2010.00907.x

Corre, B. (2017). La bordure nord de la plaque ibérique à l'Albo-Cénomanien: Architecture d'une marge passive de type ductile (Chaînons Béarnais. Pyrénées Occidentales) PhD Thesis. (Vol. *1*). Université Rennes.

Corre, B., Boulvais, P., Boiron, M. C., Lagabrielle, Y., Marasi, L., & Clerc, C. (2018). Fluid circulations in response to mantle exhumation at the passive margin setting in the North Pyrenean Zone, France. *Mineralogy and Petrology*, *112*(5), 647–670. https://doi.org/10.1007/s00710-018-0559-x

Corre, B., Lagabrielle, Y., Labaume, P., Fourcade, S., Clerc, C., & Ballevre, M. (2016). Deformation associated with mantle exhumation in a distal, hot passive margin environment: New constraints from the Saraillé Massif (Chaînons Béarnais, North-Pyrenean Zone). *Comptes Rendus Geoscience*, *348*(3–4), 279–289. https://doi.org/10.1016/j.crte.2015.11.007

Curnelle, R. (1983). Evolution structuro-sédimentaire du Trias et de l'Infra-Lias d'Aquitaine. *Bulletin des Centres de Recherches Exploration-Production Elf-Aquitaine*, *7*(1), 69–99.

Dauteuil, O., Raymond, D., & Ricou, L. E. (1987). Brèches de fracturation hydraulique dans la zone métamorphique des Pyrénées, exemple à l'Est du Saint-Barthélemy. *C. R. Acad. Sci. Paris, Ser. II*, *304*, 1025–1028.

Debrand-Passard, S., (coord.) (2001). Jurassique. In A. Barnolas & J. C. Chiron (Eds.), *Synthèse géologique et géophysique des Pyrénées* (Vol. 2, pp. 22–73). BRGM - ITGE.

Debroas, E. J. (1978). Evolution de la fosse du flysch ardoisier de l'Albien supérieur au Sénonien inferieur (zone interne metamorphique des Pyrénées navarrolanguedociennes). *Bull. Société Géologique Fr*, *7*(5), 639–648. https://doi.org/10.2113/gssgfbull.s7-xx.5.639

Debroas, E. J. (1987). Modèle de basin triangulaire à l'intersection de décrochements divergents pour le fossé albo-cénomanien de la Ballongue (Zone Nord-pyrénéenne, France). *Bull. Soc. Géol. France*, *8*(III), 887–898.

Debroas, E. J. (1990). Le Flysch noir albo-cénomanien témoin de la structuration albienne à sénonienne de la zone nord-pyrénéenne en Bigorre (Hautes-Pyrénées, France). *Bull. Soc. Géol. France*, *8*(VI), 273–285. https://doi.org/10.2113/gssgfbull.vi.2.273

Debroas, E. J. (1995). Flysch noir et rifting oblique albo-cénomanien sur la marge aquitaine du sillon nord-pyrénéen - Séance spécialisée de la Soc. géol. France " Le Bassin d'Aquitaine, évolution sédimentaire et structurale", Toulouse, 18 Septembre 1995. *Strata Toulouse, sér.*, *1*(7), 21–23.

Debroas, E. J., & Azambre, B. (2012). Des brèches aux lherzolites, la mise en place des lherzolites dans les fossés du Flysch noir albo-cénomanien de la Ballongue et d'Aulus (Zone nord-pyrénéenne, Ariège). In *AGSO, Livret-guide d'excursion, 09 et 10 Juin 2012* (p. 120). en dépôt à la SGF et Géol. France, 3.

Debroas, E. J., Canérot, J., & Bilotte, M. (2010). Les brèches d'Urdach, témoins de l'exhumation du manteau pyrénéen dans un escarpement de faille vraconnien-cénomanien inférieur (Zone nord-pyrénéenne, Pyrénées-Atlantiques, France). *Géol. Fr*, *2*, 53–63.

Debroas, E. J., Canérot, J., & Bilotte, M. (2013). Comment on: "Exhumation of subcontinental mantle rocks: Evidence from ultramafic-bearing clastic deposits nearby the Lherz peridotite body, French Pyrenees" by C. Clerc et al. *Bull. Soc. Géol. France*, *184*(6), 621–629. https://doi.org/10.2113/gssgfbull.184.6.621

DeFelipe, I., Pedreira, D., Pulgar, J. A., Iriarte, E., & Mendia, M. (2017). Mantle exhumation and metamorphism in the Basque-Cantabrian Basin (N Spain): Stable and clumped isotope analysis in carbonates and comparison with ophicalcites in the North-Pyrenean Zone (Urdach and Lherz). *Geochemistry, Geophysics, Geosystems*, *18*(2), 631–652. https://doi.org/10.1002/2016gc006690

Delfaud, J., & Henry, J. (1967). *Evolution des bassins jurassiques dans la zone nord-pyrénéenne occidentale* (pp. 75–80). 64ème Congrès AFAS.

Desmurs, L., Manatschal, G., & Bernoulli, D. (2001). The Steinmann Trinity revisited: Mantle exhumation and magmatism along an ocean-continent transition: The Platta nappe, eastern Switzerland. In R. C. L. Wilson, R. B. Whitmarsh, B. Taylor, & N. Froitzheim (Eds.), *Non-volcanic rifting of continental margins: A comparison of evidence from land and sea*, *Geological Society of London, Special Publications* (Vol. 187(1), pp. 235–266). https://doi.org/10.1144/gsl.sp.2001.187.01.12

Dobson, D. P., Jones, A. P., Rabe, R., Sekine, T., Kurita, K., Taniguchi, T., et al. (1996). In-situ measurement of viscosity and density of carbonate melts at high pressure. *Earth and Planetary Science Letters*, *143*(1–4), 207–215. https://doi.org/10.1016/0012-821x(96)00139-2

Ducoux, M., Jolivet, L., Callot, J.-P., Aubourg, C., Masini, E., Lahfid, A., et al. (2019). The Nappe des Marbres unit of the Basque-Cantabrian basin: The tectono-thermal evolution of a fossil hyperextended rift basin. *Tectonics*, *38*(11), 3881–3915. https://doi.org/10.1029/2018TC005348

Ducoux, M., Jolivet, L., Masini, E., Augier, R., Lahfid, A., Bernet, M., & Calassou, S. (2021). Distribution and intensity of high-temperature low-pressure metamorphism across the Pyrenean-Cantabrian belt: Constraints on the thermal record of the pre-orogenic hyperexten-sion rifting. *BSGF - Earth Sciences Bulletin*, *192*, 43. https://doi.org/10.1051/bsgf/2021029

Duée, G., Lagabrielle, Y., Coutelle, A., & Fortané, A. (1984). Les lherzolites associées aux Chaînons Béarnais (Pyrénées Occidentales): Mise à l'affleurement anté-dogger et resédimentation albo-cénomanienne. *Comptes-rendus des séances de l'Académie des sciences. Série 2, Mécanique-physique, chimie, sciences de l'univers, sciences de la terre*, *299*(17), 1205–1210.

Durand, C., Baumgartner, L. P., & Marquer, D. (2015). Low melting temperature for calcite at 1000 bars on the join $CaCO_3$ – H_2O – Some geological implications. *Terra Nova*, *27*(5), 364–369. https://doi.org/10.1111/ter.12168

Duretz, T., Asti, R., Lagabrielle, Y., Brun, J. P., Jourdon, A., Clerc, C., & Corre, B. (2020). Numerical modelling of syn-rift salt tectonics during Cretaceous Pyrenean Rifting. *Basin Research*, 1–16. https://doi.org/10.1111/bre.12389

Duretz, T., Petri, B., Mohn, G., Schmalholz, S. M., Schenker, F. L., & Müntener, O. (2016). The importance of structural softening for the evolution and architecture of passive margins. *Scientific Reports*, *6*(1), 38704. https://doi.org/10.1038/srep38704

Escartín, J., Mével, C., Petersen, S., Bonnemains, D., Cannat, M., Andreani, M., et al. (2017). Tectonic structure, evolution, and the nature of oceanic core complexes and their detachment fault zones (13°20'N and 13°30'N, Mid Atlantic Ridge). *Geochemistry, Geophysics, Geosystems*, *18*(4), 1451–1482. https://doi.org/10.1002/2016GC006775

Espurt, N., Angrand, P., Teixell, A., Labaume, P., Ford, M., de Saint Blanquat, M., & Chevrot, S. (2019). Crustal-scale balanced cross-section and restorations of the Central Pyrenean belt (Nestes-Cinca transect): Highlighting the structural control of Variscan belt and Permian-Mesozoic rift systems on mountain building. *Tectonophysics*, *764*, 25–45. https://doi.org/10.1016/j.tecto.2019.04.026

Fabriès, J., Lorand, J. P., & Bodinier, J. L. (1998). Petrogenetic evolution of orogenic lherzolite massifs in the central and western Pyrenees. *Tectonophysics*, *292*(1–2), 145–167. https://doi.org/10.1016/S0040-1951(98)00055-9

Fabriès, J., Lorand, J. P., Bodinier, J. L., & Dupuy, C. (1991). Evolution of the upper mantle beneath the pyrenees: Evidence from orogenic spinel lherzolite massifs. *Journal of Petrology*, Special_Volume(2), 55–76. https://doi.org/10.1093/petrology/Special_Volume.2.5

Ferrill, D. A. (1991). Calcite twin widths and intensities as metamorphic indicators in natural low-temperature deformation of limestone. *Journal of Structural Geology*, *13*(6), 667–675. https://doi.org/10.1016/0191-8141(91)90029-i

Flinch, J. F., & Soto, J. I. (2017). Allochthonous triassic and salt tectonic processes in the betic-rif orogenic arc. In *Permo-triassic salt provinces of europe, north africa and the atlantic margins* (pp. 417–446). https://doi.org/10.1016/b978-0-12-809417-4.00020-3

Floess, D., Baumgartner, L. P., & Vonlanthen, P. (2015). An observational and thermodynamic investigation of carbonate partial melting. *Earth and Planetary Science Letters*, *409*, 147–156. https://doi.org/10.1016/j.epsl.2014.10.031

Fortané, A., Duée, G., Lagabrielle, Y., & Coutelle, A. (1986). Lherzolites and the western "Chaînons Béarnais" (French Pyrenees): Structural and paleogeographical pattern. *Tectonophysics*, *129*(1–4), 81–98. https://doi.org/10.1016/0040-1951(86)90247-7

Froitzheim, N., & Manatschal, G. (1996). Kinematics of Jurassic rifting, mantle exhumation, and passive-margin formation in the Austroalpine and Penninic nappes (eastern Switzerland). *Geological Society of America Bulletin*, *108*(9), 1120–1133. https://doi.org/10.1130/0016-7606(1996)108<1120:kojrme>2.3.co;2

Ganino, C., & Arndt, N. T. (2009). Climate changes cause by degassing of sediments during the emplacement of large igneous provinces. *Geology*, *37*(4), 323–326. https://doi.org/10.1130/g25325a.1

Ganino, C., Arndt, N. T., Chauvel, C., Jean, A., & Athurion, C. (2013). Melting of carbonate wall rocks and formation of the heteregeneous aureole of the Panzhihua intrusion, China. *Geoscience Frontiers*, *4*(5), 535–546. https://doi.org/10.1016/j.gsf.2013.01.012

García-Senz, J., Rosales, I., Muñoz, J. A., Robador, A., & Pedrera, A. (2019). The North Iberian continental margin. In C. Quesada & J. T. Oliveira (Eds.), *The geology of Iberia: A geodynamic approach* (Vol. 5, pp. 171–190). Springer.

Gittins, J., & Tuttle, O. F. (1964). The system CaF_2-$Ca(OH)_2$-$CaCO_3$. *American Journal of Science*, *262*(1), 66–75. https://doi.org/10.2475/ajs.262.1.66

Golberg, J.-M. (1987). Le métamorphisme mésozoïque dans la partie orientale des Pyrénées: Relation avec l'évolution de la chaîne au Crétacé. In *Doc. Trav. Centre Geol. Geophys. Montpellier*. Université des Sciences et Techniques du Languedoc.

Golberg, J. M., & Leyreloup, A. F. (1990). High temperature-low pressure Cretaceous metamorphism related to crustal thinning (Eastern North Pyrenean Zone, France). *Contributions to Mineralogy and Petrology*, *104*(2), 194–207. https://doi.org/10.1007/BF00306443

Golberg, J. M., & Maluski, H. (1988). Données nouvelles et mise au point sur l'âge du métamorphisme pyrénéen. *CR Acad. Sci. Paris*, *306*(II), 429–435.

Golberg, J. M., Maluski, H., & Leyreloup, A. F. (1986). Petrological and age relationship between emplacement of magmatic breccia, alkaline magmatism, and static metamorphism in the North Pyrenean Zone. *Tectonophysics*, *129*(1–4), 275–290. https://doi.org/10.1016/0040-1951(86)90256-8

Gómez, J. J., Sandoval, J., Aguado, R., O'Dogherty, L., & Osete, M. L. (2019). The alpine cycle in eastern Iberia: Microplate units and geodynamic stages. In C. Quesada & J. Oliveira (Eds.), *The geology of Iberia: A geodynamic approach* (pp. 15–27). Regional Geology Reviews. Springer.

Hall, C. A., & Bennett, V. C. (1979). Significance of lherzolite at the Etang de Lherz, Central Pyrenees, southern France. *Earth and Planetary Science Letters*, *45*(2), 349–354. https://doi.org/10.1016/0012-821x(79)90135-3

Hart, N. R., Stockli, D. F., Lavier, L. L., & Hayman, N. W. (2017). Thermal evolution of a hyperextended rift basin, Mauléon Basin, western Pyrenees: Thermal evolution of hyperextended rift. *Tectonics*, *36*(6), 1103–1128. https://doi.org/10.1002/2016TC004365

Henry, P., Azambre, B., Montigny, R., Rossy, M., & Stevenson, R. K. (1998). Late mantle evolution of the Pyrenean sub-continental lithospheric mantle in the light of new 40Ar-39Ar and Sm-Nd ages on pyroxenites and peridotites (Pyrenees, France). *Tectonophysics*, *296*(1–2), 103–123. https://doi.org/10.1016/S0040-1951(98)00139-5

Hode Vuorinen, J. H., & Skelton, A. D. L. (2004). Origin of silicate minerals in carbonatites from Alnö Island, Sweden: Magmatic crystallization or wall rock assimilation? *Terra Nova*, *16*(4), 210–215. https://doi.org/10.1111/j.1365-3121.2004.00557.x

Huismans, R. S., & Beaumont, C. (2002). Asymmetric lithospheric extension; the role of frictional plastic strain softening inferred from numerical experiments. *Geology*, *30*(3), 211–214. https://doi.org/10.1130/0091-7613(2002)030<0211:aletro>2.0.co;2

Huismans, R. S., & Beaumont, C. (2003). Symmetric and asymmetric lithospheric extension: Relative effects of frictional-plastic and viscous strain softening. *Journal of Geophysical Research*, *108*(B10), 1–22. https://doi.org/10.1029/2002JB002026

Huismans, R. S., & Beaumont, C. (2008). Complex rifted continental margins explained by dynamical models of depth-dependent lithospheric extension. *Geology*, *36*(2), 163. https://doi.org/10.1130/G24231A.1

Huismans, R. S., & Beaumont, C. (2011). Depth-dependent extension, two-stage breakup and cratonic underplating at rifted margins. *Nature*, *473*(7345), 74–78. https://doi.org/10.1038/nature09988

Huismans, R. S., & Beaumont, C. (2014). Rifted continental margins: The case for depth-dependent extension. *Earth and Planetary Science Letters*, *407*, 148–162. https://doi.org/10.1016/j.epsl.2014.09.032

Jackson, M. P. A., Hudec, M. R., Jackson, M. P. A., & Hudec, M. R. (2017). Extensional salt-tectonic systems. In *Salt tectonics* (pp. 256–303). Cambridge University Press. https://doi.org/10.1017/9781139003988.014

James, V. (1998). *La plate-forme carbonatée ouest-pyrénéenne au jurassique moyen et supérieur stratigraphie séquentielle, stades d'évolution, relations avec la subsurface en aquitaine méridionale*. PhD Thesis (p. 417). Université Paul Sabatier de Toulouse.

Jammes, S., & Lavier, L. L. (2016). The effect of bimineralic composition on extensional processes at lithospheric scale. *Geochemistry, Geophysics, Geosystems*, *17*(8), 3375–3392. https://doi.org/10.1002/2016gc006399

Jammes, S., Manatschal, G., Lavier, L., & Masini, E. (2009). Tectonosedimentary evolution related to extreme crustal thinning ahead of a propagating ocean: Example of the western Pyrenees. *Tectonics*, *28*(4), TC4012. https://doi.org/10.1029/2008T.C002406

Karson, J., Früh-Green, G., Kelley, D. S., Williams, E., Yoerger, D. R., & Jakuba, M. (2006). Detachment shear zone of the Atlantis Massif core complex, Mid-Atlantic Ridge, 30 N. *Geochemistry, Geophysics, Geosystems*, *7*(6). https://doi.org/10.1029/2005gc001109

Kelemen, P. B., Aines, R., Bennett, E., Benson, S. M., Carter, E., Coggon, J. A., et al. (2018). In situ carbon mineralization in ultramafic rocks: Natural processes and possible engineered methods. *Energy Procedia*, *146*, 92–102. https://doi.org/10.1016/J.EGYPRO.2018.07.013

Kelemen, P. B., & Matter, J. (2008). In situ carbonation of peridotite for CO_2 storage. *Proceedings of the National Academy of Sciences*, *105*(45), 17295–17300. https://doi.org/10.1073/pnas.0805794105

Kruk, A., & Sokol, A. (2022). Role of volatiles in the evolution of a carbonatitic melt in peridotitic mantle: Experimental constraints at 6.3 GPa and 1200–1450° C. *Minerals*, *12*(4), 466. https://doi.org/10.3390/min12040466

Labaume, P., & Teixell, A. (2020). Evolution of salt structures of the Pyrenean rift (Chaînons Béarnais, France): From hyper-extension to tectonic inversion. *Tectonophysics*, *785*, 228451. https://doi.org/10.1016/j.tecto.2020.228451

Lacroix, A. (1894). Etude minéralogie de la lherzolite des Pyrénées et de ses phénomènes de contact. *Nouv. Arch. Mus. Hist. Paris*, *6*, 204–308.

Lacroix, A. (1895). Les phénomènes de contact de la lherzolite et de quelques ophites des Pyrénées. *Bull. Serv. Carte géol. France*, *42*(VI), 307–446.

Lacroix, A. (1900). Sur l'origine des brèches calcaires secondaires de l'Ariège: conséquences à en tirer au point de vue de l'âge de la lherzolite. *C. R. Acad. Sci. Paris*, *131*, 396–398.

Lagabrielle, Y., Asti, R., Duretz, T., Clerc, C., Fourcade, S., Teixell, A., et al. (2020). A review of cretaceous smooth-slopes extensional basins along the Iberia-Eurasia plate boundary: How pre-rift salt controls the modes of continental rifting and mantle exhumation. *Earth-Science Reviews*, *201*, 103071. https://doi.org/10.1016/j.earscirev.2019.103071

Lagabrielle, Y., Asti, R., Fourcade, S., Corre, B., Poujol, M., Uzel, J., et al. (2019a). Mantle exhumation at magma-poor passive continental margins. Part I. 3D architecture and metasomatic evolution of a fossil exhumed mantle domain (Urdach lherzolite, North-Western Pyrenees, France). *BSGF - Earth Sci. Bull*, *190*, 8. https://doi.org/10.1051/bsgf/2019007

Lagabrielle, Y., Asti, R., Fourcade, S., Corre, B., Uzel, J., Labaume, P., et al. (2019b). Mantle exhumation at magma-poor passive continental margins. Part II. Tectonic and metasomatic evolution of large displacement detachment faults preserved in a fossil distal margin domain (Saraillé lherzolites, north-western Pyrenees, France). *BSGF - Earth Sci. Bull*, *190*(1), 14. https://doi.org/10.1051/bsgf/2019013

Lagabrielle, Y., & Bodinier, J.-L. (2008). Submarine reworking of exhumed subcontinental mantle rocks: Field evidence from the Lherz peridotite, French Pyrenees. *Terra Nova*, *20*(1), 11–21. https://doi.org/10.1111/j.1365-3121.2007.00781.x

Lagabrielle, Y., Clerc, C., Vauchez, A., Lahfid, A., Labaume, P., Azambre, B., et al. (2016). Very high geothermal gradient during mantle exhumation recorded in mylonitic marbles and carbonate breccias from a Mesozoic Pyrenean palaeomargin (Lherz area, North Pyrenean Zone, France). *Comptes Rendus Géosci*, *348*(3–4), 290–300. From rifting to mountain building: the Pyrenean Belt. https://doi.org/10.1016/j.crte.2015.11.004

Lagabrielle, Y., Labaume, P., & de Saint Blanquat, M. (2010). Mantle exhumation, crustal denudation, and gravity tectonics during Cretaceous rifting in the Pyrenean realm (SW Europe): Insights from the geological setting of the lherzolite bodies. *Tectonics*, *29*(4), 1–26. https://doi.org/10.1029/2009TC002588

Lamare, P. (1936). *Recherches géologiques dans les Pyrénées basques d'Espagne*. Société géologique de France.

Larsen, H. C., Mohn, G., Nirrengarten, M., Sun, Z., Stock, J., Jian, Z., et al. (2018). Rapid transition from continental breakup to igneous oceanic crust in the South China Sea. *Nature Geoscience*, *11*(10), 782–789. https://doi.org/10.1038/s41561-018-0198-1

Lavier, L. L., & Manatschal, G. (2006). A mechanism to thin the continental lithosphere at magma-poor margins. *Nature*, *440*(7082), 324–328. https://doi.org/10.1038/nature04608

Lehujeur, M., Chevrot, S., Villasenor, A., Masini, E., Saspiturry, N., Lescoutre, R., & Sylvander, S. (2021). Three-dimensional shear velocity structure of the Mauleon and Arzacq basins (western Pyrenees). *BSGF - Earth Sciences Bulletin*, *192*(1), 47. https://doi.org/10.1051/bsgf/2021039

Lemoine, M., Tricart, P., & Boillot, G. (1987). Ultramafic and gabbroic ocean floor of the Ligurian Tethys (Alps, Corsica, Apennines): In search of a genetic model. *Geology*, *15*(7), 622. https://doi.org/10.1130/0091-7613(1987)15<622:uagofo>2.0.co;2

Lenoble, J.-L. (1992). *Les plates-formes carbonatées ouest pyrénéennes du dogger a l'Albien, stratigraphie séquentielle et évolution géodynamique*. Université Paul Sabatier de Toulouse (Sciences).

Lentz, D. R. (1999). Carbonatite genesis: A reexamination of the role of intrusion-related pneumatolytic skarn processes in limestone melting. *Geology*, *27*(4), 335–338. https://doi.org/10.1130/0091-7613(1999)027<0335:cgarot>2.3.co;2

Le Roux, V., Bodinier, J. L., Tommasi, A., Alard, O., Dautria, J. M., Vauchez, A., & Riches, A. J. V. (2007). The Lherz spinel lherzolite: Refertilized rather than pristine mantle. *Earth and Planetary Science Letters*, *259*(3–4), 599–612. https://doi.org/10.1016/j.epsl.2007.05.026

Lescoutre, R., & Manatschal, G. (2020). Role of rift-inheritance and segmentation for orogenic evolution: Example from the Pyrenean-Cantabrian system. *BSGF - Earth Sciences Bulletin*, *191*(1), 18. https://doi.org/10.1051/bsgf/2020021

Lescoutre, R., Tugend, J., Brune, S., Masini, E., & Manatschal, G. (2019). Thermal evolution of asymmetric hyperextended magma-poor rift systems: Results from numerical modeling and Pyrenean field observations. *Geochemistry, Geophysics, Geosystems*, *20*(10), 4567–4587. https://doi.org/10.1029/2019gc008600

Letargo, C. M. R., Lamb, W. M., & Park, J. S. (1995). Comparison of calcite+dolomite thermometry and carbonate+silicate equilibria: Constraints on the conditions of metamorphism of the Llano uplift, central Texas, U.S.A. *American Mineralogist*, *80*(1–2), 131–143. https://doi.org/10.2138/am-1995-1-213

Lister, G. S., & Davis, G. A. (1989). The origin of metamorphic core complexes and detachment faults formed during Tertiary continental extension in the northern Colorado River region, U.S.A. *Journal of Structural Geology*, *11*(1-2), 65–94. https://doi.org/10.1016/0191-8141(89)90036-9

Lundeen, M. T. (1978). Emplacement of the Ronda peridotite, Sierra Bermeja, Spain. *The Geological Society of America Bulletin*, *89*(2), 172. https://doi.org/10.1130/0016-7606(1978)89<172:eotrps>2.0.co;2

Mahé, S. (2013). Etude de la fracturation et de la déformation d'un massif rocheux aux abords d'une faille d'échelle crustale dans le cadre du tracé du tunnel routier de Saint-Béat. In *Université de Montpellier 2: thèse de doctorat (PhD thesis), Géosciences*. Retrieved from https://ged.biu-montpellier.fr/florabium/jsp/nnt.jsp?nnt=2013MON20254

Manatschal, G. (2004). New models for evolution of magma-poor rifted margins based on a review of data and concepts from West Iberia and the Alps. *International Journal of Earth Sciences*, *93*(3), 432–466. https://doi.org/10.1007/s00531-004-0394-7

Manatschal, G., Chenin, P., Lescoutre, R., Miró, J., Cadenas, P., Saspiturry, N., et al. (2021). The role of inheritance in forming rifts and rifted margins and building collisional orogens: A Biscay-Pyrenean perspective. *BSGF - Earth Sciences Bulletin*, *192*, 55. https://doi.org/10.1051/bsgf/2021042

Manatschal, G., & Nievergelt, P. (1997). A continent-ocean transition recorded in the Err and Platta nappes (Eastern Switzerland). *Eclogae Geologicae Helvetiae*, *90*, 3–27.

Manatschal, G., Sutra, E., & Péron-Pinvidic, G. (2010). The lesson from the Iberia-Newfoundland rifted margins: How applicable is it to other rifted margins? In *Proceedings 2nd Central and North Atlantic conjugate margins, rediscovering the Atlantic, new insights, new winds for an old sea 2* (pp. 27–37).

Martín-Chivelet, J., López-Gómez, J., Aguado, R., Arias, C., Arribas, J., Arribas, M. E., et al. (2019). The late Jurassic–Early cretaceous rifting. In C. Quesada & J. T. Oliveira (Eds.), *The geology of Iberia: A geodynamic approach. Volume 5: The alpine cycle*. Springer.

Martínez-Torres, L. M. (1989). *El manto de los mármoles (Pirineo occidental): geología estructural y evolución geodinámica (PhD Thesis)*. Universidad del País Vasco-Euskal Herriko Unibertsitatea.

Masini, E., Manatschal, G., & Mohn, G. (2013). The Alpine Tethys rifted margins: Reconciling old and new ideas to understand the stratigraphic architecture of magma-poor rifted margins. *Sedimentology*, *60*(1), 174–196. https://doi.org/10.1111/sed.12017

Masini, E., Manatschal, G., Mohn, G., & Unternehr, P. (2012). Anatomy and tectono-sedimentary evolution of a rift-related detachment system: The example of the Err detachment (Central Alps, Se Switzerland). *GSA Bulletin*, *124*, 1535–1551. https://doi.org/10.1130/B30557.1

Masini, E., Manatschal, G., Tugend, J., Mohn, G., & Flament, J. M. (2014). The tectonosedimentary evolution of a hyper-extended rift basin: The example of the Arzacq–Mauléon rift system (Western Pyrenees, SW France). *International Journal of Earth Sciences*, *103*(6), 1569–1596. https://doi.org/10.1007/s00531-014-1023-8

Mazzoli, S., & Martín-Algarra, A. (2011). Deformation partitioning during transpressional emplacement of a 'mantle extrusion wedge': The Ronda peridotites, western Betic Cordillera, Spain. *Journal of the Geological Society*, *168*(2), 373–382. https://doi.org/10.1144/0016-76492010-126

Mazzoli, S., Martín-Algarra, A., Reddy, S. M., Sánchez-Vizcaíno, V. L., Fedele, L., & Noviello, A. (2013). The evolution of the footwall to the Ronda subcontinental mantle peridotites: Insights from the Nieves Unit (western Betic Cordillera). *Journal of the Geological Society*, *170*(3), 385–402. https://doi.org/10.1144/jgs2012-105

McKenzie, D. (1978). Some remarks on the formation of sedimentary basins. *Earth and Planetary Science Letters*, *40*(1), 25–32. https://doi.org/10.1016/0012-821x(78)90071-7

Mendia, M. S., & Ibarguchi, J. I. G. (1991). High-grade metamorphic rocks and peridotites along the Leiza Fault (Western Pyrenees, Spain). *Geologische Rundschau*, *80*(1), 93–107. https://doi.org/10.1007/BF01828769

Menzel, M. D., Garrido, C. J., Sánchez-Vizcaíno, V. L., Marchesi, C., Hidas, K., Escayola, M. P., & Huertas, A. D. (2018). Carbonation of mantle peridotite by CO_2-rich fluids: The formation of listvenites in the Advocate ophiolite complex (Newfoundland, Canada). *Lithos*, *323*, 238–261. https://doi.org/10.1016/j.lithos.2018.06.001

Miller, E. L., Gans, P. B., & Garing, J. (1983). The Snake Range décollement: An exhumed mid-Tertiary ductile–brittle transition. *Tectonics*, *2*(3), 239–263. https://doi.org/10.1029/TC002i003p00239

Minnigh, L. D., Van Castelren, P. W. C., & Den Tex, E. (1980). Quenching an additional model for emplacement of lherzolite at Lers, French Pyrenees. *Geology*, *8*, 18–21.

Mitchell, R. H. (2005). Carbonatites and carbonatites and carbonatites. *The Canadian Mineralogist*, *43*(6), 2049–2068. https://doi.org/10.2113/gscanmin.43.6.2049

Mizuochi, H., Satish-Kumar, M., Motoyoshi, Y., & Michibayashi, K. (2010). Exsolution of dolomite and application of calcite–dolomite solvus geo-thermometry in high-grade marbles: An example from Skallevikshalsen, East Antarctica. *Journal of Metamorphic Geology*, *28*(5), 509–526. https://doi.org/10.1111/j.1525-1314.2010.00877.x

Mohn, G., Manatschal, G., Beltrando, M., Masini, E., & Kusznir, N. (2012). Necking of continental crust in magma-poor rifted margins: Evidence from the fossil Alpine Tethys margins. *Tectonics*, *31*(1), TC1012. https://doi.org/10.1029/2011TC002961

Monchoux, P. (1970). *Les lherzolites pyrénéennes: contribution à l'étude de leur minéralogie, de leur genèse et de leurs transformations*. Ph.D. thesis (p. 180). Univ. of Toulouse, Toulouse, France.

Montigny, R., Azambre, B., Rossy, M., & Thuizat, R. (1986). K-Ar Study of cretaceous magmatism and metamorphism in the Pyrenees: Age and length of rotation of the Iberian Peninsula. *Tectonophysics*, *129*(1–4), 257–273. https://doi.org/10.1016/0040-1951(86)90255-6

Morgan, P. (1982). Heat flow in rift zones. *Geodynamics Series, Continental and Oceanic Rifts*, *8*, 107–122. https://doi.org/10.1029/gd008p0107

Motus, M., Nardin, E., Mouthereau, F., & Denèle, Y. (2022). Evolution of rift-related cover-basement decoupling revealed by brecciation processes in the eastern Pyrenees. *BSGF - Earth Sci Bull*, *193*, 14. https://doi.org/10.1051/bsgf/2022013

Mouthereau, F., Filleaudeau, P.-Y., Vacherat, A., Pik, R., Lacombe, O., Fellin, M. G., et al. (2014). Placing limits to shortening evolution in the Pyrenees: Role of margin architecture and implications for the Iberia/Europe convergence. *Tectonics*, *33*(12), 2283–2314. https://doi.org/10.1002/2014TC003663

Negro, F., Beyssac, O., Goffe, B., Saddiqi, O., & Bouybaouene, M. L. (2006). Thermal structure of the Alboran Domain in the Rif (northern Morocco) and the Western Betics (southern Spain). Constraints from Raman spectroscopy of carbonaceous material. *Journal of Metamorphic Geology*, *24*(4), 309–327. https://doi.org/10.1111/j.1525-1314.2006.00639.x

Nováková, M., Gallay, M., Šupinský, J., Ferré, E., Asti, R., de Saint Blanquat, M., et al. (2022). Correcting laser scanning intensity recorded in a cave environment for high-resolution lithological mapping: A case study of the Gouffre Georges, France. *Remote Sensing of Environment*, *280*, 113210. https://doi.org/10.1016/j.rse.2022.113210

Nteme Mukonzo, J., Boiron, M. C., Lagabrielle, Y., Cathelineau, M., & Quesnel, B. (2021). Fluid-rock interactions along detachment faults during continental rifting and mantle exhumation: The case of the Urdach lherzolite body (North Pyrenees). *Journal of the Geological Society*, *178*(2). https://doi.org/10.1144/jgs2020-116

Oliva-Urcia, B., Román-Berdiel, T., Casas, A. M., Pueyo, E. L., & Osácar, C. (2010). Tertiary compressional overprint on Aptian–Albian extensional magnetic fabrics, North-Pyrenean Zone. *Journal of Structural Geology*, *32*(3), 362–376. https://doi.org/10.1016/j.jsg.2010.01.009

Ortí, F., Pérez-López, A., & Salvany, J. M. (2017). Triassic evaporites of Iberia: Sedimentological and palaeogeographical implications for the western Neotethys evolution during the Middle Triassic–Earliest Jurassic. *Palaeogeography, Palaeoclimatology, Palaeoecology*, *471*, 157–180. https://doi.org/10.1016/j.palaeo.2017.01.025

Pérez-Gussinyé, M., & Reston, T. J. (2001). Rheological evolution during extension at passive non-volcanic margins: Onset of serpentinization and development of detachments to continental break-up. *Journal of Geophysical Research*, *106*, 3691–3975.

Pérez-Gussinyé, M., Xin, Y., Cunha, T., Ram, R., Andrés-Martínez, M., Dong, D., & García-Pintado, J. (2024). Synrift and post-rift thermal evolution of rifted margins: A re-evaluation of classic models of extension. In B. Kilhams, S. Holford, D. Gardiner, S. Gozzard, L. Layfield, C. McLean, et al. (Eds.), *The impacts of igneous systems on sedimentary basins and their energy resources*, *Geological Society, London, Special Publications* (p. 547).

Péron-Pinvidic, G., & Manatschal, G. (2009). The final rifting evolution at deep magma-poor passive margins from Iberia-Newfoundland: A new point of view. *International Journal of Earth Sciences*, *98*(7), 1581–1597. https://doi.org/10.1007/s00531-008-0337-9

Péron-Pinvidic, G., Manatschal, G., Minshull, T. A., & Sawyer, D. S. (2007). Tectonosedimentary evolution of the deep Iberia-Newfoundland margins: Evidence for a complex breakup history. *Tectonics*, *26*(2), TC2011. https://doi.org/10.1029/2006tc001970

Péron-Pinvidic, G., Manatschal, G., & Osmundsen, P. T. (2013). Structural comparison of archetypal Atlantic rifted margins: A review of observations and concepts. *Marine and Petroleum Geology*, *43*, 21–47. https://doi.org/10.1016/j.marpetgeo.2013.02.002

Péron-Pinvidic, G., & Osmundsen, P. T. (2016). Architecture of the distal and outer domains of the mid-Norwegian Vøring rifted margin: Insights from the Rån Ridge system. *Marine and Petroleum Geology*, *77*, 280–299. https://doi.org/10.1016/j.marpetgeo.2016.06.014

Persikov, E. S., & Bukhtiyarov, P. G. (2004). Experimental study of the mechanisms of calcite and dolomite melting at high fluid pressures. In *Informational bulletin of the annual seminar of experimental mineralogy, petrology and geochemistry*.

Petri, B., Duretz, T., Mohn, G., Schmalholz, S. M., Karner, G. D., & Müntener, O. (2019). Thinning mechanisms of heterogeneous continental lithosphere. *Earth and Planetary Science Letters*, *512*, 147–162. https://doi.org/10.1016/j.epsl.2019.02.007

Peybernès, B. (1976). *Le Jurassique et le Crétace inferieur des Pyrénées franco-espagnoles entre la Garonne et la Méditérranée*. Toulouse.

Peybernès, B. (1979). L'Urgonien des Pyrénées, Essai de synthèse. *Geobios*, *12*, 79–87. https://doi.org/10.1016/s0016-6995(79)80052-2

Peybernès, B. (1982). Création puis évolution de la marge nord-ibérique des Pyrénées au Crétacé inférieur. *Cuadernos de Geologia Iberica*, *8*, 987–1004.

Picazo, S., Cannat, M., Delacour, A., Escartín, J., Rouméjon, S., & Silantyev, S. (2012). Deformation associated with the denudation of mantle-derived rocks at the Mid-Atlantic Ridge 13°–15°N: The role of magmatic injections and hydrothermal alteration. *Geochemistry, Geophysics, Geosystems*, *13*(9). https://doi.org/10.1029/2012GC004121

Picazo, S., Manatschal, G., Cannat, M., & Andréani, M. (2013). Deformation associated to exhumation of serpentinized mantle rocks in a fossil ocean continent transition: The Totalp unit in SE Switzerland. *Lithos*, *175*, 255–271. https://doi.org/10.1016/j.lithos.2013.05.010

Platt, J. P., Argles, T. W., Carter, A., Kelley, S. P., Whitehouse, M. J., & Lonergan, L. (2003). Exhumation of the Ronda peridotite and its crustal envelope: Constraints from thermal modelling of a P–T–time array. *Journal of the Geological Society*, *160*(5), 655–676. https://doi.org/10.1144/0016-764902-108

Platt, J. P., Behr, W. M., & Cooper, F. J. (2015). Metamorphic core complexes: Windows into the mechanics and rheology of the crust. *Journal of the Geological Society of London*, *172*(1), 9–27. https://doi.org/10.1144/jgs2014-036

Précigout, J., Gueydan, F., Garrido, C. J., Cogné, N., & Booth-Rea, G. (2013). Deformation and exhumation of the Ronda peridotite (Spain). *Tectonics*, *32*(4), 1011–1025. https://doi.org/10.1002/tect.20062

Puigdefàbregas, C., & Souquet, P. (1986). Tecto-sedimentary cycles and depositional sequences of the Mesozoic and Tertiary from the Pyrenees. *Tectonophysics*, *129*(1–4), 173–203. https://doi.org/10.1016/0040-1951(86)90251-9

Puustinen, K. (1974). Dolomite exsolution textures in calcite from the Siilinjärvi carbonatite complex, Finland. *Bulletin of the Geological Society of Finland*, *46*(2), 151–159. https://doi.org/10.17741/bgsf/46.2.008

Rahl, J. M., Anderson, K. M., Brandon, M., & Fassoulas, C. (2005). Raman spectroscopic carbonaceous material thermometry of low-grade metamorphic rocks – Calibration and application to tectonic exhumation in Crete, Greece. *Earth and Planetary Science Letters*, *240*(2), 339–354. https://doi.org/10.1016/j.epsl.2005.09.055

Ravier, J. (1959). Le métamorphisme des terrains secondaires des Pyrénées. *Mém. Soc. géol. Fr*, *86*, 250.

Razin, P. (1989). *Evolution tecto-sédimentaire alpine des Pyrénées basques à l'ouest de la transformante de Pamplona, Province du Labourd*. PhD Thesis (Vol. 3, p. 464). University of Bordeaux.

Reston, T. J. (2005). Polyphase faulting during the development of the west Galicia rifted margin. *Earth and Planetary Science Letters*, *237*(3–4), 561–576. https://doi.org/10.1016/j.epsl.2005.06.019

Reston, T. J. (2007). The formation of non-volcanic rifted margins by the progressive extension of the lithosphere: The example of the West Iberian margin. *Geol. Soc. Lond. Spec. Publ.*, *282*(1), 77–110. https://doi.org/10.1144/sp282.5

Reston, T. J. (2009). The structure, evolution and symmetry of the magma-poor rifted margins of the North and Central Atlantic: A synthesis. *Tectonophysics*, *468*(1–4), 6–27. https://doi.org/10.1016/j.tecto.2008.09.002

Reston, T. J., Leythaeuser, T., Booth-Rea, G., Sawyer, D., Klaeschen, D., & Long, C. (2007). Movement along a low-angle normal fault. The S reflector west of Spain. *Geochemistry, Geophysics, Geosystems*, *8*(6), Q06002. https://doi.org/10.1029/2006GC001437

Reston, T. J., & Morgan, J. P. (2004). Continental geotherm and the evolution of rifted margins. *Geology*, *32*(2), 133. https://doi.org/10.1130/g19999.1

Reston, T. J., Pennell, J., Stubenrauch, A., Walker, I., & Pérez-Gussinyé, M. (2001). Detachment faulting, mantle serpentinization and serpentinite mud volcanism beneath the Porcupine Basin SW Ireland. *Geology*, *29*(7), 587–590. https://doi.org/10.1130/0091-7613(2001)029<0587:dfmsas>2.0.co;2

Reston, T. J., & Pérez-Gussinyé, M. (2007). Lithospheric extension from rifting to continental breakup at magma-poor margins: Rheology, serpentinisation and symmetry. *International Journal of Earth Sciences*, *96*(6), 1033–1046. https://doi.org/10.1007/s00531-006-0161-z

Ring, U., Gessner, K., Gungor, T., & Passchier, C. W. (1999). The Menderes Massif of western Turkey and the cycladic massif in the Aegean - Do they really correlate? *Journal of the Geological Society*, *156*(1), 3–6. https://doi.org/10.1144/gsjgs.156.1.0003

Rouméjon, S., Cannat, M., Agrinier, P., Godard, M., & Andreani, M. (2015). Serpentinization and fluid pathways in tectonically exhumed peridotites from the southwest Indian Ridge (62°-65° E). *Journal of Petrology*, *56*(4), 703–734. https://doi.org/10.1093/petrology/egv014

Rouméjon, S., Früh-Green, G. L., & Orcutt, B. N., & IODP Expedition 357 Science Party. (2018). Alteration heterogeneities in peridotites exhumed on the southern wall of the Atlantis massif (IODP Expedition 357). *Journal of Petrology*, *59*(7), 1329–1358. https://doi.org/10.1093/petrology/egy065

Roux, J.-C. (1983). Recherches stratigraphiques et sédimentologiques sur les flyschs crétacés pyrénéens au sud d'Oloron (Pyrénées Atlantiques). *Université Paul Sabatier de Toulouse (Sciences)*.

Rowan, M. G. (2014). Passive-margin salt basins: Hyperextension, evaporite deposition, and salt tectonics. *Basin Research*, *26*(1), 154–182. https://doi.org/10.1111/bre.12043

Saint-Blanquat de, M., Bajolet, F., Boulvais, P., Boutin, A., Clerc, C., Delacour, A., et al., (2017). Pyrenean hyper-extension: Breaking, thinning, or stretching of the crust? A view from the central north-Pyrenean zone. *Geophysical Research Abstracts*, *19*, EGU2017-8934-1.

Saint-Blanquat de, M., Bajolet, F., Grand'Homme, A., Proietti, A., Zanti, M., Boutin, A., et al. (2016). Cretaceous mantle exhumation in the central Pyrenees: New constraints from the peridotites in eastern Ariege (North Pyrenean zone, France). *CR Geosciences*, *348*(3–4), 268–278. https://doi.org/10.1016/j.crte.2015.12.003

Saint-Blanquat de, M., Brunel, M., & Mattauer, M. (1986). Les zones de cisaillements du massif Nord Pyrénéen du Saint Barthélémy, témoins probables de l'extension crustale d'âge crétacé. *Comptes Rendus de l'Académie des Sciences, Paris, Série II*, *303*, 1339–1344.

Salardon, R., Carpentier, C., Bellahsen, N., Pironon, J., & France-Lanord, C. (2017). Interactions between tectonics and fluid circulations in an inverted hyper-extended basin: Example of mesozoic carbonate rocks of the western North Pyrenean Zone (Chaînons Béarnais, France). *Marine and Petroleum Geology*, *80*, 563–586. https://doi.org/10.1016/j.marpetgeo.2016.11.018

Salas, R., Guimerà, J., Mas, R., Martín-Closas, C., Meléndez, A., & Alonso, A. (2001). Evolution of the Mesozoic central Iberian rift system and its Cainozoic inversion (Iberian chain). *Mém. Mus. Hist. Nat.*, *186*, 145–185.

Sallarès, V., Martínez-Loriente, S., Prada, M., Gràcia, E., Ranero, C., Gutscher, M. A., et al. (2013). Seismic evidence of exhumed mantle rock basement at the Gorringe Bank and the adjacent Horseshoe and Tagus abyssal plains (SW Iberia). *Earth and Planetary Science Letters*, *365*, 120–131. https://doi.org/10.1016/j.epsl.2013.01.021

Sapin, F., Ringenbach, J.-C., & Clerc, C. (2021). Rifted margins classification & forcing parameters. *Scientific Reports*, *11*(1), 8199. https://doi.org/10.1038/s41598-021-87648-3

Saspiturry, N., Allanic, C., & Peyrefitte, A. (2024). Serpentinization and Magmatic distribution in a Hyperextended Rift Suture: Implication for Natural Hydrogen Exploration (Mauléon Basin, Pyrenees). *Tectonics*, *43*(8), e2024TC008385. https://doi.org/10.1029/2024TC008385

Saspiturry, N., Allanic, C., Razin, P., Issautier, B., Baudin, T., Lasseur, E., et al. (2020a). Closure of a hyperextended system in an orogenic lithospheric pop-up, Western Pyrenees: The role of mantle buttressing and rift structural inheritance. *Terra Nova*, *32*(4), 253–260. https://doi.org/10.1111/ter.12457

Saspiturry, N., Allanic, C., Serrano, O., Courrioux, G., Baudin, T., Le Bayon, B., et al. (2022). Upper lithospheric transfer zones driving the non-cylindricity of the West-Pyrenean orogenic prism (Mauléon hyperextended basin). *Journal of Structural Geology*, *156*, 104535. https://doi.org/10.1016/j.jsg.2022.104535

Saspiturry, N., Cochelin, B., Razin, P., Leleu, S., Lemirre, B., Bouscary, C., et al. (2019b). Tectono-sedimentary evolution of a rift system controlled by Permian post-orogenic extension and metamorphic core complex formation (Bidarray Basin and Ursuya dome, Western Pyrenees). *Tectonophysics*, *768*, 228180. https://doi.org/10.1016/j.tecto.2019.228180

Saspiturry, N., Issautier, B., Razin, P., Andrieu, S., Lasseur, E., Allanic, C., et al. (2021b). Review of the syn-rift to early post-rift depositional systems of the Cretaceous Mauléon Rift: Sedimentary record of continental crust hyperextension and mantle denudation (Western Pyrenees). *BSGF - Earth Science Bulletin*, *192*, 49. https://doi.org/10.1051/bsgf/20221044

Saspiturry, N., Issautier, B., Razin, P., Baudin, T., Asti, R., Lagabrielle, Y., et al. (2021a). Review of Iberia-Eurasia plate-boundary basins: Role of sedimentary burial and salt tectonic during rifting and continental breakup. *Basin Research*, *33*(2), 1626–1661. https://doi.org/10.1111/bre.12529

Saspiturry, N., Lahfid, A., Baudin, T., Guillou-Frottier, L., Razin, P., Issautier, B., et al. (2020b). Paleogeothermal gradients across an inverted hyperextended rift system: Example of the Mauléon fossil rift (Western Pyrenees). *Tectonics*, *39*(10), e2020TC006206. https://doi.org/10.1029/2020TC006206

Saspiturry, N., Razin, P., Baudin, T., Serrano, O., Issautier, B., Lasseur, E., et al. (2019a). Symmetry vs. asymmetry of a hyper-thinned rift: Example of the Mauléon Basin (Western Pyrenees, France). *Marine and Petroleum Geology*, *104*, 86–105. https://doi.org/10.1016/j.marpetgeo.2019.03.031

Sauter, D., Manatschal, G., Kusznir, N., Masquelet, C., Werner, P., Ulrich, M., et al. (2023). Ignition of the southern Atlantic seafloor spreading machine without hot-mantle booster. *Scientific Reports*, *13*(1), 1195. https://doi.org/10.1038/s41598-023-28364-y

Schwarzenbach, E. M., Früh-Green, G. L., Bernasconi, S. M., Alt, J. C., & Plas, A. (2013). Serpentinization and carbon sequestration: A study of two ancient peridotite-hosted hydrothermal systems. *Chemical Geology*, *351*, 115–133. https://doi.org/10.1016/j.chemgeo.2013.05.016

Soares, D. M. (2014). *Sedimentological and stratigraphical aspects of the syn- to post-rift transition on fully separated conjugate margins*. PhD thesis (305 p.). Cardiff University.

Soares, D. M., Alves, T. M., & Terrinha, P. (2012). The breakup sequence and associated lithospheric breakup surface: Their significance in the context of rifted continental margins (West Iberia and Newfoundland margins, North Atlantic). *Earth and Planetary Science Letters*, *355–356*, 311–326. https://doi.org/10.1016/j.epsl.2012.08.036

Sorriaux, P., Guinot, R., Ferré, E., Gallay, M., Šupinský, J., de Saint Blanquat, M., & Asti, R. (2019). Expédition spéléo-scientifique au gouffre Georges: Relevé 3D de la Grande galerie. *Spelunca*, *5*, 5–13.

Souquet, P., Debroas, E. J., Boirie, J. M., Pons, P., Fixari, G., Dol, J., et al. (1985). Le Groupe du Flysch Noir (Albo-Cénomanien) dans les Pyrénées. *Bull Cent Rech Exlpo-Prod Elf-Aquitaine, Pau*, *9*, 183–252.

Teixell, A., Labaume, P., & Lagabrielle, Y. (2016). The crustal evolution of the west-central Pyrenees revisited: Inferences from a new kinematic scenario. *Comptes Rendus Geoscience*, *348*(3), 257–267. https://doi.org/10.1016/j.crte.2015.10.010

Ternet, Y., Colchen, M., Debroas, E.-J., Azambre, B., Debon, F., Bouchez, J.-L., et al. (1997). In O. BRGM (Ed.), *Notice explicative, Carte géol. France (1/50 000), feuille Aulus-les-Bains (1086) BRGM éditions*.

Tichadou, C., Godard, M., Munoz, M., Labaume, P., Vauchez, A., Gaucher, E., & Calassou, S. (2021). Mineralogical and geochemical study of serpentinized peridotites from the north-western Pyrenees: New insights on serpentinization along magma-poor continental passive margins. *Lithos*, *406*.

Tubía, J. M., Cuevas, J., & Ibarguchi, J. G. (1997). Sequential development of the metamorphic aureole beneath the Ronda peridotites and its bearing on the tectonic evolution of the Betic Cordillera. *Tectonophysics*, *279*(1–4), 227–252. https://doi.org/10.1016/s0040-1951(97)00124-8

Tugend, J., Manatschal, G., Kusznir, N. J., Masini, E., Mohn, G., & Thinon, I. (2014). Formation and deformation of hyperextended rift systems: Insights from rift domain mapping in the Bay of Biscay-Pyrenees. *Tectonics*, *33*(7), 1239–1276. https://doi.org/10.1002/2014TC003529

Tugend, J., Mohn, G., Duretz, T., Petri, B., & Le Pourhiet, L. (2024). Extension of continental lithosphere in rifted margins: A review of thinning mechanisms. In *Comptes Rendus. Géoscience - Sciences de la Planète, Special Issue: Geodynamics of Continents and Oceans – A tribute to Jean Aubouin*. https://doi.org/10.5802/crgeos.257

Uzel, J., Lagabrielle, Y., Fourcade, S., Chopin, C., Monchoux, P., Clerc, C., & Poujol, M. (2020). The sapphirine-bearing rocks in contact with the Lherz peridotite body: New mineralogical data, age and interpretation. *BSGF - Earth Sci. Bull.*, *191*, 5. https://doi.org/10.1051/bsgf/2019015

Vacherat, A., Mouthereau, F., Pik, R., Bernet, M., Gautheron, C., Masini, E., et al. (2014). Thermal imprint of rift-related processes in orogens as recorded in the Pyrenees. *Earth and Planetary Science Letters*, *408*, 296–306. https://doi.org/10.1016/j.epsl.2014.10.014

Vergés, J., & García-Senz, J. (2001). Mesozoic evolution and Cainozoic inversion of the Pyrenean Rift. In: P. A. Ziegler, W. Cavazza, A. H. F. Robertson, & S. Crasquin-Soleau (Eds.), *Peri-Tethyan Rift/wrench basins and passive margins* (Vol. 186, pp. 187–212). Mém. Mus. Hist. Nat.

Vielzeuf, D., & Kornprobst, J. (1984). Crustal splitting and the emplacement of Pyrenean lherzolites and granulites. *Earth and Planetary Science Letters*, *67*(1), 87–96. https://doi.org/10.1016/0012-821X(84)90041-4

Vissers, R. L. M., Drury, M. R., Newman, J., & Flliervoet, T. F. (1997). Mylonitic deformation in upper mantle peridotites of the North Pyrenean Zone (France): Implications for strength and strain localization in the lithosphere. *Tectonophysics*, *279*(1–4), 303–325. https://doi.org/10.1016/S0040-1951(97)00128-5

Wernicke, B. (1981). Low-angle normal faults in the basin and Range Province: Nappe tectonics in an extending orogen. *Nature*, *291*(5817), 645–648. https://doi.org/10.1038/291645a0

Wernicke, B. (1985). Uniform-sense normal simple shear of the continental lithosphere. *Canadian Journal of Earth Sciences*, *22*(1), 108–125. https://doi.org/10.1139/e85-009

Whitmarsh, R. B., Manatschal, G., & Minshull, T. A. (2001). Evolution of magma-poor continental margins from rifting to sea-floor spreading. *Nature*, *413*(6852), 150–154. https://doi.org/10.1038/35093085

Wyllie, P. J., & Tuttle, O. F. (1960). The system $CaO–CO_2–H_2O$ and the origin of carbonatites. *Journal of Petrology*, *1*, 1–46. https://doi.org/10.1093/petrology/1.1.1

Yaxley, G., Anenburg, M., Tappe, S., Decrée, S., & Guzmics, T. (2022). Carbonatites – Classification, Sources, Evolution and Emplacement. *Annual Review of Earth and Planetary Sciences*, *50*(1), 261–293. https://doi.org/10.1146/annurev-earth-032320-104243

Zaitsev, A., & Polezhaeva, L. (1994). Dolomite-calcite textures in early carbonatites of the Kovdor ore deposit, Kola peninsula, Russia: Their genesis and application for calcite-dolomite geothermometry. *Contributions to Mineralogy and Petrology*, *115*(3), 339–344. https://doi.org/10.1007/BF00310772

Ziegler, A. M. (1988). *Evolution of arctic-North Atlantic and western Tethys* (Vol. 43, p. 198). AAPG Memoir.